CODE OPTIMIZATION AND ANALYSIS FOR MULTIPLE-INPUT AND MULTIPLE-OUTPUT COMMUNICATION SYSTEMS

A Dissertation

by

GUOSEN YUE

Submitted to the Office of Graduate Studies of
Texas A&M University
in partial fulfillment of the requirements for the degree of

DOCTOR OF PHILOSOPHY

August 2004

Major Subject: Electrical Engineering

CODE OPTIMIZATION AND ANALYSIS FOR MULTIPLE-INPUT AND MULTIPLE-OUTPUT COMMUNICATION SYSTEMS

A Dissertation

by

GUOSEN YUE

Submitted to Texas A&M University
in partial fulfillment of the requirements
for the degree of

DOCTOR OF PHILOSOPHY

Approved as to style and content by:

Xiaodong Wang (Co-Chair of Committee)	Krishna R. Narayanan (Co-Chair of Committee)
Scott L. Miller (Member)	Aydin Karsilayan (Member)
Du Li (Member)	Chanan Singh (Head of Department)

August 2004

Major Subject: Electrical Engineering

ABSTRACT

Code Optimization and Analysis for Multiple-input and

Multiple-output Communication Systems. (August 2004)

Guosen Yue, B.S., Nanjing University, P.R. China;

M.S., Nanjing University, P.R. China

Co–Chairs of Advisory Committee: Dr. Xiaodong Wang
Dr. Krishna R. Narayanan

Design and analysis of random-like codes for various multiple-input and multiple-output communication systems are addressed in this work. Random-like codes have drawn significant interest because they offer capacity-achieving performance. We first consider the analysis and design of low-density parity-check (LDPC) codes for turbo multiuser detection in multipath CDMA channels. We develop techniques for computing the probability density function (pdf) of the extrinsic messages at the output of the soft-input soft-output (SISO) multiuser detectors as a function of the pdf of input extrinsic messages, user spreading codes, channel impulse responses, and signal-to-noise ratios. Using these techniques, we are able to accurately compute the thresholds for LDPC codes and design good irregular LDPC codes. We then apply the tools of density evolution with mixture Gaussian approximations to optimize irregular LDPC codes and to compute minimum operational signal-to-noise ratios for ergodic MIMO OFDM channels. In particular, the optimization is done for various MIMO OFDM system configurations which include different number of antennas, different channel models and different demodulation schemes. We also study the coding-spreading tradeoff in LDPC coded CDMA systems employing multiuser joint decoding. We solve the coding-spreading optimization based on the extrinsic information SNR evolution curves for the SISO multiuser detectors and the SISO LDPC decoders. Both single-cell and multi-cell scenarios will be considered. For

each of these cases, we will characterize the extrinsic information for both finite-size systems and the so-called large systems where asymptotic performance results must be evoked. Finally, we consider the design optimization of irregular repeat accumulate (IRA) codes for MIMO communication systems employing iterative receivers. We present the density evolution-based procedure with Gaussian approximation for optimizing the IRA code ensemble. We adopt an approximation method based on linear programming to design an IRA code with the extrinsic information transfer (EXIT) chart matched to that of the soft MIMO demodulator.

To my family

ACKNOWLEDGMENTS

I would first like to thank my advisors, Dr. Xiaodong Wang and Dr. Krishna R. Narayanan, not only for their inspirational guidance and consistent support, but also for their encouragement and patience, during my Ph.D. program. Without their help, this dissertation would not be finished. I would also like to thank my committee members, Dr. Scott L. Miller, Dr. Aydin Karsilayan, and Dr. Du Li for their valuable comments and insightful advice on my research.

I wish to thank Dr. Xiaobo Zhou and Dr. Ben Lu. Cooperation and discussion with them has significantly diversified my research. I also wish to acknowledge all my colleagues in the wireless communication lab at Texas A&M University, especially to Dr. Shengjie Zhao, Dr. Zigang Yang, Dr. Jing Li, Dr. Yan Wang, Dong Guo, Yongzhe Xie, Dung Ngoc Doan, Zemin Zhu, Wenyan He, Jun Zheng, Yong Sun, Kai Shi, Beminihennadige Janath Peiris, and Jing Jiang for the constructive and insightful discussions.

I am very grateful to my grandma, my parents, Wenzhe Yue and Yulan Zhang, my sister Jiangyan Yue for their continuous support and endless love to me. I am especially grateful to my wife, Xuechao Du, for her love, understanding, patience, and full support during my hard time.

TABLE OF CONTENTS

CHAPTER Page

CHAPTER Page

LIST OF TABLES

LIST OF FIGURES

FIGURE Page

FIGURE Page

FIGURE Page

CHAPTER I

INTRODUCTION

A. Background

During the past decade, random-like codes have drawn significant interest because they offer near capacity performance [1, 2, 3]. The first breakthrough in this area is the invention of turbo codes [4]. This novel approach to error control coding has revolutionalized coding theory and techniques. Another important milestone is the re-discovery of the low-density parity-check (LDPC) codes [5], which were originally proposed by Gallager [6]. In fact, Gallager's remarkable paper in 1962 already contains many new concepts of fundamental importance for capacity-approaching coding. Irregular LDPC codes were introduced in [7], which were shown to asymptotically achieve the capacity of the binary erasure channel (BEC) under iterative message-passing decoding. The complete design and performance analysis of irregular LDPC codes for memoryless channels based on density evolution and Gaussian approximation were treated recently in [8, 9, 10]. It has been shown in the limit of infinite block lengths, carefully designed irregular LDPC codes can achieve within 0.0045dB of the Shannon limit [11].

The ideas behind turbo codes have also spread to impact many aspects of signal processing and communications. One of significant techniques is iterative processing for joint demodulation and decoding. An iterative algorithm invokes demodulation and decoding iteratively to approximate the optimum decision. Soft extrinsic messages are iteratively exchanged between the demodulator and decoder. This so-called "turbo principle" [12] has been successfully applied to many detection/decoding prob-

---

The journal model is *IEEE Transactions on Automatic Control*.

lems such as equalization, coded modulation, multiuser detection, joint source and channel decoding, and turbo-BLAST systems [12, 13, 14, 15]. Iterative processing is indeed an instance of message-passing. A graph presentation of iterative receiver with both coding and modulation is elaborated in [16].

The code design for memoryless channels is studied in [7, 9, 11, 17]. However, these code design methods for memoryless channels no longer provide optimized code for iterative systems. It is important to consider code design for the iterative system in order to achieve optimal gain and this is addressed in this dissertation.

More detailed introductions can be found in subsequent chapters.

B. Dissertation Outline

This dissertation presents some topics on code design and analysis for some wireless communication systems with iterative demodulation and decoding. The dissertation is organized as follows.

In Chapter II, we consider the analysis and design of low-density parity-check (LDPC) codes for turbo multiuser detection in multipath CDMA channels. We develop techniques for computing the probability density function (pdf) of the extrinsic messages at the output of the soft-input soft-output (SISO) multiuser detectors as a function of the pdf of input extrinsic messages, user spreading codes, channel impulse responses, and signal-to-noise ratios. Of particular interest is the SIC-MMSE multiuser detector, for which the pdf of the extrinsic messages can be characterized analytically. For the case of additive white Gaussian noise (AWGN) channels, the extrinsic messages can be well-approximated as symmetric Gaussian distributed. For the case of asynchronous multipath fading channels, the extrinsic messages can be approximated by a mixture of symmetric Gaussian distributions. We show that the

expectation-maximization (EM) algorithm can be used to compute the parameters of this mixture. Using these techniques, we are able to accurately compute the thresholds for LDPC codes and design good irregular LDPC codes. Simulation results are in good agreement with the computed thresholds and the designed irregular LDPC codes outperform regular ones significantly.

In Chapter III, we consider the performance analysis and design optimization of LDPC coded multiple-input multiple-output (MIMO) orthogonal frequency-division multiplexing (OFDM) systems for high data rate wireless transmission. The tools of density evolution with mixture Gaussian approximations are used to optimize irregular LDPC codes and to compute minimum operational signal-to-noise ratios for ergodic MIMO OFDM channels. In particular, the optimization is done for various MIMO OFDM system configurations which include different number of antennas, different channel models and different demodulation schemes; and the optimized performance is compared to the corresponding channel capacity. From the LDPC profiles that already optimized for ergodic channels, we heuristically construct small block-size irregular LDPC codes for outage MIMO OFDM channels; as shown from simulation results, the irregular LDPC codes constructed here are helpful to expedite the convergence of the iterative receivers.

In Chapter IV, we consider the problem of coding-spreading tradeoff in CDMA systems employing multiuser joint decoding. In particular, we assume the users employing the capacity-achieving LDPC codes and at the receiver, turbo multiuser detection is used to implement joint decoding. We solve the coding-spreading optimization based on the extrinsic information SNR evolution curves for the SISO multiuser detectors and the SISO LDPC decoders. Two types of SISO multiuser detectors are treated, namely, the SIC-MMSE detector and the SIC-MF detector. Moreover, both single-cell and multi-cell scenarios are considered. For each of these cases, we are able

to characterize the extrinsic information SNR analytically, for both finite-size systems and the so-called large systems where asymptotic performance results must be evoked. Our analysis indicates that the SIC-MMSE-based system offers a significant gain in spectral efficiency compared with the SIC-MF counterpart, in both single-cell and multi-cell scenarios. This is in contrast to the single-user decoding case, where it has been shown that the MMSE detector offers little advantage over the conventional matched-filter in terms of capacity in multi-cell scenario. Moreover, the results on coding-spreading tradeoff for finite-size systems and large-system match very well.

In Chapter V, we consider the design optimization of the random-like ensemble of irregular repeat accumulate (IRA) codes for MIMO communication systems employing iterative receivers. We first present the density evolution-based procedure for optimizing the IRA code ensemble. An approximation method based on linear programming is adopted to design an IRA code with the extrinsic information transfer (EXIT) chart matched to that of the soft MIMO demodulator. We then reveal the relationship between the IRA codes and the LDPC codes. With a code ensemble mapping relationship between an IRA code and an LDPC code, an optimal IRA code can also be obtained by transforming an optimal LDPC code designed for MIMO systems. The results show that with the MAP receiver, the designed IRA codes can perform within 1dB from the ergodic capacities of the MIMO systems under consideration. We also treat the short-length IRA code design for block fading MIMO channels. We adopt design techniques for short-length LDPC codes to improve the performance of the short-length IRA code and to reduce the error floor.

Finally, Chapter VI contains the conclusions.

CHAPTER II

LDPC CODE OPTIMIZATION FOR TURBO CDMA SYSTEMS

A. Introduction

Most works on turbo multiuser detection are confined to the use of convolutional codes or parallel concatenated convolutional codes (PCCC) [18]. Recent results [9, 10] show that carefully designed irregular low-density parity-check (LDPC) codes can outperform PCCC for long code lengths and provide near-capacity performance on memoryless channels. It is then natural to attempt to design good LDPC code ensembles for turbo multiuser detection.

The main idea used in the design of LDPC codes is to employ the technique of density evolution [19, 10], where the probability density function (pdf) of extrinsic messages is computed as a function of iteration and the given degree profiles for the LDPC code, in order to compute the thresholds (in SNR or E_b/N_o). Then, an optimization procedure is used to find optimum degree profiles that result in the least thresholds (or, near capacity performance). It has been shown that for a small sacrifice in the resulting thresholds, the design procedure can be simplified by making the assumption that the messages (extrinsic information) at the output of the check nodes and the bit nodes have a Gaussian distribution [8]. For turbo multiuser detection, the LDPC codes will be used in conjunction with a soft-input soft-output (SISO) multiuser detector. In order to extend the afore-mentioned technique to design good LDPC codes for turbo multiuser receiver, we need a technique to characterize the pdf of the extrinsic messages at the output of the detector as a function of the input pdf and channel characteristics. In this chapter, we will primarily focus on the SISO multiuser detector based on soft interference cancellation (SIC)

and instantaneous linear MMSE filtering, a technique first proposed in [14]. Other receivers, i.e., the optimal detector and the matched filter are also discussed. We show how to characterize the input-output pdf's of the extrinsic information *analytically* for these multiuser detectors and use this to design good LDPC codes.

B. Turbo Multiuser Receiver for LDPC-coded CDMA

We consider an LDPC-coded CDMA system with K users, employing normalized modulation waveforms $s_1,\ s_2, \cdots, s_K$, and signaling through their respective multipath channels with additive white Gaussian noise. The block diagram of the transmitter-end of such a system is shown in the upper half of Fig. 1. The binary information data $\{d_k(m)\}$ for user k are LDPC encoded. The interleaved code bits of the kth user are BPSK symbol-mapped. Each data symbol $b_k(i)$ is then modulated by a spreading waveform $s_{k,i}(t)$, and transmitted through its multipath channel. Shown in the lower part of Fig. 1, the overall receiver is an iterative receiver which performs turbo multiuser detection by passing extrinsic messages on the code bits between a soft-input soft-output (SISO) multiuser detector and an LDPC decoder. In each turbo iteration, several inner iterations are performed within the LDPC decoder during which extrinsic messages are passed along the edges in the bipartite graph of the code.

Notation: The variable L is used to refer to extrinsic messages (in log-likelihood form). The variable f is used to denote the pdf of the extrinsic information L, and m is used to denote the mean of L. Superscript (p, q) is used to denote quantities during the pth round of inner decoding within the LDPC decoder and qth stage of outer iteration between the LDPC decoder and the multiuser detector. For the quantities passed between the multiuser detector and the decoder, only one superscript q, namely the turbo multiuser detection iteration number is used. A subscript $m \rightarrow L$

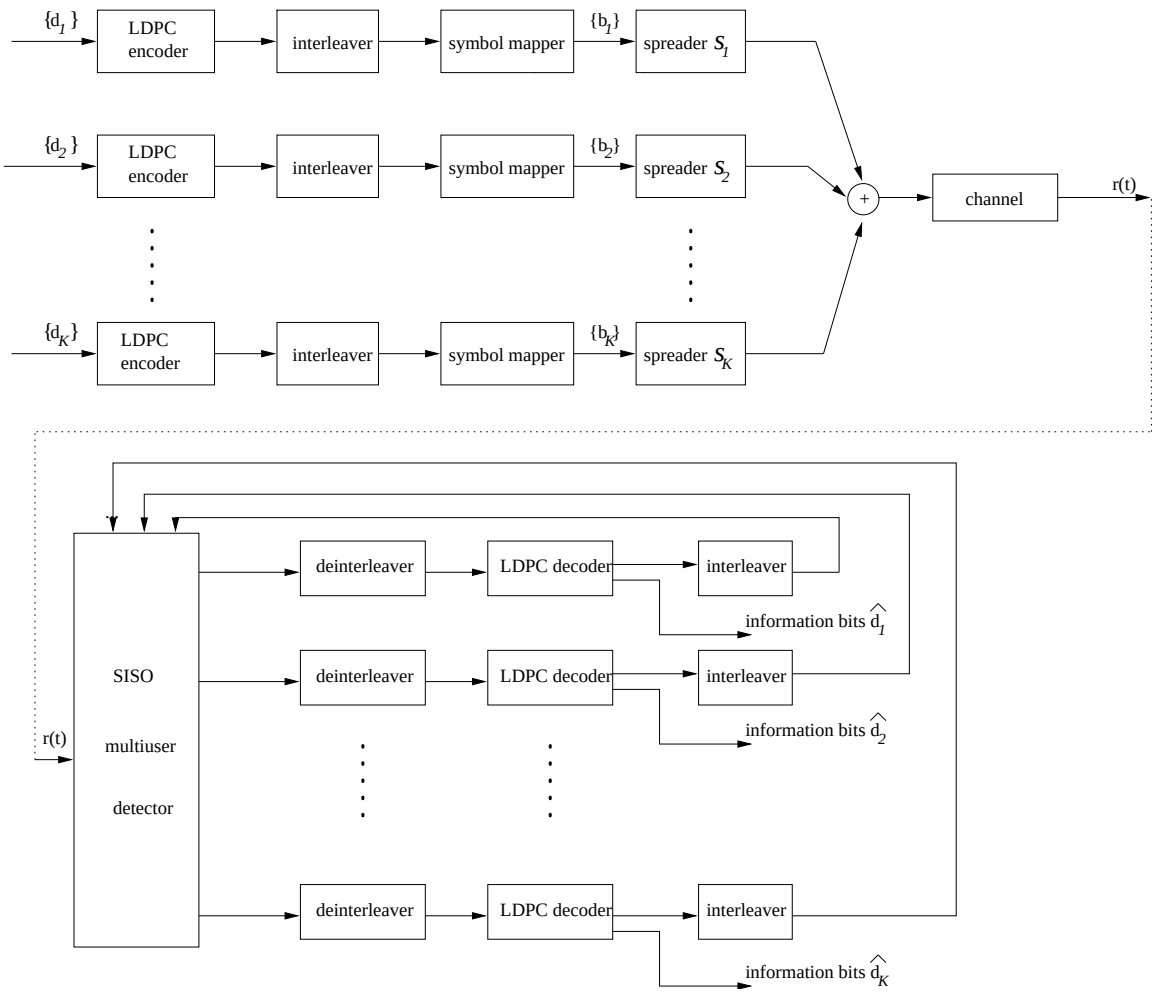

Fig. 1. An LDPC coded CDMA system with iterative receiver.

denotes quantities passed from the multiuser detector to the LDPC decoder, and vice versa. Similarly, quantities passed between the bit nodes and the check nodes of the LDPC code are denoted by $b \rightarrow c$ and $b \leftarrow c$, respectively. The degree of the ith bit node is denoted by ν_i and the degree of the ith check node is denoted by Δ_i. Denote by $\{e^b_{i,1}, e^b_{i,2}, \ldots, e^b_{i,\nu_i}\}$ the set of edges connected to the ith bit node and by $\{e^c_{i,1}, e^c_{i,2}, \ldots, e^c_{i,\Delta_i}\}$ the set of edges connected to the ith check node. The particular edge or bit associated with an extrinsic information is denoted as the argument of L.

The turbo multiuser detection algorithm for LDPC-coded CDMA systems is as follows:

[0:] Initialization: $L^{0,0}_{b\leftarrow c}(e^b_{i,n}) = 0, \forall(i,n)$, and $L^0_{m\leftarrow L}[b_k(i)] = 0, \forall(i,k)$.

[1:] *Turbo multiuser detection iterations:* For $q = 1, 2, \ldots, Q$

[1-a:] *SISO multiuser detection:* The SISO multiuser detector computes

$$L^q_{m\rightarrow L}[b_k(i)] = g\Big(\{r(t)\}, \{L^{q-1}_{m\leftarrow L}[b_{k'}(i)]\}_{k'\neq k}\Big), \tag{2.1}$$

where $g(\cdot)$ denotes the SISO multiuser detector.

[1-b:] *LDPC decoding:* For $k = 1, 2, \ldots, K$

Iterate between bit node update and check node update: For $p = 1, 2, \ldots, P$

Bit node update: For each of the bit nodes i, and for all edges connected to it, compute

$$L^{p,q}_{b\rightarrow c}(e^b_{i,j}) = L^q_{m\rightarrow L}[b_k(i)] + \sum_{n=1, n\neq j}^{\nu_i} L^{p-1,q}_{b\leftarrow c}(e^b_{i,n}). \tag{2.2}$$

Check node update: For each of the check nodes i, and for all edges connected to it, compute [20]

$$L^{p,q}_{b\leftarrow c}(e^c_{i,j}) = 2\tanh^{-1}\left[\prod_{n=1, n\neq j}^{\Delta_i} \tanh\left(\frac{L^{p,q}_{b\rightarrow c}(e^c_{i,n})}{2}\right)\right]. \tag{2.3}$$

[1-c:] *Compute extrinsic messages passed back to the multiuser detector:*

$$L^q_{m\leftarrow L}[b_k(i)] = \sum_{n=1}^{\nu_i} L^{P,q}_{b\leftarrow c}(e^b_{i,n}). \tag{2.4}$$

[1-d:] *Store check to bit messages:* For all edges, set

$$L^{0,q+1}_{b\leftarrow c}(e^b_{i,n}) = L^{P,q}_{b\leftarrow c}(e^b_{i,n}). \tag{2.5}$$

[2:] *Final hard decisions on information and parity bits:*

$$\hat{b}_k(i) \;=\; \text{sign}\left\{ L^{Q}_{m\to L}[b_k(i)] + L^{Q}_{m\leftarrow L}[b_k(i)] \right\}. \tag{2.6}$$

C. SISO Multiuser Detectors

In this section, we outline three SISO multiuser detectors. For clarity, we first discuss these detectors in the context of a synchronous CDMA systems, in which the received (real-valued) signal is given by

$$r(t) = \sum_{k=1}^{K} A_k \sum_{i=0}^{M-1} b_k(i) s_{k,i}(t) + \sigma n(t), \tag{2.7}$$

where $s_{k,i}(t)$ is the spreading waveform of the kth user, ith symbol, and M is the number of the data symbols per user. A sufficient statistic for demodulating $\{b_k(i), k = 1, \cdots, K\}$ is given by

$$y_k(i) \triangleq \int_{iT}^{(i+1)T} s_{k,i}(t) r(t) \mathrm{d}t, \quad k = 1, \cdots, K. \tag{2.8}$$

Denote $\underline{y}(i) = [y_1(i), \cdots, y_K(i)]^T$, then

$$\underline{y}(i) = \underline{R}(i)\underline{A}\underline{b}(i) + \sigma \underline{n}(i), \tag{2.9}$$

where $[\underline{R}(i)]_{k,l} \triangleq \int_{iT}^{(i+1)T} s_{k,i}(t) s_{l,i}(t) \mathrm{d}t$; $\underline{A} \triangleq \text{diag}(A_1, \cdots, A_k)$; $\underline{b}(i) = [b_1(i), \cdots, b_K(i)]^T$; and $\underline{n}(i) \sim \mathcal{N}(\underline{0}, \underline{R}(i))$ is independent of $\underline{b}(i)$.

Exact SISO multiuser detector: [14] Denote

$$\mathcal{B}_k^{+} \triangleq \{(b_1, \cdots, b_{k-1}, +1, b_{k+1}, \cdots, b_K) : b_j \in \{+1, -1\}\}.$$

Similarly define $\mathcal{B}_k^{-}$. We have the following exact expression for the extrinsic messages

from the multiuser detector

$$L^q_{m\to L}[b_k(i)] = \frac{2A_k y_k(i)}{\sigma^2} + \log \frac{\sum_{\underline{b}\in\mathcal{B}_k^+}\left\{\exp\left[-\underline{b}^T\underline{AR}(i)\underline{Ab}/(2\sigma^2)\right]\prod_{j\neq k}[1+b_j\tanh(A_j y_j(i)/\sigma^2)]\left[1+b_j\tanh\left(\frac{1}{2}L^{q-1}_{m\leftarrow L}[b_j(i)]\right)\right]\right\}}{\sum_{\underline{b}\in\mathcal{B}_k^-}\left\{\exp\left[-\underline{b}^T\underline{AR}(i)\underline{Ab}/(2\sigma^2)\right]\prod_{j\neq k}[1+b_j\tanh(A_j y_j(i)/\sigma^2)]\left[1+b_j\tanh\left(\frac{1}{2}L^{q-1}_{m\leftarrow L}[b_j(i)]\right)\right]\right\}}. \quad (2.10)$$

SIC-MMSE SISO multiuser detector: [14] A low-complexity approximate SISO multiuser detector was developed in [14] which is based on soft interference cancellation and instantaneous linear MMSE filtering, and is summarized as follows. Denote $\underline{e}_k$ as the k-th unit vector in $\mathbb{R}^K$. Define

$$\tilde{b}_j(i) \triangleq \tanh\left(\frac{1}{2}L^{q-1}_{m\leftarrow L}[b_j(i)]\right), \quad j=1,\cdots,K, \quad (2.11)$$

$$\text{and} \quad \underline{V}_k(i) \triangleq \sum_{j\neq k} A_j^2[1-\tilde{b}_j(i)^2]\underline{e}_j\underline{e}_j^T + A_k^2\underline{e}_k\underline{e}_k^T. \quad (2.12)$$

Denote $\underline{\tilde{b}}(i) \triangleq [\tilde{b}_1(i)\cdots\tilde{b}_K(i)]^T$ and $\underline{\tilde{b}}_k(i) \triangleq \underline{\tilde{b}}(i) - \tilde{b}_k(i)\underline{e}_k$. Then we have

$$L^q_{m\to L}[b_k(i)] = \frac{2z_k(i)}{1-\mu_k(i)}, \quad (2.13)$$

$$\text{where} \quad z_k(i) = A_k\underline{e}_k^T[\underline{V}_k(i)+\sigma^2\underline{R}(i)^{-1}]^{-1}[\underline{R}(i)^{-1}\underline{y}(i) - \underline{A}\underline{\tilde{b}}_k(i)]. \quad (2.14)$$

$$\mu_k(i) = A_k^2\underline{e}_k^T\left[\underline{V}_k(i)+\sigma^2\underline{R}(i)^{-1}\right]^{-1}\underline{e}_k. \quad (2.15)$$

SIC-MF SISO multiuser detector: A further simplification on the above SIC-MMSE detector is to skip the linear MMSE filtering step. In this case, the output is a scaled version of the matched filter output after ideal interference cancellation, given by

$$L^q_{m\to L}[b_k(i)] = \frac{2}{\gamma_k(i)}\left(y_k(i) - \sum_{j\neq k} A_j[\underline{R}(i)]_{k,j}\tilde{b}_j(i)\right), \quad (2.16)$$

$$\text{where} \quad \gamma_k(i) = \left[\underline{R}(i)\underline{V}_k(i)\underline{R}(i)+\sigma^2\underline{R}(i)\right]_{k,k} - 1. \quad (2.17)$$

1. Extension to Asynchronous CDMA with Multipath Fading

The received signal in an asynchronous CDMA system with multipath fading channels can be written as

$$r(t) = \sum_{k=1}^{K} A_k \sum_{i=0}^{M-1} b_k(i) \sum_{l=1}^{\ell_P} g_{kl}(i) s_{k,i}(t-\tau_{kl}) + \sigma n(t), \tag{2.18}$$

where ℓ_P is the number of resolvable paths in each user's channel; $g_{kl}(i)$ and τ_{kl} are respectively the complex gain corresponding to the ith symbol and the delay of the l-th path of the kth user's channel. Assume that the multipath spread of any user signal is limited to at most Δ symbol intervals, where Δ is a positive integer. Define

$$\rho^{[j]}_{(k,l)(k',l')}(i) \triangleq \int_{-\infty}^{\infty} s_{k,i}(t-\tau_{kl}) s_{k',i-j}(t-\tau_{k'l'}) dt, \quad -\Delta \le j \le \Delta. \tag{2.19}$$

The received signal $r(t)$ in (2.18) is first passed through a matched filter, to obtain

$$\begin{aligned} z_{kl}(i) &\triangleq \int_{-\infty}^{\infty} r(t) s_{k,i}(t-\tau_{kl}) dt \\ &= \sum_{j=-\Delta}^{\Delta} A_{k'} b_{k'}(i+j) \sum_{l'=1}^{\ell_P} g_{k'l'}(i) \rho^{[-j]}_{(k,l)(k',l')}(i) + \sigma u_{kl}(i), \end{aligned} \tag{2.20}$$

where $\{u_{kl}(i)\}$ are zero-mean complex Gaussian random sequences with covariance

$$E\{u_{kl}(i) u_{k'l'}(i')^*\} = \int_{-\infty}^{\infty} s_{k,i}(t-\tau_{kl}) s_{k',i'}(t-\tau_{k'l'}) dt = \rho^{[i-i']}_{(k,l)(k',l')}(i). \tag{2.21}$$

Define the following quantities

$$\underline{R}^{[j]}(i) \triangleq \begin{bmatrix} \rho^{[j]}_{(1,1)(1,1)}(i) & \cdots & \rho^{[j]}_{(1,1)(K,1)}(i) & \cdots & \rho^{[j]}_{(1,1)(K,\ell_P)}(i) \\ \rho^{[j]}_{(2,1)(1,1)}(i) & \cdots & \rho^{[j]}_{(2,1)(K,1)}(i) & \cdots & \rho^{[j]}_{(2,1)(K,\ell_P)}(i) \\ \vdots & \vdots & \vdots & \vdots & \vdots \\ \rho^{[j]}_{(K,\ell_P)(1,1)}(i) & \cdots & \rho^{[j]}_{(K,\ell_P)(K,1)}(i) & \cdots & \rho^{[j]}_{(K,\ell_P)(K,\ell_P)}(i) \end{bmatrix}_{[(K\ell_P \times K\ell_P)]}$$

$$\underline{\zeta}(i) \triangleq [z_{11}(i), \cdots, z_{1\ell_P}(i), \cdots, z_{K1}(i), \cdots, z_{K\ell_P}(i)]^T \ \ [(K\ell_P \times 1)]$$

$$\underline{u}(i) \triangleq [u_{11}(i), \cdots, u_{1\ell_P}(i), \cdots, u_{K1}(i), \cdots, u_{K\ell_P}(i)]^T \ \ [(K\ell_P \times 1)]$$

$$\underline{g}_k(i) \triangleq [g_{k1}(i), \cdots, g_{k\ell_P}(i)]^T \quad [(\ell_P \times 1)]$$

$$\underline{G}(i) \triangleq \text{diag}\left(\underline{g}_1(i), \cdots, \underline{g}_K(i)\right) \ \ [(K\ell_P \times K)]$$

We can then write (2.20) in the following vector form

$$\underline{\zeta}(i) = \sum_{j=-\Delta}^{\Delta} \underline{R}^{[-j]}(i)\underline{G}(i+j)\underline{Ab}(i+j) + \sigma\underline{u}(i), \tag{2.22}$$

and from (2.21), the covariance matrix of the complex Gaussian vector sequence $\{\underline{u}(i)\}$ is $E\left\{\underline{u}(i)\underline{u}(i+j)^H\right\} = \underline{R}^{[-j]}(i)$. Define $y_k(i) \triangleq \sum_{l=1}^{\ell} g_{kl}(i)^* z_{kl}(i)$. Then, $\underline{y}(i) \triangleq [y_1(i), \cdots, y_K(i)]^T$ is given by

$$\underline{y}(i) \triangleq \underline{G}(i)^H\underline{\zeta}(i) = \sum_{j=-\Delta}^{\Delta} \underbrace{\underline{G}(i)^H\underline{R}^{[-j]}(i)\underline{G}(i+j)}_{\underline{H}^{[-j]}(i)}\underline{Ab}(i+j) + \sigma\underbrace{\underline{G}(i)^H\underline{u}(i)}_{\underline{v}(i)}, \tag{2.23}$$

where $\underline{v}(i)$ is a sequence of zero-mean complex Gaussian vectors with covariance matrix

$$E\left\{\underline{v}(i)\underline{v}(i+j)^H\right\} = \underline{G}(i)^H\underline{R}^{[-j]}(i)\underline{G}(i+j) \triangleq \underline{H}^{[-j]}(i). \tag{2.24}$$

Now define $\boldsymbol{H}(i) \triangleq [\underline{H}^{[1]}(i)\ \underline{H}^{[0]}(i)\ \underline{H}^{[-1]}(i)]$ ($K \times 3K$ matrix), $\boldsymbol{A} \triangleq \text{diag}(\underline{A}, \underline{A}, \underline{A})$ ($3K \times 3K$ diagonal matrix) and $\boldsymbol{b}(i) \triangleq [\underline{b}(i-1)^T\ \underline{b}(i)^T\ \underline{b}(i+1)^T]^T$ ($3K$-vector). We

can then write $\underline{y}(i)$ in (2.23) in a matrix form as

$$\underline{y}(i) = \boldsymbol{H}(i)\boldsymbol{A}\boldsymbol{b}(i) + \sigma\underline{v}(i), \tag{2.25}$$

where $\underline{v}(i) \sim \mathcal{N}_c\Big(\underline{0}, \underline{H}^{[0]}(i)\Big)$. Based on (2.25), both the SIC-MMSE and the SIC-MF SISO multiuser detectors can be similarly applied as in the synchronous and AWGN case. Specifically, the extrinsic information $L^q_{m\to L}[b_k(i)]$ is given by

$$L^q_{m\to L}[b_k(i)] = \frac{4\Re\Big(\mu_k(i)z_k(i)\Big)}{\nu_k(i)^2}, \tag{2.26}$$

where as before, $z_k(i)$, $\mu_k(i)$ and $\nu_k(i)$ are respectively the output, mean, and variance of the MMSE or matched filter (after soft interference cancellation).

D. Distribution of Multiuser Extrinsic Messages

In this section, we describe how to compute the pdf of the extrinsic LLRs at the output of the SISO multiuser detector, as a function of the pdf of the input *a priori* LLRs.

1. AWGN Channels

SIC-MMSE SISO multiuser detector: We first consider the SIC-MMSE SISO detector in a synchronous CDMA system. The extrinsic message in this case is given by (2.13). As discussed in [14], the output $z_k(i)$ of the instantaneous linear MMSE filter is well approximated by a Gaussian distribution. Hence $L^q_{m\to L}[b_k(i)]$ has a Gaussian distribution with mean and variance given respectively by

$$E\{L^q_{m\to L}[b_k(i)]\} = \left(\frac{2}{1-\mu_k(i)}\right) E\{z_k(i)\} = \frac{2\mu_k(i)b_k(i)}{1-\mu_k(i)}, \tag{2.27}$$

$$\mathrm{Var}\{L^q_{m\to L}[b_k(i)]\} = \left(\frac{2}{1-\mu_k(i)}\right)^2 \mathrm{Var}\{z_k(i)\} = \frac{4\mu_k(i)}{1-\mu_k(i)}. \tag{2.28}$$

Thus the extrinsic message has a Gaussian distribution of the form $L^q_{m\to L}[b_k(i)] \sim \mathcal{N}(m_k(i)b_k(i), 2m_k(i))$, with $m_k(i) \triangleq \frac{2\mu_k(i)}{1-\mu_k(i)}$. Given $\underline{R}(i)$, $\underline{A}$ and σ^2, and the *a priori* code bit LLR distribution $f^{q-1}_{m\leftarrow L}$. we can compute $\{m_k(i), k = 1, \cdots, K\}$ as follows:
For $j = 1, 2, \ldots, N$ (number of samples) and for $k = 1, 2, \ldots, K$

- Draw i.i.d. $\Omega^{(j)}_k \sim f^{q-1}_{m\leftarrow L}$. Let $\underline{V}^{(j)}_k \triangleq \text{diag}\Big\{1 - \tanh\left(\Omega^{(j)}_1/2\right)^2, \ldots, 1 - \tanh\left(\Omega^{(j)}_{k-1}/2\right)^2, 1, 1 - \tanh\left(\Omega^{(j)}_{k+1}/2\right)^2, \ldots, 1 - \tanh\left(\Omega^{(j)}_K/2\right)^2\Big\}$;
- Compute $\mu^{(j)}_k \triangleq A^2\underline{e}^T_k\left[\underline{V}^{(j)}_k + \sigma^2\underline{R}^{-1}\right]^{-1}\underline{e}_k$, and $m^{(j)}_k \triangleq \frac{2\mu^{(j)}_k}{1-\mu^{(j)}_k}$.

Finally $m_k(i)$ is calculated as $m_k(i) \cong \frac{1}{N}\sum_{j=1}^N m^{(j)}_k$. Note that the *a priori* code bit LLR from the LDPC decoder is typically modelled as mixture symmetric Gaussian, i.e.,

$$f^{q-1}_{m\leftarrow L} = \sum_{\ell=1}^{L} \lambda_\ell \mathcal{N}(m_\ell, 2m_\ell), \tag{2.29}$$

where m_ℓ and $2m_\ell$ are respectively the mean and the variance of the ℓth component. Here λ_ℓ is the fraction of the bit nodes of degree ℓ and we assume that the output extrinsic LLR at a node of degree ℓ is symmetric Gaussian with mean m_ℓ [8, 21].

Exact and SIC-MF SISO multiuser detector: For these two detectors, simulations show that the extrinsic messages are also well approximated by symmetric Gaussian distributions. The means can be calculated via Monte Carlo as follows:
For $j = 1, 2, \ldots, N$ (number of samples)

- For $k = 1, \cdots, K$: Draw i.i.d. $b_k(i)^{(j)} \in \{+1, -1\}$, $n_k(i)^{(j)} \sim \mathcal{N}(0, 1)$, $\Omega^{(i)}_k \sim f^{q-1}_{m\leftarrow L}$; Set $L^{q-1}_{m\leftarrow L}[b_k(i)] = \Omega^{(i)}_k b_k(i)$; Compute $y_k(i)^{(j)}$ according to (2.9).
- For $k = 1, \cdots, K$: Compute the extrinsic information $L^q_{m\to L}[b_k(i)]^{(j)}$ according to (2.10) for the exact SISO detector, or according to (2.14) for the SIC-MF SISO detector. Set $m^{(j)}_k = L^q_{m\to L}[b_k(i)]^{(j)}b_k(i)^{(j)}$.

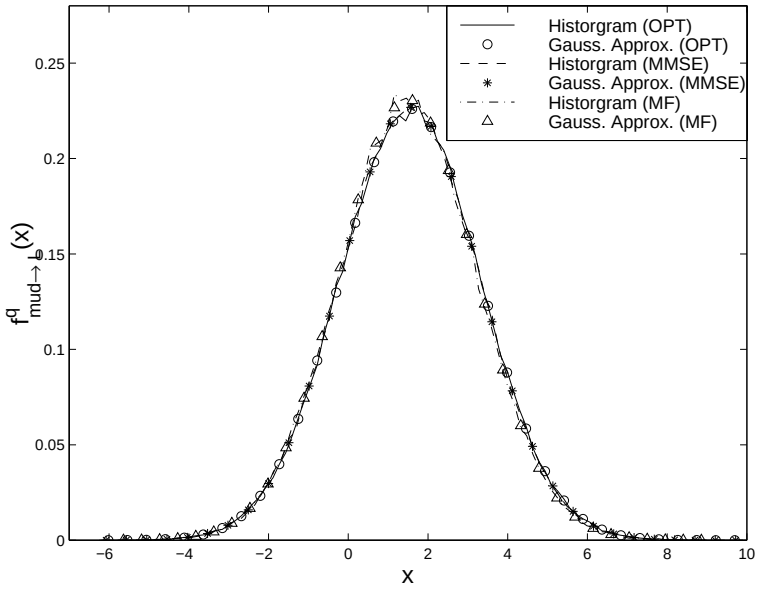

Fig. 2. The histograms for the multiuser detectors extrinsic information in a 2-user synchronous CDMA system, and the symmetric Gaussian approximations by Monte Carlo simulation.

We now demonstrate the validity of Gaussian assumption through following example. Consider estimating the pdf of extrinsic information at the output of the multiuser detector for a two-user synchronous system with ρ_{jk} fixed at 0.5 for $j \neq k$ when $E_s/N_o = -1$ dB. The pdf of the input *a priori* information to the multiuser detector is $f^{q-1}_{m\leftarrow L} = 0.05\mathcal{N}(0.1, 0.2) + 0.25\mathcal{N}(1.0, 2.0) + 0.7\mathcal{N}(5.0, 10.0)$. Fig. 2 shows the histograms of the extrinsic information at the optimal, SIC-MMSE, MF multiuser detectors by simulating the channel and the detector. The symmetric Gaussian pdf's with same means are also shown in the same figure. It can be seen that the match is quite close for each detector, indicating that the underlying pdf is well approximated by the symmetric Gaussian.

2. Fading Channels

Consider the SIC-MMSE detector in a synchronous CDMA system with fading channels. Conditioned on the channels $\boldsymbol{\alpha}(i) = [\alpha_1(i), \cdots, \alpha_K(i)]$, the extrinsic message from the multiuser detector has a Gaussian distribution, i.e., $f^q_{m\to L}(\boldsymbol{\alpha}(i)) \sim \mathcal{N}(m(\boldsymbol{\alpha}(i)), 2m(\boldsymbol{\alpha}(i)))$, with $m(\boldsymbol{\alpha}(i)) \stackrel{\triangle}{=} \frac{4\mu_k(i)}{1-\mu_k(i)}$. Hence the pdf of the output extrinsic message is given by

$$f^q_{m\to L} \stackrel{\triangle}{=} \int f^q_{m\to L}\Big(\boldsymbol{\alpha}(i)\Big) p\Big(\boldsymbol{\alpha}(i)\Big) \mathrm{d}\boldsymbol{\alpha}(i). \tag{2.30}$$

In general, the pdf in (2.30) can not be well approximated as Gaussian. However, we can approximate $f^q_{m\to L}$ as a mixture of symmetric Gaussian pdf's, i.e., $f^q_{m\to L} \cong \sum_{j=1}^{J} \pi_j \, \mathcal{N}(m_j, 2m_j)$. Note that in the limit as $J \to \infty$, this can approximate (2.30) arbitrarily closely. For fixed number of mixtures J, based on the observations $\boldsymbol{\Xi} \stackrel{\triangle}{=} \{\xi_t, t = 1, \ldots, N\}$, the parameters $\boldsymbol{\theta} \stackrel{\triangle}{=} \{\pi_j, m_j, j = 1, \cdots, J\}$, can be estimated using the expectation-maximization (EM) algorithm as follows.

Denote $\phi(x; \mu, \sigma^2)$ as the pdf of an $\mathcal{N}(\mu, \sigma^2)$ random variable. Then the maximum likelihood (ML) estimate of the parameters $\boldsymbol{\theta}$ is given by

$$\begin{aligned} \hat{\boldsymbol{\theta}} &= \arg \max_{\boldsymbol{\theta}: \sum_{j=1}^{J} \pi_j = 1} \log p_{\boldsymbol{\theta}}(\boldsymbol{\Xi}) \\ &= \arg \max_{\boldsymbol{\theta}: \sum_{j=1}^{J} \pi_j = 1} \sum_{t=1}^{N} \log \sum_{j=1}^{J} \pi_j \phi(\xi_t; m_j, 2m_j). \end{aligned} \tag{2.31}$$

Direct solution to the above maximization problem is very difficult. The expectation-maximization (EM) algorithm [22, 23] is an iterative procedure for solving this ML estimation problem. In the EM algorithm, the observation $\boldsymbol{\Xi}$ is termed as *incomplete* data. The algorithm postulates that one has access to *complete* data $\boldsymbol{X}$, which is such that $\boldsymbol{\Xi}$ can be obtained through a many-to-one mapping. Typically the complete data

is chosen such that the conditional density $p_{\boldsymbol{\theta}}(\boldsymbol{X})$ is easy to obtain and optimize. Starting from some initial estimate $\boldsymbol{\theta}^{(0)}$, the EM algorithm solves the ML estimation problem (2.31) by the following iterative procedure:

- E-step: Compute $Q\left(\boldsymbol{\theta} \mid \boldsymbol{\theta}^{(i)}\right) = E_{\boldsymbol{\theta}^{(i)}}\left\{\log p_{\boldsymbol{\theta}}(\boldsymbol{X}) \mid \boldsymbol{\Xi}\right\}$.
- M-step: Solve $\boldsymbol{\theta}^{(i+1)} = \arg\max_{\boldsymbol{\theta}} Q\left(\boldsymbol{\theta} \mid \boldsymbol{\theta}^{(i)}\right)$.

Define the following hidden data $\boldsymbol{Z} = \{\boldsymbol{z}_t, t = 1, \ldots, N\}$, where $\boldsymbol{z}_t$ is a J-dimensional indicator vector such that $z_{t,j} = 1, \text{if } \xi_t \sim \mathcal{N}(m_j, 2m_j)$, and $z_{t,j} = 0, \text{otherwise}$. The complete data is then $\boldsymbol{X} \stackrel{\triangle}{=} (\boldsymbol{\Xi}, \boldsymbol{Z})$. We have

$$p_{\boldsymbol{\theta}}(\boldsymbol{\Xi}, \boldsymbol{Z}) = \prod_{t=1}^{N}\prod_{j=1}^{J}\left[\pi_j\, \phi(\xi_t; m_j, 2m_j)\right]^{z_{t,j}},$$

where $\phi(x; \mu, \sigma^2) = \frac{1}{\sqrt{2\pi\sigma^2}} e^{-\frac{(x-\mu)^2}{2\sigma^2}}$, hence

$$\log p_{\boldsymbol{\theta}}(\boldsymbol{\Xi}, \boldsymbol{Z}) = \sum_{t=1}^{N}\sum_{j=1}^{J} z_{t,j} \log \pi_j + \sum_{t=1}^{N}\sum_{j=1}^{J} z_{t,j}\left[-\frac{1}{2}\log 2m_j - \frac{(\xi_t - m_j)^2}{4m_j}\right] + C, \tag{2.32}$$

where C is some constant. The E-step can then be calculated as follows:

$$\begin{aligned} Q(\boldsymbol{\theta}, \boldsymbol{\theta}') &\stackrel{\triangle}{=} E_{\boldsymbol{\theta}'}\left\{\log p_{\boldsymbol{\theta}}(\boldsymbol{\Xi}, \boldsymbol{Z}) \mid \boldsymbol{\Xi}\right\} \\ &= \sum_{t=1}^{N}\sum_{j=1}^{J} \hat{z}_{t,j}\left[\log \pi_j - \frac{1}{2}\log 2m_j - \frac{(\xi_t - m_j)^2}{4m_j}\right] + C, \qquad (2.33) \\ &\quad \text{where} \quad \hat{z}_{t,j} \stackrel{\triangle}{=} E_{\boldsymbol{\theta}'}\left\{z_{t,j} \mid \boldsymbol{\Xi}, \boldsymbol{\theta}'\right\} = \frac{\phi(\xi_t; m'_j, 2m'_j)\,\pi'_j}{\sum_{l=1}^{J}\phi(\xi_t; m'_l, 2m'_l)\,\pi'_l}. \qquad (2.34) \end{aligned}$$

And the M-step is calculated as follows.

$$\frac{\partial Q(\boldsymbol{\theta}, \boldsymbol{\theta}')}{\partial \pi_j} = 0 \quad \Rightarrow \quad \pi_j = \frac{1}{N}\sum_{t=1}^{N} \hat{z}_{t,j}, \quad j = 1, \cdots, J. \tag{2.35}$$

$$\frac{\partial Q(\boldsymbol{\theta}, \boldsymbol{\theta}')}{\partial m_j} = 0 \quad \Rightarrow \quad m_j = -1 + \sqrt{1 + \frac{\sum_{t=1}^{N}\hat{z}_{t,j}\xi_t^2}{\sum_{t=1}^{N}\hat{z}_{t,j}}}, \quad j = 1, \cdots, J. \tag{2.36}$$

Finally the EM algorithm for calculating the Gaussian mixture parameters for the extrinsic messages in fading channels is summarized as follows: Given the detector extrinsic messages $\{\xi_t\}$, the number of mixture components J, the total number of EM iterations I, starting from the initial parameters $\boldsymbol{\theta}^{(0)}$, for $i = 1, \ldots, I$:

- Let $\boldsymbol{\theta}' = \boldsymbol{\theta}^{(i-1)}$ and calculate $\{\hat{z}_{t,j}, t = 1, \ldots, N; j = 1, \ldots, J\}$ according to (2.34).
- Calculate $\{\pi_j, j = 1, \cdots, J\}$ according to (2.35); and calculate $\{m_j, j = 1, \cdots, J\}$ according to (2.36). Set $\boldsymbol{\theta}^{(i)} = \boldsymbol{\theta}$.

The algorithm can be applied to the SISO multiuser detector in fading channels by letting $\xi_k(i) \triangleq b_k(i) L^q_{m \to L}[b_k(i)]$, where $L^q_{m \to L}[b_k(i)]$ is given by (2.26).

In the above EM algorithm the number of mixture components J is fixed. Note that when J increases, $\log p_{\boldsymbol{\theta}}(\boldsymbol{\Xi})$ increases, or $-\log p_{\boldsymbol{\theta}}(\boldsymbol{\Xi})$ decreases. The minimum description length (MDL) principle can be used to select the optimal number of the components in a Gaussian mixture [24, 25]. In the MDL criterion, a penalty term $\frac{J}{2} \log N$ is introduced. And the optimal number of components is given by

$$\hat{J}_{\text{MDL}} = \arg\min_{J} \left\{ -\log p_{\boldsymbol{\theta},J}(\boldsymbol{\Xi}) + \frac{J}{2} \log N \right\}. \tag{2.37}$$

Hence we can first set an upper bound of the number of mixture components, $J_{\max}$. And for each $J \leq J_{\max}$, we run the above EM algorithm and calculate the corresponding MDL value. Finally, we choose the optimal J with the minimum MDL.

We now demonstrate the efficiency of the mixture Gaussian modeling of the multiuser detector extrinsic information developed in this section through the following example. Consider a five-user asynchronous CDMA system in independently Rayleigh fading channel and an $E_s/N_o = 0$ dB employing MMSE multiuser detector when the input LLR distribution is $f^{q-1}_{m \leftarrow L} = 0.05\mathcal{N}(0.1, 0.2) + 0.25\mathcal{N}(1.0, 2.0) + 0.7\mathcal{N}(5.0, 10.0)$.

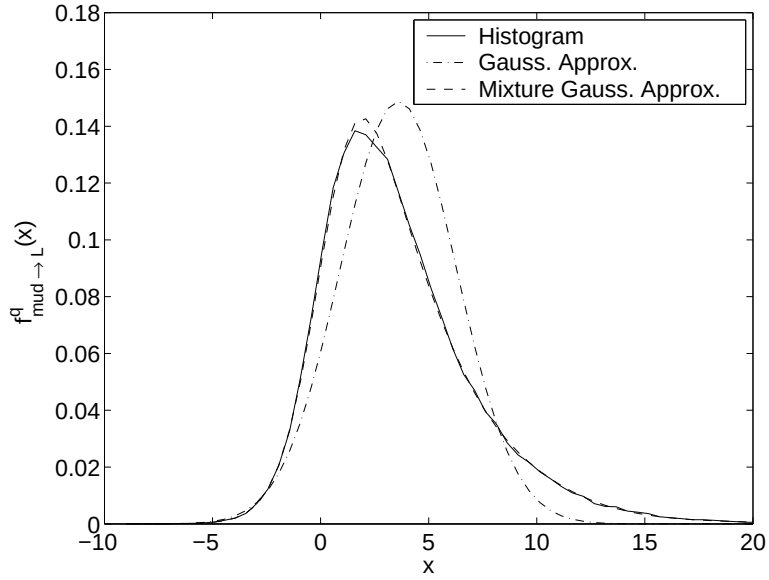

Fig. 3. The histogram for the SIC-MMSE multiuser detector extrinsic information in a 5-user asynchronous CDMA system with fading, and the approximations by a single symmetric Gaussian pdf, and by a mixture of symmetric Gaussian pdf's obtained using the EM algorithm.

The histogram of the multiuser detector output extrinsic information obtained using Monte Carlo simulations is plotted in Fig. 3. The approximation of the pdf using a mixture of symmetric Gaussian distributions computed via the EM algorithm is also shown in the figure. Note that the two curves are almost indistinguishable indicating that the approximation is very accurate. On the other hand, a symmetric Gaussian pdf which has the same mean as that of the histogram is also shown. It is seen that such a single symmetric Gaussian approximation of the extrinsic information distribution is quite inaccurate. This confirms that the extrinsic information delivered by the SIC-MMSE multiuser detector in fading channels cannot be assumed to be Gaussian, whereas a mixture of symmetric Gaussian pdf offers a good approximation. In this example, the codeword length is $N = 20000$ for each user. The average number of mixture components given by the MDL criterion is $\hat{J}_{\mathrm{MDL}} = 12$.

E. Design of LDPC Codes

1. Computing Threshold

In this section, we first describe how to compute the thresholds for LDPC codes with the afore-mentioned receiver employing turbo multiuser detection. The main idea is to treat the extrinsic LLRs as i.i.d random variables and to compute their pdf at each iteration [8, 7, 10]. In [8], the pdf of the extrinsic LLRs at each bit or check node was assumed to be Gaussian and symmetric (variance is twice the mean) and, hence, it is sufficient to track the mean of the extrinsic LLRs. While this is a good approximation for the single user AWGN channel, this is not a good approximation for fading channels. Therefore, we will assume that the output of the multiuser detector and, hence, the input at every bit node is a mixture of symmetric Gaussian densities. We will show that this assumption allows us to track the pdf's of the extrinsic LLRs accurately without having to numerically convolve or evaluate pdf's. In computing the pdf's of the extrinsic LLRs, we will assume that the all-zeros codeword is transmitted but the coded bits are modulated into ± 1 in a random order which is known to the receiver. Therefore, density evolution can still be performed assuming the all-zeros codeword as reference even though the overall system is not geometrically uniform. We next specify the procedure for computing the pdf's of the extrinsic messages passed around in the turbo multiuser detection algorithm described in Section B. Denote $\psi(x) \stackrel{\triangle}{=} E\left\{\tanh\left[\frac{1}{2}\mathcal{N}(x, 2x)\right]\right\}$.

[0:] *Initialization:* Set $f_{b\leftarrow c}^{0,0}(x) = \delta(x)$, and $f_{m\leftarrow L}^{0}(x) = \delta(x)$.

[1:] *Turbo multiuser detection iterations:* For $q = 1, 2, \ldots, Q$

[1-a:] *Compute the pdf of the multiuser detector extrinsic messages:* $f_{m\rightarrow L}^{q}$ is computed as a function of E_b/N_o and $f_{m\leftarrow L}^{q-1}$ using the appropriate procedure from

Section D, to obtain

$$f^q_{m\to L} = \sum_{j=1}^{J} \pi_j \, \mathcal{N}(\mu_j, 2\mu_j). \tag{2.38}$$

[1-b:] *Compute the pdf of the LDPC extrinsic messages:*

[1-b-i:] *Iterate between bit node update and check node update:* For $p = 1, 2, \ldots, P$

◇ *At a bit node of degree i:* The pdf of the extrinsic LLR passed along an edge connected to a bit node of degree i is denoted by $f^{p,q}_{b\to c,i}$. From (2.2), we can see that $f^{p,q}_{b\to c,i}$ is given by

$$f^{p,q}_{b\to c,i} \;=\; f^q_{m\to L} \otimes f^{p-1,q\otimes(i-1)}_{b\leftarrow c}, \tag{2.39}$$

where $\otimes$ denotes convolution, $(\cdot)^{\otimes i}$ denotes i-fold convolution. We can simplify this by making the assumption that the output extrinsic from the bit node of degree i excluding the contribution from the channel is Gaussian. The same assumption has been made in [8]. That is,

$$\begin{aligned} f^{p,q}_{b\to c,i} &= f^q_{m\to L} \otimes \mathcal{N}\Big((i-1)m^{p-1,q}_{b\leftarrow c},\; 2(i-1)m^{p-1,q}_{b\leftarrow c}\Big) \\ &= \sum_{j=1}^{J} \pi_j \mathcal{N}\Big(\mu_j + (i-1)m^{p-1,q}_{b\leftarrow c},\; 2[\mu_j + (i-1)m^{p-1,q}_{b\leftarrow c}]\Big). \end{aligned} \tag{2.40}$$

The pdf of the extrinsic message passed from the bit to check nodes along an edge is then

$$\begin{aligned} f^{p,q}_{b\to c} &= \sum_{j=2}^{d_{l,max}} \lambda_i \; f^{p,q}_{b\to c,i} \\ &= \sum_{j=1}^{J} \sum_{i=2}^{d_{l,max}} \pi_j \lambda_i \mathcal{N}\Big(\mu_j + (i-1)m^{p-1,q}_{b\leftarrow c},\; 2[\mu_j + (i-1)m^{p-1,q}_{b\leftarrow c}]\Big) \end{aligned} \tag{2.41}$$

◇ *At check node of degree j:* Assume that the ith check node is of degree j and that the extrinsic LLR at the output of this check node is Gaussian with mean

$m^{p,q}_{b\leftarrow c,j}$. To compute $m^{p,q}_{b\leftarrow c,j}$, we take the expectation on both sides of (2.3) and get

$$\begin{aligned} E\left\{\tanh\left(L^{p,q}_{b\leftarrow c}(e^c_{i,r})/2\right)\right\} &= E\Big\{\Big[\prod_{k=1,k\neq r}^{j}\tanh\left(L^{p,q}_{b\to c}(e^c_{i,k})/2\right)\Big]\Big\} \\ &= \left[E\left\{\tanh\left(L^{p,q}_{b\to c}(e^c_{i,k})/2\right)\right\}\right]^{j-1}, \end{aligned} \tag{2.42}$$

where (2.42) follows from the fact that $L^{p,q}_{b\to c}(e^c_{i,k})$ and $L^{p,q}_{b\to c}(e^c_{i,s})$ are identically distributed and are independent for $k \neq s$. Since the distribution of $L^{p,q}_{b\leftarrow c}(e^c_{i,r})$ will be same for all r, we can drop r. Therefore,

$$m^{p,q}_{b\leftarrow c,j} = \sum_j \rho_j \ \psi^{-1}\Big[\Big(\sum_{l=1}^{J}\sum_{i=2}^{d_{l,max}} \pi_l\,\lambda_i\ \psi(m^{p,q}_{b\to c,i})\Big)^{j-1}\Big]. \tag{2.43}$$

[1-b-ii:] *Message passed back to the multiuser detector:* At bit node of degree i, by taking expectation on both sides of (2.4), we get $m^q_{m\leftarrow L}(i) = i m^{p-1,q}_{b\leftarrow c}$. Since $\tilde{\lambda}_i$ of the *nodes* have degree i,

$$f^q_{m\leftarrow L} = \sum_{i=2}^{d_{l,max}} \tilde{\lambda}_i \mathcal{N}\left(m^q_{m\leftarrow L}(i),\ 2m^q_{m\leftarrow L}(i)\right). \tag{2.44}$$

The threshold is defined as the minimum E_b/N_o for which the mean $m^Q_{m\leftarrow L}$ or $m^{P,Q}_{b\leftarrow c}$ tends to ∞. That is,

$$(E_b/N_o)_{\text{th}} = \min\ E_b/N_o : \lim_{N\to\infty}\lim_{Q\to\infty} m^{P,Q}_{b\leftarrow c} \to \infty. \tag{2.45}$$

2. Design of LDPC Codes

The procedure for computing the threshold for a given degree profile $(\lambda(x), \rho(x))$ can be used in conjunction with an optimization procedure to design optimal LDPC codes for the multiuser detection. The idea is to find optimal $\lambda(x)$ and $\rho(x)$ such that the threshold is minimized. Note that the rate of the LDPC code is $R = 1 - \frac{\int_0^1 \rho(x)\ dx}{\int_0^1 \lambda(x)\ dx}$.

If a rate of R_o is required, the optimization problem can be stated as follows: Find $\lambda(x)$ and $\rho(x)$ such that we minimize E_b/N_o subject to the following constraints (1) $1 - \frac{\int_0^1 \rho(x)\ dx}{\int_0^1 \lambda(x)\ dx} = R_o$; and (2) $m_{b\leftarrow c}^{P,Q} \to \infty$ (computed using (2.38) - (2.44)).

A non-linear optimization procedure called differential evolution [9, 26] has been used to perform this optimization. This technique involves choosing several candidates for $\lambda(x)$ and $\rho(x)$ and computing thresholds for each pair during the optimization. Without the Gaussian mixture assumption for the extrinsic LLR pdf's, the pdf's have to be evaluated numerically within the LDPC decoder and by using Monte Carlo in the multiuser detector. However, with this assumption only the means of the components in the mixture need to be evaluated which is a very significant reduction in complexity. This is a key advantage of the SIC-MMSE multiuser detection since the output pdf from the multiuser detector can be computed relatively easily.

F. Results

1. Two-user Synchronous CDMA System with Periodic Spreading Sequences

We first present results for a two-user synchronous CDMA system in AWGN channel. With periodic spreading sequences, the cross correlation matrix is fixed. Set $\rho_{jk} = 0.5$ for $j \neq k$. Three different receivers were simulated (i.e., optimal, SIC-MMSE and matched filter). The theoretical thresholds for a $(3, 6)$ rate $\frac{1}{2}$ regular LDPC code, and the simulation results for a $(3, 6)$ rate $\frac{1}{2}$ regular LDPC code of length $N = 100,000$ bits are shown in Fig. 4, Fig. 5 and Fig. 6. It is seen that the actual simulation results are within 0.2dB of the theoretical thresholds for three different detectors, indicating that the Gaussian assumption and the characterization of the input-output pdf of the multiuser detector extrinsic information is quite accurate. Optimum degree profiles were computed for the same channel using algorithms and the technique

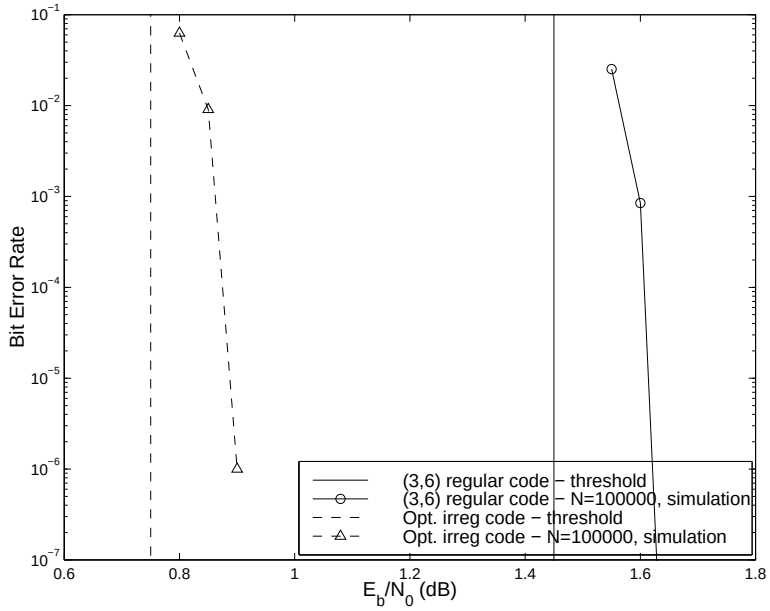

Fig. 4. Thresholds and simulation results for the $(3, 6)$ regular LDPC codes and for the optimum irregular LDPC codes in a 2-user synchronous system with optimal receiver.

discussed in Section E. The optimum degree profile for optimal multiuser detector was $\lambda(x) = 0.255869x + 0.144624x^2 + 0.069450x^3 + 0.076102x^4 + 0.028071x^5 + 0.048760x^6 + 0.013873x^8 + 0.021780x^9 + 0.026336x^{12} + 0.015840x^{13} + 0.011756x^{17} + 0.287539x^{19}$ and $\rho(x) = 0.721952x^7 + 0.278048x^8$. The resulting threshold is shown in Fig. 4. The performance of a randomly constructed LDPC code with the afore-mentioned degree profile of length $N = 100000$ is also shown in Fig. 4. It is seen that the performance is about 0.15 dB from the threshold at BER of 10^{-6}.

The optimum degree profile for MMSE multiuser detector was $\lambda(x) = 0.244164x^1 + 0.168476x^2 + 0.093799x^3 + 0.047910x^4 + 0.022387x^5 + 0.025506x^6 + 0.015051x^8 + 0.038143x^9 + 0.035043x^{10} + 0.014559x^{11} + 0.024455x^{14} + 0.011258x^{17} + 0.259249x^{19}$ and $\rho(x) = 0.775041x^7 + 0.224959x^8$. The performance of the constructed irregular LDPC code, shown in Fig. 5, is around 0.15 dB from the threshold. The perfor-

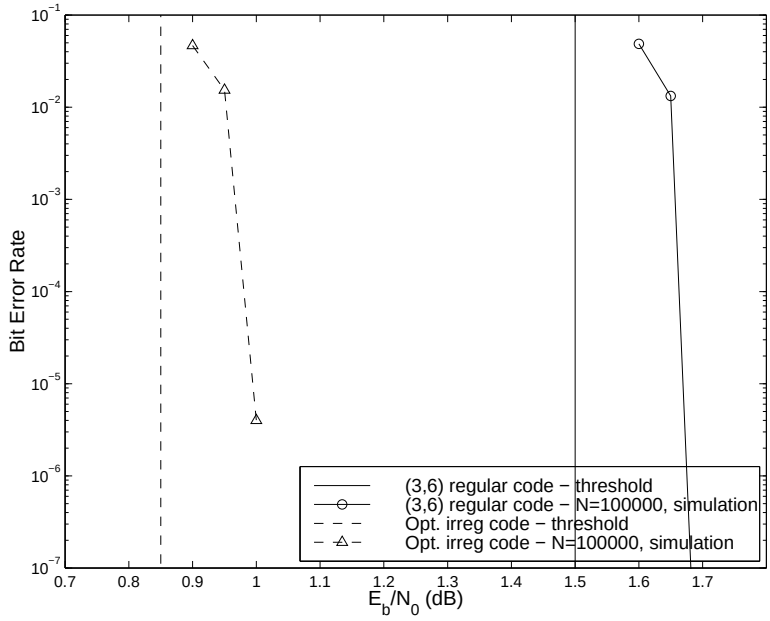

Fig. 5. Thresholds and simulation results for the $(3, 6)$ regular LDPC codes and for the optimum irregular LDPC codes in a 2-user synchronous system with MMSE receiver.

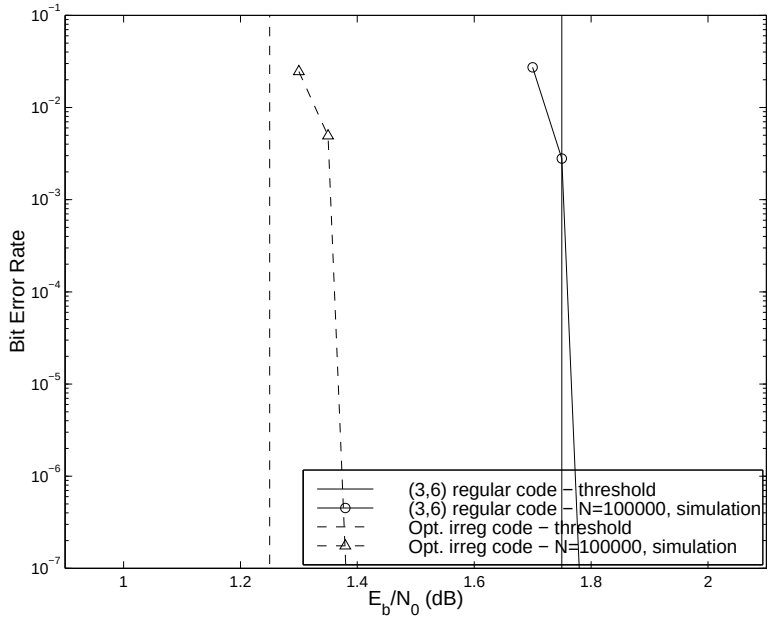

Fig. 6. Thresholds and simulation results for the $(3, 6)$ regular LDPC codes and for the optimum irregular LDPC codes in a 2-user synchronous system with MF receiver.

mance fo MMSE receiver is only 0.1dB worse than optimal receiver. The optimum degree profile for MF detector was $\lambda(x) = 0.259484x + 0.146658x^2 + 0.114980x^3 + 0.056695x^4 + 0.023731x^5 + 0.019086x^6 + 0.015051x^8 + 0.042996x^9 + 0.034469x^{10} + 0.016299x^{11} + 0.033337x^{14} + 0.010720x^{17} + 0.226495x^{19}$ and $\rho(x) = x^7$. Shown in Fig. 6, the simulation result of the randomly constructed LDPC code is about 0.15dB from the threshold 1.25dB. The results presented here show that the irregular codes provide about 0.5dB better performance than the regular codes.

a. Achievable Information Rate

The achievable information rate for a two-user synchronous CDMA system with binary modulation can be computed for a given E_s/N_0 and $\rho_{12} = \rho$ as follows. The equivalent signal space diagram for the two-user system can be obtained by projecting the received signal on to two basis functions $\phi_1(t) = -\frac{\rho}{\sqrt{1-\rho^2}}s_1(t) + \frac{1}{\sqrt{1-\rho^2}}s_2(t)$ and $\phi_2(t) = s_1(t)$ [27]. The four points in the two-dimensional signal space corresponding to the transmitted bits $(-1,-1), (-1,1), (1,-1)$ and $(1,1)$ can then be shown to be $\boldsymbol{x}_0 = [-\sqrt{1-\rho^2},\ -1-\rho]$, $\boldsymbol{x}_1 = [\sqrt{1-\rho^2},\ -1+\rho]$, $\boldsymbol{x}_2 = [-\sqrt{1-\rho^2},\ 1-\rho]$, $\boldsymbol{x}_3 = [\sqrt{1-\rho^2},\ 1+\rho]$. The sufficient statistic $\underline{y}$ can be expressed as

$$\underline{y} = \underline{x} + \underline{n}, \quad \underline{x} \in \{\boldsymbol{x}_0, \boldsymbol{x}_1, \boldsymbol{x}_2, \boldsymbol{x}_3\} \tag{2.46}$$

with the choice of basis functions given above, $\underline{n} \sim \mathcal{N}(\underline{0}, \sigma^2 \boldsymbol{I}_2)$, where $\sigma^2 = N_0/(2E_s)$ and $\boldsymbol{I}_2$ is the 2×2 identity matrix. For non-cooperative coding between the two users, the information rate is maximized by the equiprobable distribution $p(\underline{x} = \boldsymbol{x}_i) = 1/4, \forall i$. The achievable information rate can be computed using

$$\begin{aligned} I_{2-user} &= h(\underline{y}) - h(\underline{y}|\underline{x}) && (2.47) \\ &= \sum_i -\frac{1}{4}\int_{\mathcal{R}^2} p(\underline{y}|\boldsymbol{x}_i)\ \log_2(p(\underline{y}|\boldsymbol{x}_i))\ d\underline{y}\ - \log_2(2\pi e\sigma^2) && (2.48) \end{aligned}$$

The integral in (2.48) can be computed numerically after noting that $p(\underline{y}|\boldsymbol{x}_i)$ is $\mathcal{N}(\boldsymbol{x}_i, \sigma^2 \boldsymbol{I}_2)$.

For $\rho_{12} = 0.5$, the required E_b/N_0 to achieve 0.5 bits/user/channel use is 0.46 dB. The threshold for the optimized irregular LDPC code with the optimal receiver (in Fig. 4) is less than 0.3 dB away corroborating the effectiveness of the proposed design methodology.

2. Five-user Synchronous System with Aperiodic Spreading Sequence

Next, we present some simulation results for five-user synchronous system using aperiodic spreading in AWGN channel. For each user, the spreading code is random code with processing gain $N_c = 10$ which varies with symbol i. The randomly chosen spreading sequences is an accurate model when pseudo-noise sequences span many symbol periods [28]. With aperiodic random spreading, the cross correlation matrix after matched filter dynamically changes symbol by symbol. The theoretical thresholds for the $(3, 6)$ rate-$\frac{1}{2}$ regular LDPC code with maximum number of iterations between the multiuser detector and decoder, $P = 30$, is shown in Fig. 7 and Fig. 8 with MMSE and MF receiver, respectively. Both receivers have the performance for the regular LDPC code within 0.05 dB from the thresholds. The irregular LDPC code was designed and the resulting optimum degree profiles of MMSE receiver with $d_{l_{max}} = 20$ was $\lambda(x) = 0.257632x^1 + 0.154468x^2 + 0.070704x^3 + 0.076268x^4 + 0.028071x^5 + 0.048760x^6 + 0.015496x^8 + 0.021936x^9 + 0.028388x^{12} + 0.015840x^{13} + 0.016623x^{17} + 0.265814x^{19}$ and $\rho(x) = 0.867663x^7 + 0.132337x^8$. The threshold for the above degree profile and simulation results for a randomly constructed LDPC code of length $N = 100000$ are shown in Fig. 7. It is seen that the simulation results agree well with the theoretical thresholds, and that the irregular LDPC code is about 0.65 dB better than the $(3, 6)$ regular LDPC code, indicating the usefulness of the

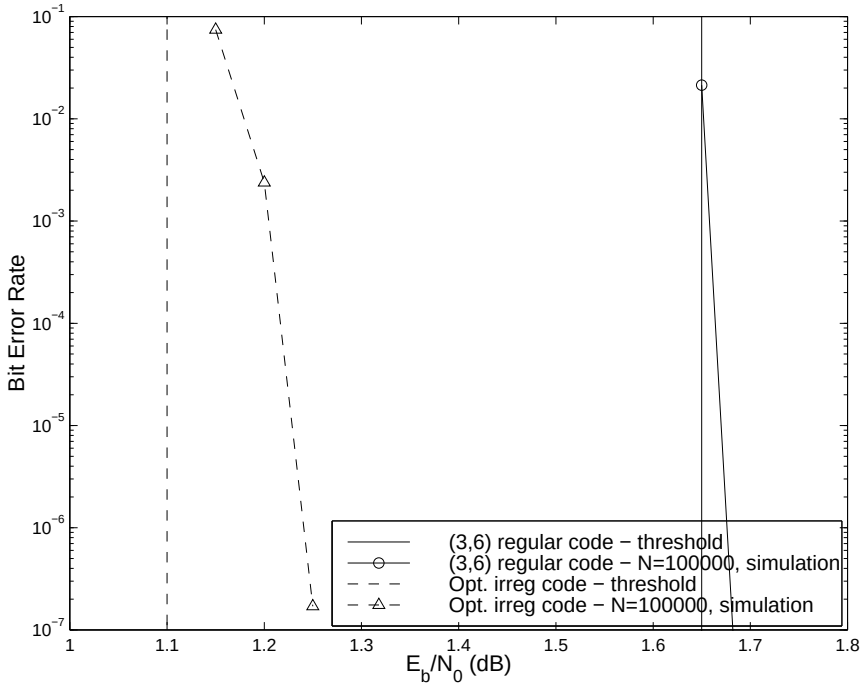

Fig. 7. Thresholds and simulation results for the $(3, 6)$ regular LDPC codes and for the optimum irregular LDPC codes in a 5-user synchronous system with MMSE receiver.

proposed techniques for designing good LDPC codes. The optimum degree profile for MF detector was $\lambda(x) = 0.291442x^1 + 0.146740x^2 + 0.017766x^3 + 0.050683x^4 + 0.066068x^5 + 0.044891x^7 + 0.015843x^8 + 0.052557x^9 + 0.019073x^{11} + 0.022182x^{12} + 0.016018x^{16} + 0.013343x^{17} + 0.243395x^{19}$ and $\rho(x) = x^7$. Shown in Fig. 8, the performance is only 0.1 dB from the threshold, and the irregular LDPC codes is 0.5 dB better than the $(3, 6)$ regular LDPC code.

3. Five-user Asynchronous System in Fading

Finally, we consider a 5-user asynchronous CDMA system in random fading channel with aperiodic random spreading. Each user's channel contains four paths, i.e., $\ell_P = 4$. The relative path power gains are $0, -3, -6$ and -9 dB and the relative delay

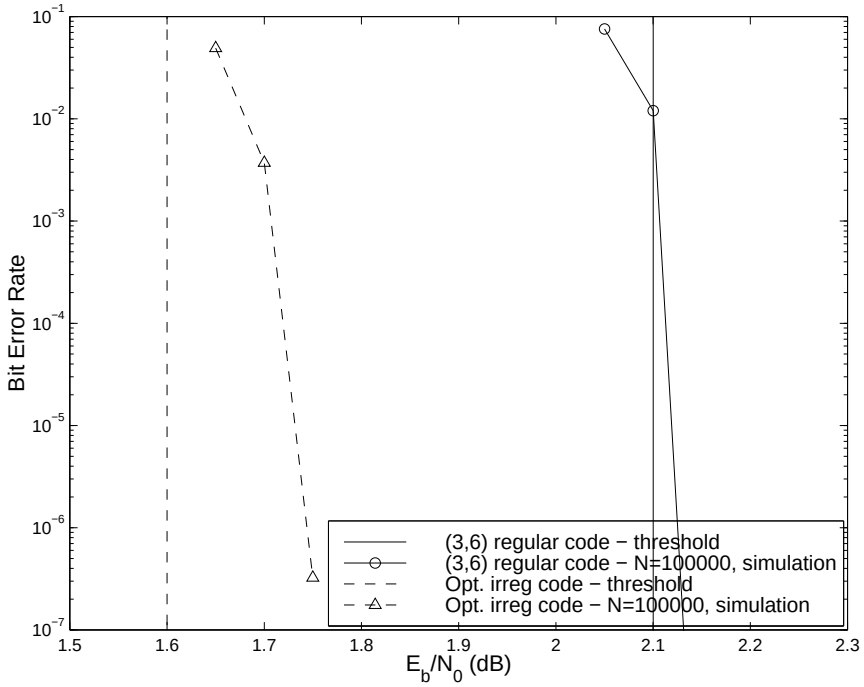

Fig. 8. Thresholds and simulation results for the $(3, 6)$ regular LDPC codes and for the optimum irregular LDPC codes in a 5-user synchronous system with MF receiver.

is $0, T_c, 2T_c, 3T_c$. The theoretical thresholds for a $(3, 6)$ rate-$\frac{1}{2}$ regular LDPC code and simulation results for a randomly constructed regular LDPC code of length $N = 100,000$ are shown in Fig. 9 for MMSE receiver and in Fig. 10 for MF receiver. It is seen that the simulated BER performance matched quite well with the thresholds, indicating that the threshold computation is fairly accurate. Then, we designed optimal degree profiles with $d_{l_{max}} = 20$, and rate-$\frac{1}{2}$ for both receivers. The resulting optimal degree profiles for the MMSE receiver were $\lambda(x) = 0.246553x^1 + 0.146658x^2 + 0.093799x^3 + 0.022387x^5 + 0.019086x^6 + 0.015051x^8 + 0.038143x^9 + 0.032978x^{10} + 0.014559x^{11} + 0.017916x^{14} + 0.010720x^{17} + 0.294241x^{19}$ and $\rho(x) = 0.562658x^7 + 0.437342x^8$. The resulting optimal degree profiles for the MF receiver were $\lambda(x) = 0.281703x^1 + 0.146740x^2 + 0.041345x^3 + 0.050683x^4 + 0.066068x^5 + 0.045004x^7 +$

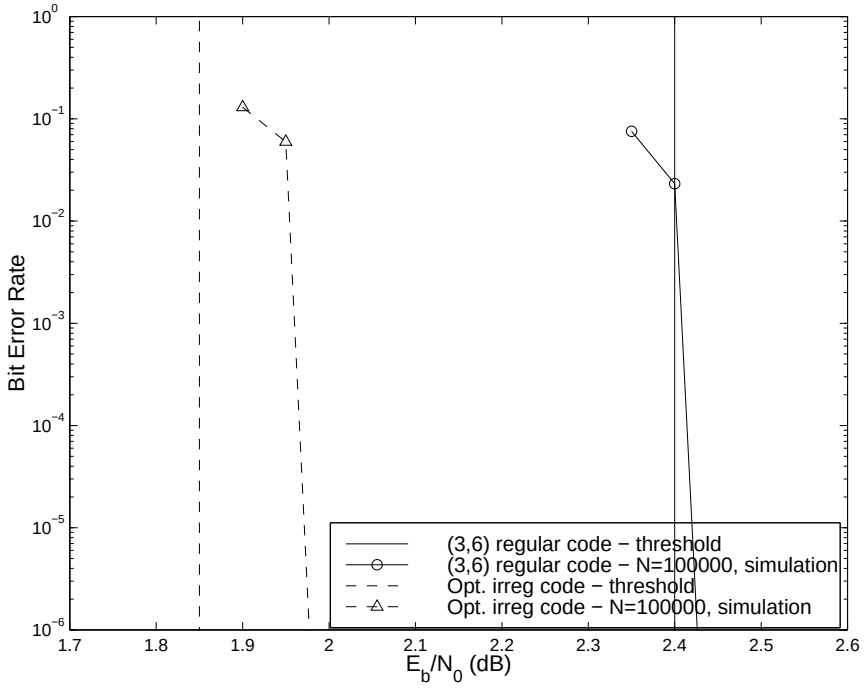

Fig. 9. Thresholds and simulation results for the $(3, 6)$ regular LDPC codes and for the optimum irregular LDPC codes in a 5-user asynchronous system with fading using MMSE receiver.

$0.020060x^8 + 0.047036x^9 + 0.014923x^{11} + 0.014942x^{12} + 0.017153x^{16} + 0.013343x^{17} + 0.241000x^{19}$ and $\rho(x) = x^7$. The simulation results for a randomly constructed LDPC code with these degree profiles for a length of $N = 100,000$ are shown in Fig. 9 and Fig. 10. At a BER of 10^{-6}, the performance is about 0.2 dB away from the thresholds. The irregular codes outperform the regular ones by about 0.6 dB for both receivers. These results show that by using the EM algorithm, we can accurately model the extrinsic information as a mixture of Gaussian densities and use this to design good irregular LDPC codes.

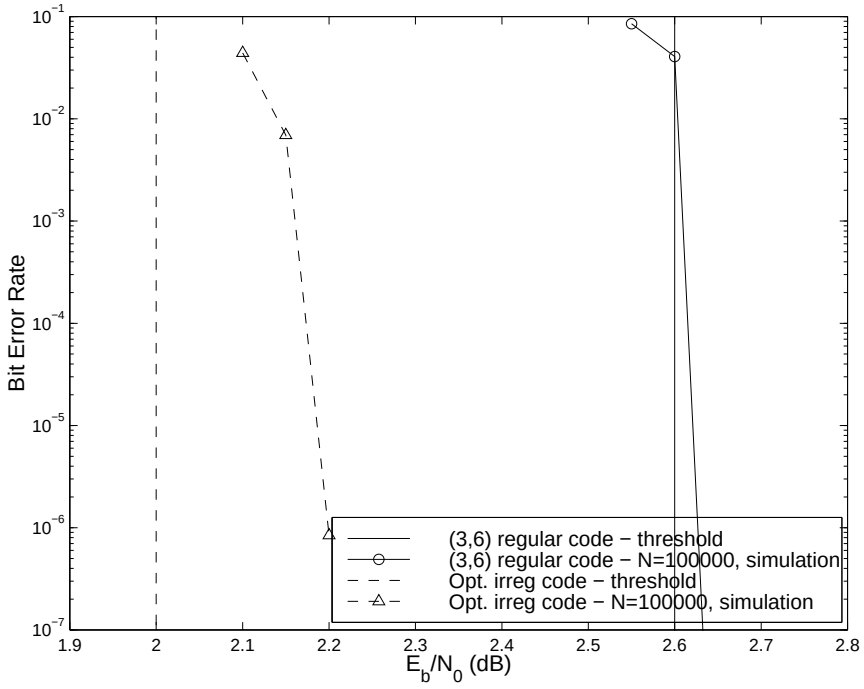

Fig. 10. Thresholds and simulation results for the $(3, 6)$ regular LDPC codes and for the optimum irregular LDPC codes in a 5-user asynchronous system with fading using MF receiver.

G. Conclusions

In this chapter, we have shown how to characterize the pdf of the extrinsic information at the output of the multiuser detector as a function of the pdf of the input extrinsic information, the E_b/N_o and cross correlation matrix of spreading codes for CDMA systems through AWGN channels or multipath fading channels. For synchronous system in AWGN, we have shown that the pdf can be assumed to be symmetric Gaussian, whereas for asynchronous system with multipath fading the pdf can be approximated as a mixture of symmetric Gaussian densities. Then, we have shown how to compute the thresholds for a given irregular LDPC code degree profile and to design good irregular LDPC codes. In all cases, the computed thresholds match very well with simulations and the designed irregular codes significantly outperform regular

LDPC codes. The differences between computed thresholds and the simulations are within 0.2dB. From the simulation, the performance of the designed irregular codes are about 0.6dB closer to the capacity than regular LDPC codes for synchronous system through AWGN, and 0.45 dB for the asynchronous CDMA system with multipath fading. Finally, we note that the proposed framework can also be applied to optimize the turbo equalization systems [29] and turbo BLAST systems [15].

CHAPTER III

PERFORMANCE ANALYSIS AND DESIGN OPTIMIZATION OF LDPC CODED MIMO OFDM SYSTEMS

A. Introduction

One of the ambitious design goals of 4G wireless cellular systems is to reliably provide very high data rate transmission: around 100 Mbps peak rate for downlink and around 30 Mbps sum rate for uplink transmission. Due to its higher rate requirement, the downlink transmission is especially considered to be a bottleneck in system design. In this chapter, we demonstrate the feasibility of *downlink transmission* in 4G wireless systems through the physical-layer (PHY) design and optimization of LDPC coded wireless multiple-input multiple-output (MIMO) orthogonal frequency-division multiplexing (OFDM) communications. In the considered systems, different users access the downlink channels in a time-division multiple accessing (TDMA) manner, most possibly with certain scheduling scheme [30]. Compared to other alternative solutions, the MIMO-OFDM-TDMA downlink transmission proposed here attempts to balance between high rate transmission and low receiver complexity of mobile devices, where the former primarily counts on the LDPC coded MIMO techniques and the latter is owing to the orthogonal structure of OFDM-TDMA.

A large number of works on the physical-layer study of MIMO techniques has been done in past decade. Various MIMO schemes could be distinguished by different design goals, for example the BLAST systems [31] aimed at the highest data-rate, or the orthogonal space-time block code (STBC) [32] aimed at the full transmit-diversity. On the other hand, these MIMO schemes could also be categorized according to the different ways of making use of channel state information (CSI), for example the

space-time codes [33] that assume no CSI at transmitter side, or the optimal eigen-beamforming schemes [34] that assume perfect CSI at transmitter. In this work, we restrict our attention to the schemes that require no CSI at transmitter and aim to achieve very high data rate. In particular, we focus on an LDPC coded MIMO OFDM scheme proposed in [35, 36].

In this chapter, for a fixed target data rate (e.g., 100 Mbps), we optimize and compare the performance of the LDPC coded MIMO OFDM systems with different configurations. For a fair comparison, we adopt the quantity $\mathrm{SNR}_{min.op}(\mathrm{dB}) - C^{-1}(R)(\mathrm{dB})$ as the performance measure, which measures how many dB's the minimum operational $\mathrm{SNR}_{min.op}$ is above the SNR required by the information theoretic channel capacity $C(\cdot)$ to support a target information rate R. We also remark that in this chapter the concept of *data rate* (in the unit of bits/sec) shall be discriminated from that of *information rate* (in the unit of bits/sec/Hz), when the bandwidth (in the unit of Hz) is not specified or fixed. Specifically, we are interested in the following problems:

- Different number of antennas: We consider MIMO system with N transmitter antennas and M receiver antennas. As a well known result from information theory[37, 34], at high SNR's a narrow-band MIMO system can support $m = \min(N, M)$ times higher information rate than that in single-antenna ($M = N = 1$) systems. One may wonder whether in wide-band transmission such a MIMO system is capable of providing the same data rate with one m-th bandwidth of that in single-antenna systems?

- Different soft-input-soft-output demodulation schemes: We consider both the optimal maximum *a posteriori* (MAP) demodulator with a complexity at $\mathcal{O}(|\Omega|^N)$, where $|\Omega|$ is the constellation size of modulator and N is the number of trans-

mitter antennas; and the suboptimal linear minimum mean-square-error based soft interference cancellation (SIC-MMSE) demodulator with a complexity at $\mathcal{O}(|\Omega|^3)$. What is the performance penalty of applying SIC-MMSE in LDPC coded MIMO OFDM?

- Different MIMO channel models: We consider both the spatially uncorrelated MIMO channel model and the spatially correlated model. As a result shown by information theory [38], the channel capacity can be substantially reduced for spatially correlated MIMO channels. What is the impact of spatial correlation on the LDPC code design and optimization?

Many previous works have addressed the different aspects of the above problems, e.g., [39, 31, 37, 40, 36]. However, only very lately, the work in [36] studied the LDPC code design in the MIMO systems under the framework of turbo iterative signal processing and decoding via the tools of EXIT charts. In this work, for each system configuration described above, we employ the techniques of density evolution with mixture Gaussian approximations [11, 7, 10, 29] to design and optimize the irregular LDPC codes, as well as to compute the $\text{SNR}_{min.op}$ for ergodic MIMO OFDM channels. Furthermore, from the LDPC profiles that are optimized for the ergodic channels, we heuristically construct small block-size irregular LDPC codes for outage MIMO OFDM channels. In the end, quantitative results from both the density evolution analysis/design and computer simulations give rise to a number of useful observations and conclusions in the design and optimization of the LDPC MIMO OFDM systems.

The chapter is organized as follows. In Section B, we describe an LDPC coded MIMO OFDM system, with brief summary of the system model and channel capacity of MIMO OFDM modulation. A turbo iterative receiver is introduced with the different demodulation schemes. In Section C, we brief the procedures of analyz-

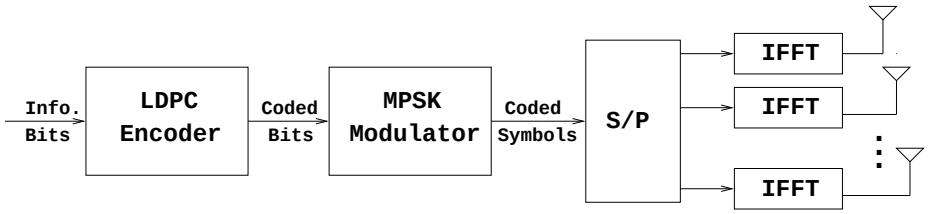

Fig. 11. Transmitter structure of an LDPC coded MIMO OFDM system.

ing and optimizing the LDPC codes for MIMO OFDM systems. In Sections D, the performance analysis and LDPC code optimization results for LDPC coded MIMO OFDM systems with different system configurations are demonstrated and discussed. Section E contains the conclusions.

B. System Description of LDPC Coded MIMO OFDM

We consider an LDPC coded MIMO OFDM system with K subcarriers, N transmitter antennas and M receiver antennas, signaling through frequency-selective fading channels. The transmitter structure is illustrated in Figure 11. A block of k bits of information data is encoded by a rate $r = k/n$ LDPC code. The output n coded bits are interleaved. The interleaved bits are modulated by QAM constellation Ω into a block of $n/\log_2|\Omega|$ QAM symbols. During each OFDM slot, NK out of the total $n/\log_2|\Omega|$ QAM symbols are transmitted from K OFDM subcarriers and N transmitter antennas simultaneously. Due to the inherent random structure of LDPC codes, the NK symbols can be mapped to K subcarriers and N transmitter antennas in any order. Without loss of generality, we assume $(n/\log_2|\Omega|)/(NK) = \tilde{n}$, i.e., the total block of QAM symbols is transmitted in $\tilde{n}$ OFDM slots.

Note that in Figure 11, LDPC could also be replaced by other error-control codes such as Turbo codes, however the relatively low and scalable decoding complexity and the freedom for code optimization make LDPC codes a more favorable candidate.

1. MIMO OFDM Modulation

Consider a quasi-static block fading model for the studied MIMO OFDM modulation, as in Figure 12. It is assumed that the fading channels remain static during each OFDM slot but vary independently from one OFDM slot to another. Furthermore, for practical MIMO OFDM systems with spatial (antenna) correlations, the frequency domain channel response matrix at the k-th ($k = 0, \ldots, K-1$) subcarrier and the p-th ($p = 0, \ldots, \tilde{n}-1$) OFDM slot is given by [41]

$$\boldsymbol{H}[p,k] \;=\; \sum_{l=0}^{L-1} \boldsymbol{R}_l^{1/2} \boldsymbol{H}_l[p] \boldsymbol{S}_l^{1/2} \exp(-j2\pi lk/K)\;, \tag{3.1}$$

where $\boldsymbol{R}_l = \boldsymbol{R}_l^{1/2}\boldsymbol{R}_l^{1/2}$ and $\boldsymbol{S}_l = \boldsymbol{S}_l^{1/2}\boldsymbol{S}_l^{1/2}$ represent the receive and transmit spatial-correlation matrices, which are determined by the spacing and the angle spread of MIMO antennas as what will be explained in Section 3; L is the number of resolvable paths of the frequency-selective fading channels; $\boldsymbol{H}_l[p]$ is the matrix with entries being independent and identically distributed (i.i.d.) circularly symmetric complex Gaussian distributed as $\sim \mathcal{N}_c(0, \beta_l^2)$, and is assumed to be independent for different l and different p; in addition, the power of $\boldsymbol{H}_l[p], \forall l$ is normalized by letting $\sum_{l=0}^{L-1} \beta_l^2 \equiv 1$.

Assume proper cyclic insertion and sampling, the MIMO OFDM system with K subcarriers decouples frequency-selective channels into K correlated flat-fading channels with the following input-output relation

$$\boldsymbol{y}[p,k] = \sqrt{\frac{\mathrm{SNR}}{N}} \boldsymbol{H}[p,k]\boldsymbol{x}[p,k] + \boldsymbol{z}[p,k]\;, \qquad k = 0, \ldots, K-1, \quad p = 0, \ldots, \tilde{n}-1, \tag{3.2}$$

where $\boldsymbol{H}[p,k] \in \mathcal{C}^{M\times N}$ is the matrix of complex channel frequency responses defined in (3.1); $\boldsymbol{x}[p,k] \in \Omega^N$ and $\boldsymbol{y}[p,k] \in \mathcal{C}^M$ are respectively the transmitted signals and the

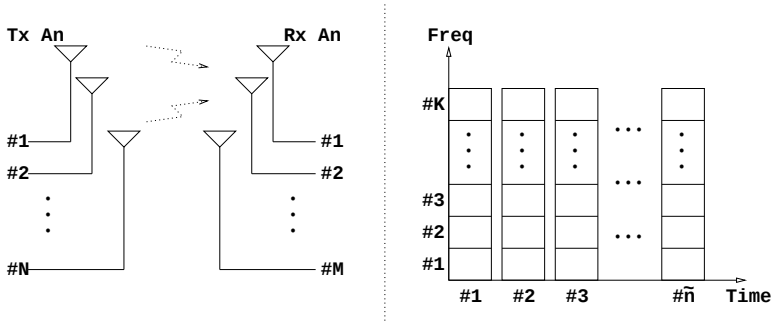

Fig. 12. A quasi-static block-fading MIMO OFDM channel model. For each OFDM slot, the fading channel responses remain static but are correlated in different OFDM subcarriers. For different OFDM slots, the fading channel responses are independent. [Note that the spatial relation of fading channels associated with different transmit-receive-antenna-pairs is defined through $\boldsymbol{R}_l$ and $\boldsymbol{S}_l$ in Eq.(3.1).]

received signals at the k-th subcarrier and the p-th slot; $\boldsymbol{z}[p,k] \in \mathcal{C}^M$ is the additive noise with i.i.d. entries $\boldsymbol{z}[p,k] \sim \mathcal{N}_c(\boldsymbol{0}, \boldsymbol{I})$; SNR denotes the average signal-to-noise ratio at each receiver antenna. Note that in this work, only the fixed/deterministic (in contrast to variable/adaptive) signal constellation Ω is considered, and its averaged power is normalized to be one.

With no channel state information (CSI) at the transmitter side, the channel capacity for the above MIMO OFDM modulation has been studied in [37, 34]. Assume Gaussian signaling (i.e., $\Omega \to \mathcal{C}$), for MIMO OFDM channels with infinite fading channel observations (i.e, $\tilde{n} \to \infty$), the *ergodic capacity* is given by

$$C_{erg}(\mathrm{SNR}) \triangleq \mathrm{E}\Bigg\{ \underbrace{\frac{1}{K\tilde{n}} \sum_{k=0}^{K-1} \sum_{p=0}^{\tilde{n}-1} \left[\log_2 \det \left(\boldsymbol{I}_M + \frac{\mathrm{SNR}}{N} \boldsymbol{H}[p,k] \boldsymbol{H}^{\mathrm{H}}[p,k] \right) \right]}_{\mathcal{I}_{|\mathcal{H}}(\mathrm{SNR})} \Bigg\} \quad (3.3)$$

where $^{\mathrm{H}}$ denotes the Hermitian transpose; the expectation is taken over random channel states $\mathcal{H}$, with $\mathcal{H} \triangleq \{\boldsymbol{H}[p,k]\}_{p,k}$; $\mathcal{I}_{|\mathcal{H}}(\mathrm{SNR})$ is the instantaneous mutual information conditioned on $\mathcal{H}$. For MIMO OFDM channels with finite fading channel

observations (i.e, $\tilde{n} \ll \infty$), the *outage capacity/probability* is a more sensible measure. For a target information rate R, the outage probability is given by

$$P_{\text{out}}(R, \text{SNR}) = P(\mathcal{I}_{|\mathcal{H}}(\text{SNR}) < \text{R}) \ . \tag{3.4}$$

However, in practice, the transmitted signals usually take values from constraint constellation, i.e., $\boldsymbol{x} \in \Omega^N$. In this case, following [42], the mutual information is computed instead as

$$\begin{aligned} \mathcal{I}_{|\mathcal{H}}(\text{SNR}) \quad &= \quad N \log_2 |\Omega| - \frac{1}{K\tilde{n}|\Omega|^N} \sum_{k=0}^{K-1} \sum_{p=0}^{\tilde{n}-1} \sum_{j=0}^{|\Omega|^N-1} \\ &\qquad \text{E}\Bigg\{ \log_2 \sum_{i=0}^{|\Omega|^N-1} \exp\left[-\left\| \sqrt{\text{SNR}/N}\ \boldsymbol{H}[p,k] \left(\boldsymbol{x}^j - \boldsymbol{x}^i \right) + \boldsymbol{z} \right\|^2 + \left\| \boldsymbol{z} \right\|^2 \right] \Bigg\}, \end{aligned} \tag{3.5}$$

where the expectation is taken over random noise vector $\boldsymbol{z} \sim \mathcal{N}_c(\boldsymbol{0}, \boldsymbol{I})$.

2. Iterative Receiver Structure

A serial concatenated turbo iterative receiver is employed (as shown in Figure 13) to approach the maximum likelihood (ML) receiver performance of joint MIMO OFDM demodulation and LDPC decoding. The extrinsic information of the LDPC coded bits is iteratively passed between a soft-input-soft-output demodulator and a soft belief-propagation LDPC decoder; in each demodulator-decoder iteration, a number of inner iterations is performed within the soft LDPC decoder during which extrinsic information is passed along the edges in the bipartite graph.

In the next, we stick to the following notations. All extrinsic information (message) is in log-likelihood (LLR) form and the variable L is used to refer to extrinsic information. The variable f is used to denote the probability density function (pdf)

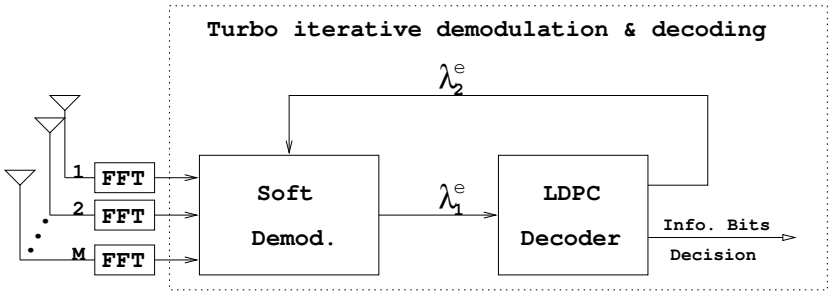

Fig. 13. The turbo receiver structure, which employs a soft demodulator and a soft LDPC decoder, for an LDPC coded MIMO OFDM system.

of the extrinsic information L, and m is used to denote the mean of L. Superscript (p, q) is used to denote quantities during the p-th round of inner decoding within the LDPC decoder and q-th stage of outer iteration between the LDPC decoder and the MIMO OFDM demodulator. For the quantities passed between the soft MIMO OFDM demodulator and the soft LDPC decoder, only one superscript q, namely the iteration number of turbo iterative receiver is used. A subscript $D \rightarrow L$ denotes quantities passed from the demodulator to the LDPC decoder, and vice versa does $D \leftarrow L$.

Demodulation of MIMO OFDM

Assume the perfect CSI at the receiver, it is clear from (3.1) that the demodulation of the received signals at a particular subcarrier and in a particular slot can be carried out independently. For notational convenience, in this subsection we temporarily drop the index $[p, k]$.

As illustrated in Figure 13, at the q-th turbo iteration, the soft MIMO OFDM demodulator computes extrinsic information of the LDPC code bit b_i as

$$L^q_{D\rightarrow L}(b_i) = g(\boldsymbol{y}, \{L^{q-1}_{D\leftarrow L}(b_j)\}_j) \tag{3.6}$$

where $\boldsymbol{y}$ is the received data; $\{L^{q-1}_{D\leftarrow L}(b_j)\}_j$ is the extrinsic information computed by LDPC decoder in the previous turbo iteration, at the first turbo iteration $L^{q-1}_{D\leftarrow L}(b_j) \equiv 0, \forall j$; $g(\cdot)$ denotes the demodulation function, which is described below.

At a given subcarrier and time slot, N symbols or correspondingly $N\log_2|\Omega|$ LDPC code bits are transmitted from N transmitter antennas. In maximum *a posterior* (MAP) MIMO OFDM demodulator, $L^q_{D\rightarrow L}(b_i)$ $(i = 1, \ldots, N\log_2|\Omega|)$ is computed as

$$\begin{aligned}
L^q_{D\rightarrow L}(b_i) &\triangleq \log\frac{P(b_i=+1|\boldsymbol{y})}{P(b_i=-1|\boldsymbol{y})} - \underbrace{\log\frac{P(b_i=+1)}{P(b_i=-1)}}_{L^{q-1}_{D\leftarrow L}(b_i)} \\
&= \log\frac{\sum_{\boldsymbol{x}^+\in\mathcal{C}_i^+} P(\boldsymbol{x}=\boldsymbol{x}^+|\boldsymbol{y})}{\sum_{\boldsymbol{x}^-\in\mathcal{C}_i^-} P(\boldsymbol{x}=\boldsymbol{x}^-|\boldsymbol{y})} - L^{q-1}_{D\leftarrow L}(b_i) \\
&= \log\frac{\sum_{\boldsymbol{x}^+\in\mathcal{C}_i^+} P(\boldsymbol{y}|\boldsymbol{x}=\boldsymbol{x}^+)\,P(\boldsymbol{x}=\boldsymbol{x}^+)}{\sum_{\boldsymbol{x}^-\in\mathcal{C}_i^-} P(\boldsymbol{y}|\boldsymbol{x}=\boldsymbol{x}^-)\,P(\boldsymbol{x}=\boldsymbol{x}^-)} - L^{q-1}_{D\leftarrow L}(b_i) \\
&= \log\frac{\displaystyle\sum_{\boldsymbol{x}^+\in\mathcal{C}_i^+} \exp\left(-\|\boldsymbol{y}-\sqrt{\frac{\mathrm{SNR}}{N}}\boldsymbol{H}\boldsymbol{x}^+\|^2 + \sum_{j=1}^{N\log_2|\Omega|}\{\boldsymbol{x}^+\}_j\cdot L^{q-1}_{D\leftarrow L}(b_j)/2\right)}{\displaystyle\sum_{\boldsymbol{x}^-\in\mathcal{C}_i^-} \exp\left(-\|\boldsymbol{y}-\sqrt{\frac{\mathrm{SNR}}{N}}\boldsymbol{H}\boldsymbol{x}^-\|^2 + \sum_{j=1}^{N\log_2|\Omega|}\{\boldsymbol{x}^-\}_j\cdot L^{q-1}_{D\leftarrow L}(b_j)/2\right)} \\
&\quad - L^{q-1}_{D\leftarrow L}(b_i), \qquad (3.7)
\end{aligned}$$

where $\mathcal{C}_i^+$ is the set of $\boldsymbol{x}$ for which the i-th LDPC coded bit is "+1", and $\mathcal{C}_i^-$ is similarly defined; $\{\boldsymbol{x}^+\}_j$ denotes the corresponding j-th binary bit of the symbol $\boldsymbol{x}^+$, and similarly does $\{\boldsymbol{x}^-\}_j$. The soft MAP demodulator in (3.7) has a complexity at $\mathcal{O}(|\Omega|^N)$, and can only be used in practice for small constellation size and small number of transmit antennas.

We next describe a suboptimal soft demodulator, which is based on the linear minimum-mean-square-error soft-interference-cancellation (SIC-MMSE) techniques [14]

and has a relatively low complexity at $\mathcal{O}(|\Omega|^3)$.

Based on the *a priori* LLR of the code bits provided by the LDPC decoder, $\{L_{D\leftarrow L}^{q-1}(b_i)\}$, we first form soft estimates of the symbol transmitted from the j-th $(j = 1, 2, \ldots, N)$ antenna as

$$\tilde{x}_j \triangleq \sum_{\hat{x}\in\Omega} \hat{x} P\left(x_j = \hat{x}\right) = \sum_{\hat{x}\in\Omega} \hat{x} \prod_{j=1}^{\log_2|\Omega|} \left[1 + \exp\left(-\{\hat{x}\}_j \cdot L_{D\leftarrow L}^{q-1}(b_j)\right)\right]^{-1} \quad (3.8)$$

Denote

$$\tilde{\boldsymbol{x}}_j \triangleq \left[\tilde{x}_1, \ldots, \tilde{x}_{j-1}, 0, \tilde{x}_{j+1}, \ldots, \tilde{x}_{N-1}\right]^T. \quad (3.9)$$

We then perform a soft interference cancellation $\boldsymbol{y}_j$ to obtain

$$\tilde{\boldsymbol{y}}_j \triangleq \boldsymbol{y} - \boldsymbol{H}\tilde{\boldsymbol{x}}_j = \boldsymbol{H}\left(\boldsymbol{x} - \tilde{\boldsymbol{x}}_j\right) + \boldsymbol{n}. \quad (3.10)$$

Next an instantaneous linear MMSE filter is applied to $\tilde{\boldsymbol{y}}_j$, to obtain

$$z_j = \boldsymbol{w}_j^{\mathrm{H}} \tilde{\boldsymbol{y}}_j, \quad (3.11)$$

where the filter $\boldsymbol{w}_j \in \mathcal{C}^M$ is chosen to minimize the mean-square error between the transmit symbol x_j and the filter output z_j, i.e.,

$$\begin{aligned} \boldsymbol{w}_j &= \arg\min_{\boldsymbol{w}\in\mathcal{C}^M} E\left\{|x_j - \boldsymbol{w}^H \tilde{\boldsymbol{y}}_j|^2\right\} \\ &= \sqrt{\frac{N}{\mathrm{SNR}}} \left(\boldsymbol{H}\boldsymbol{\Delta}_j \boldsymbol{H}^{\mathrm{H}} + \frac{N}{\mathrm{SNR}}\boldsymbol{I}\right)^{-1} \boldsymbol{H}\boldsymbol{e} \quad (3.12) \\ \text{where} \quad \boldsymbol{\Delta}_j &\triangleq \mathrm{cov}\left\{\boldsymbol{x}_j - \tilde{\boldsymbol{x}}_j\right\} \\ &= \mathrm{diag}\left\{1 - |\tilde{x}_1|^2, \ldots, 1 - |\tilde{x}_{j-1}|^2, 1, 1 - |\tilde{x}_{j+1}|^2, \ldots, 1 - |\tilde{x}_N|^2\right\}; \quad (3.13) \end{aligned}$$

and $\boldsymbol{e}$ denotes a M-sized vector with all-zero entries, except for the j-th entry being 1. The detailed derivation of (3.12) is further referred to [14].

As in [14], we approximate the soft instantaneous MMSE filter output z_j in (3.11) as Gaussian distributed, i.e.,

$$p(z_j \mid x_j) \;\sim\; \mathcal{N}_c\left(\mu_j x_j, \eta_j^2\right). \tag{3.14}$$

Conditioned on x_j, the mean and variance of z_j are given respectively by

$$\mu_j \;\triangleq\; E\{z_j\, x_j^*\} \;=\; \boldsymbol{e}^{\mathrm{T}}\boldsymbol{H}^{\mathrm{H}}\left(\boldsymbol{H}\boldsymbol{\Delta}_j\boldsymbol{H}^{\mathrm{H}} + \frac{N}{\mathrm{SNR}}\boldsymbol{I}\right)^{-1}\boldsymbol{H}\boldsymbol{e}, \tag{3.15}$$

$$\eta_j^2 \;\triangleq\; \mathrm{var}\{z_j\} \;=\; E\{|z_j|^2\} - \mu_j^2 \;=\; \mu_j - \mu_j^2. \tag{3.16}$$

The extrinsic information $L^q_{D\to L}(b_i)$ delivered by the SIC-MMSE demodulator is calculated as

$$\begin{aligned}
L^q_{D\to L}(b_i) \;&\triangleq\; \log\frac{P\left(b_i=+1|z_j\right)}{P\left(b_i=-1|z_j\right)} - \underbrace{\log\frac{P\left(b_i=+1\right)}{P\left(b_i=-1\right)}}_{L^{q-1}_{D\leftarrow L}(b_i)} \\
&=\; \log\frac{\sum_{x^+\in\mathcal{S}^+_{i,j}} P\left(x_j=x^+|z_j\right)}{\sum_{x^-\in\mathcal{S}^-_{i,j}} P\left(x_j=x^-|z_j\right)} - L^{q-1}_{D\leftarrow L}(b_i) \\
&=\; \log\frac{\sum_{x^+\in\mathcal{S}^+_{i,j}} P\left(z_j|x_j=x^+\right)P\left(x_j=x^+\right)}{\sum_{x^-\in\mathcal{S}^-_{i,j}} P\left(z_j|x_j=x^-\right)P\left(x_j=x^-\right)} - L^{q-1}_{D\leftarrow L}(b_i) \\
&=\; \log\frac{\sum_{x^+\in\mathcal{S}^+_{i,j}} \exp\left(-\|z_j-\mu_j x^+\|^2/\eta_j^2 + \sum_{k=1}^{\log_2|\Omega|}\{x_j^+\}_k\cdot L^{q-1}_{D\leftarrow L}(b_k)/2\right)}{\sum_{x_j^+\in\mathcal{S}^-_{i,j}} \exp\left(-\|z_j-\mu_j x^-\|^2/\eta_j^2 + \sum_{k=1}^{\log_2|\Omega|}\{x_j^-\}_k\cdot L^{q-1}_{D\leftarrow L}(b_k)/2\right)} \\
&\quad -L^{q-1}_{D\leftarrow L}(b_i),
\end{aligned} \tag{3.17}$$

where $\mathcal{S}^+_{i,j}$ is the set of all possible values of x_i for which the i-th LDPC coded bit is "+1", and $\mathcal{S}^-_{i,j}$ is similarly defined; $\{x_j^+\}_k$ denotes the corresponding k-th binary bit of the symbol x_j^+, and similarly does $\{x_j^-\}_k$. Note that, SIC-MMSE demodulator extracts the extrinsic LLR of code bit b_i from z_j, the *scalar* output of the LMMSE filter in (3.11), whereas MAP demodulator collects the extrinsic LLR from $\boldsymbol{y}$, the M-size *vector* of the received signals. The complexity of soft SIC-MMSE demodulator

hence is significantly lower than that of soft MAP demodulator, especially when N and $|\Omega|$ are large.

Decoding of LDPC codes

The message-passing (also known as belief-propagation) decoding algorithm is used to decode the LDPC codes [10]. The detailed decoding algorithm is described in the turbo multiuser detection in Chapter II.

C. Analysis and Optimization of LDPC Coded MIMO OFDM

We analyze and optimize the LDPC coded MIMO OFDM systems via the techniques of density evolution with mixture Gaussian approximations [43]. The principal idea of density evolution [11, 7, 10] is to treat the extrinsic information that is passed in the iterative process as random variables. Then, by estimating the pdf of the random variables as a function of SNR and iteration number, we can compute the probability of error at every iteration. When the length of the codewords $n \to \infty$, the extrinsic information passed along the edges connected to every check node and variable node can be assumed to be independent variables. This makes it possible to compute the pdf's relatively easily. The minimum SNR for which the probability of error tends to zero is called the minimum operational SNR, denoted by $\text{SNR}_{min.op}$. The detail procedures of LDPC code optimization using density evolution with mixture Gaussian approximation are similar to that in Chapter II for turbo multiuser detection. Here we omit them for the sake of conciseness.

D. Numerical Results

In this section, we present numerical results for the design and optimization of LDPC coded MIMO OFDM systems. For each transmit-receive-antenna pair, DoCoMo's physical fading channel model, exponentially distributed frequency-selective fading with $88.8ns$ maximum delay spread, is adopted. OFDM modulation is used with subcarrier spacing 131.836 kHz and cyclic prefix interval of 1.54 μs; as a parameter to be discussed, the number of subcarriers K is specified next. It is clear that the total bandwidth is approximately K times of the subcarrier spacing, and the multipath resolution of the frequency-selective fading channel is the inverse of total bandwidth. For instance, with $K = 1024$ there are 12 resolvable paths in DoCoMo's channel model, but with $K = 512$ the number of resolvable paths is reduced to 6. The modulator uses the QPSK constellation with Gray mapping; for the considered MIMO systems with large number of antennas, the capacity (both ergodic and outage) difference between QPSK signaling and Gaussian signaling is small (e.g., ~ 0.2dB at 4 bits/Hz/sec when $N = M = 4$). All the LDPC codes designed and optimized below have rate 1/2 and appropriate code lengths. For clarity, the rate loss due to cyclic prefix is not counted in this chapter.

All the regular LDPC codes are $(s = 3, t = 6)$ codes taken from [5]. All the irregular LDPC codes are obtained from the design procedure proposed in this chapter. For example, the optimized degree profile for the spatially uncorrelated 2×2 MIMO OFDM systems employing the MAP demodulator is $\lambda(x) = 0.269052x + 0.135031x^2 + 0.024564x^4 + 0.028685x^5 + 0.075819x^6 + 0.033661x^7 + 0.024360x^8 + 0.020951x^9 + 0.018975x^{10} + 0.014373x^{12} + 0.035585x^{13} + 0.015569x^{14} + 0.013611x^{16} + 0.289765x^{19}$ and $\rho(x) = 0.307710x^7 + 0.692290x^8$, and that for the spatially uncorrelated 2×2 MIMO OFDM systems employing the SIC-MMSE demodulator is

$\lambda(x) = 0.294388x + 0.100255x^2 + 0.056131x^3 + 0.042069x^4 + 0.032675x^5 + 0.065028x^7 + 0.030813x^8 + 0.027357x^9 + 0.025533x^{10} + 0.029996x^{11} + 0.014911x^{15} + 0.020255x^{17} + 0.013650x^{18} + 0.246939x^{19}$ and $\rho(x) = 0.738497x^7 + 0.261503x^8$.

In Sections 1-3, the performance of the LDPC codes in ergodic MIMO OFDM channels is demonstrated by bit-error-rate (BER) versus SNR (see Eq.(3.2)); in Section 4, the performance in outage MIMO OFDM channels is demonstrated by frame-error-rate (FER) versus SNR.

1. Different Number of Antennas

If only single-transmit-receive-antenna is used, a cellular system designed for 100 Mbps peak rate downlink transmission requires very broad spectrum, as well as broadband transceiver circuitry; either of which could be costly for commercial applications. MIMO techniques provide a promising means to ameliorate this issue. For example, to achieve a fixed data rate of 100 Mbps, traditional single-antenna system requires 100 MHz bandwidth (assume QPSK modulation and coding rate 1/2), whereas a 4-transmit-4-receive-antenna system could potentially transmit the same 100 Mbps data rate using only 25MHz bandwidth. We note that the information rate in the single-antenna system is 1 bit/Hz/sec, whereas in the 4×4 MIMO system it increases to 4 bits/Hz/sec (higher information rate implies a more efficient use of spectral resource).

In our study, it is assumed that the number of receive antennas is the same as the number of transmit antennas, i.e., $N = M$. We consider 1×1, 2×2 and 4×4 MIMO OFDM systems. Without spatial correlation, $\boldsymbol{R}_l = \boldsymbol{S}_l = \boldsymbol{I}$ in (3.1), (the systems with spatial correlation will be discussed in Section 3). The design and optimization results are shown in Figures 14-16. In these figures, the ergodic channel capacity computed from (3.3) and (3.5) is denoted by "Capacity". First, we focus on the performance

of iterative receiver employing soft MAP demodulator, i.e., the curves denoted by "MAP+regLDPC –D.E.", "MAP+regLDPC –Simu", "MAP+irrLDPC –D.E." and "MAP+irrLDPC –Simu", where suffix "D.E." denotes the results from density evolution analysis and "Simu" denotes that from computer simulations. In order to achieve ergodic channel capacity, large block-size LDPC codes ($n = 880640$) are used to capture large number of fading channel realizations ($\tilde{n} = 430$). It is seen that by applying MIMO techniques, the information rate is increased to N bits/Hz/sec, while the ergodic capacity (the "Capacity" curve) is also slightly improved. Moreover, by employing the optimized irregular LDPC codes and the turbo iterative receiver employing the MAP demodulator, the operational $\text{SNR}_{min.op}$ of LDPC coded MIMO OFDM systems is within 1 dB from the information theoretic ergodic capacity. It is also seen that the performance calculated by density evolution analysis (the "D.E." curves) is in match with that obtained from simulations (the "Simu" curves). At last, we observe that the performance gap between the regular and the irregular LDPC codes tends to be smaller for systems with larger number of antennas.

2. Different Demodulation Schemes

The performance when employing sub-optimal SIC-MMSE demodulator is demonstrated in Figures 14-16, by the curves "SIC+regLDPC –D.E.", "SIC+regLDPC –Simu", "SIC+irrLDPC –D.E." and "SIC+irrLDPC –Simu". Compared to the MAP demodulator based performance (as in Section 1), the use of the SIC-MMSE demodulator brings less than 1dB performance loss for 1×1, 2×2 and 4×4 systems. Therefore, in spatially uncorrelated ergodic MIMO OFDM channels, SIC-MMSE demodulator appears to be a promising choice in practical implementation, for its good performance and relatively low-complexity. (Note that the similar conclusion is not verified yet for systems with even larger number of antennas, e.g., $N = M = 8$, as

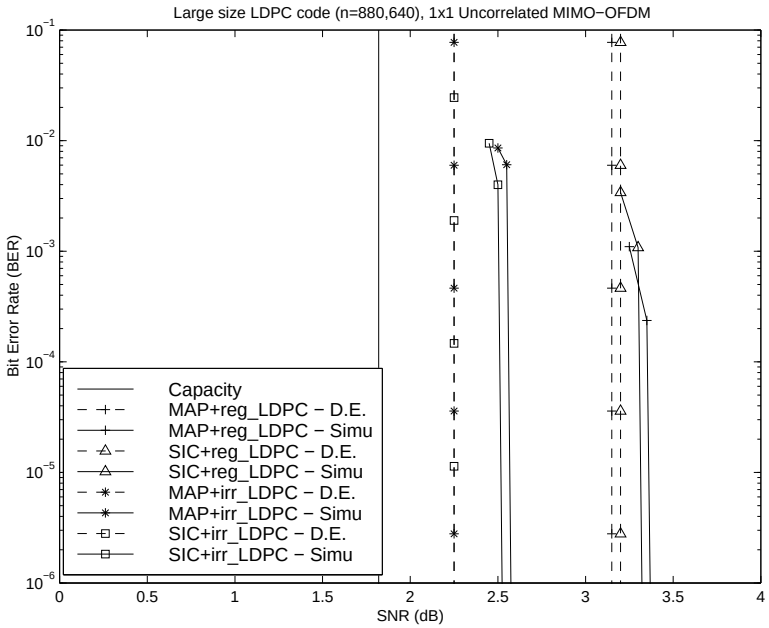

Fig. 14. Performance computed by density evolution analysis and computer simulations for ergodic 1×1 MIMO OFDM channels with no spatial correlation.

the computational complexity of the design procedure for MAP based systems soon becomes unmanageable.)

3. Spatial Correlation

In this subsection, we discuss the performance of MIMO OFDM systems with spatial (antenna) correlation. Following [41], we assume uniform linear antenna placement at both the transmitter and the receiver. The antenna correlation matrices $\boldsymbol{R}_l$ and $\boldsymbol{S}_l$ are given by

$$[\boldsymbol{S}_l]_{m,n} = \exp\left[-j2\pi(n-m)d_T\cos(\bar{\theta}_{T,l}) - (2\pi(n-m)d_T\sin(\bar{\theta}_{T,l})\sigma_{\theta_{T,l}})^2/2\right], \tag{3.18}$$

$$[\boldsymbol{R}_l]_{m,n} = \exp\left[-j2\pi(n-m)d_R\cos(\bar{\theta}_{R,l}) - (2\pi(n-m)d_R\sin(\bar{\theta}_{R,l})\sigma_{\theta_{R,l}})^2/2\right], \tag{3.19}$$

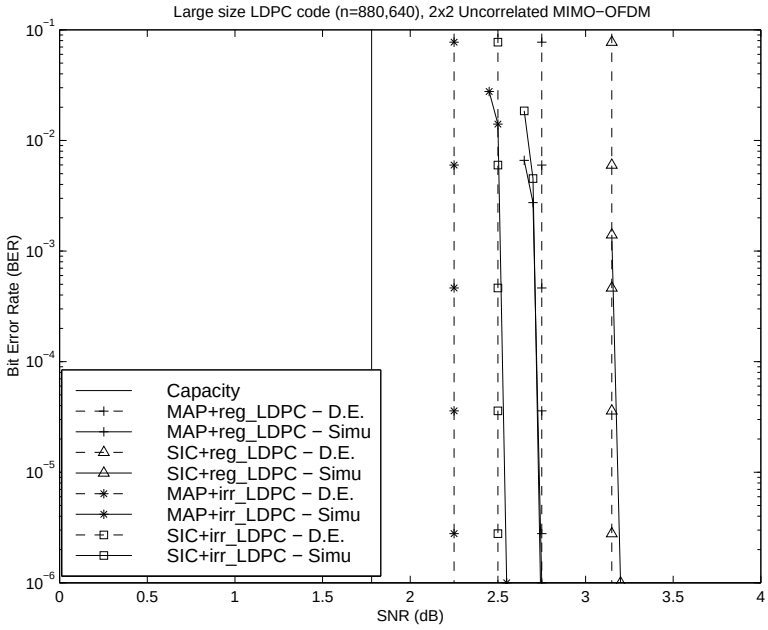

Fig. 15. Performance computed by density evolution analysis and computer simulations for ergodic 2×2 MIMO OFDM channels with no spatial correlation.

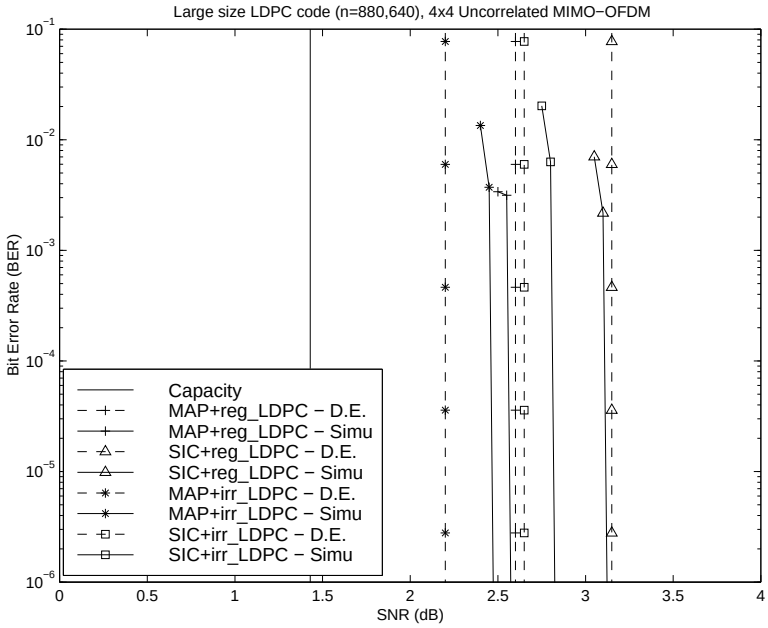

Fig. 16. Performance computed by density evolution analysis and computer simulations for ergodic 4×4 MIMO OFDM channels with no spatial correlation.

where $[\boldsymbol{A}]_{m,n}$ denotes the (m,n)-th entry of matrix $\boldsymbol{A}$; d_T denotes the transmitter antenna spacing normalized by carrier wavelength; $\bar{\theta}_{T,l}$ denotes the mean angle of departure for each scatterer cluster at the transmitter; $\sigma_{\theta_{T,l}}$ denotes the root-mean-square (RMS) of angle of departure at the transmitter; d_R, $\bar{\theta}_{R,l}$ and $\sigma_{\theta_{R,l}}$ denote the corresponding variables at the receiver side. In our experiments, we consider an urban micro-cell scenario [44] and for simplicity assume that all L paths follow the same spatial parameters as $\bar{\theta}_{T,l} = 53$, $\bar{\theta}_{R,l} = 18$, $\sigma_{\theta_{T,l}} = 8$, $\sigma_{\theta_{R,l}} = 2$; we also let $d_T = 4.0$ and $d_R = 0.5$ to reflect the situations that the antennas at base station are easier to be sparsely placed than the antennas at mobile devices. It is worth to note that some parameters (e.g., $\sigma_{\theta_{R,l}} = 2$) here are intentionally set to be worse than typical scenarios in order to highlight the effect of spatial correlation. Going through the same design and optimization procedure, we obtain the analysis and design results in Figures 17-18. (The issue of antenna correlation does not exist for 1×1 systems.) Compared to spatially uncorrelated systems, antenna correlation causes channel capacity loss for the systems considered here. Nevertheless, the optimized irregular LDPC codes along with the MAP demodulator based iterative receiver can yield a performance within 1dB from the capacity of correlated channels. This demonstrates again the generality and efficacy of the methods of density evolution with mixture Gaussians in optimizing LDPC OFDM MIMO systems. However, compared to the corresponding result in spatially uncorrelated channels (4×4 systems in particular) the performance of the SIC-MMSE based receivers is degraded. We conjecture that the correlation matrices $\boldsymbol{R}_l$ and $\boldsymbol{S}_l$ lead to a larger matrix conditional number of $\boldsymbol{H}_l$ than it in uncorrelated MIMO channels, and therefore the matrix operations (e.g., matrix inverse) in the SIC-MMSE are more subject to numerical instability. (It is possible that some signal processing techniques be used to alleviate this issue; further discussion is out of the scope of this chapter.)

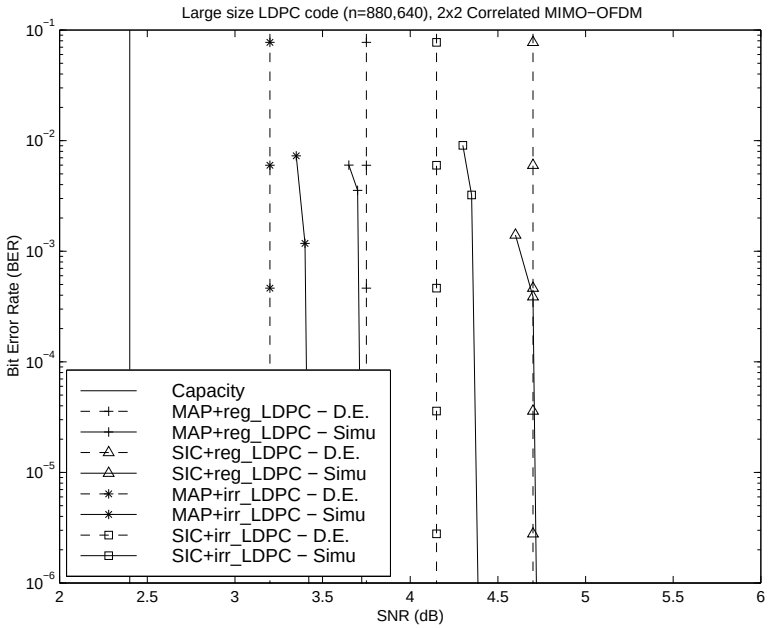

Fig. 17. Performance computed by density evolution analysis and computer simulations for ergodic 2×2 MIMO OFDM systems with spatial correlation.

4. Small Block-size LDPC Coded MIMO OFDM

So far, we have focused on the design and optimization of the LDPC MIMO OFDM systems aiming to achieve the ergodic capacity. In doing so, large block-size LDPC codes were employed for the following reasons. (1) In order to achieve the ergodic channel capacity, the LDPC code word must be long enough to experience a very large number of fading channel realizations. (2) The results of the density evolution analysis are based on the assumption that extrinsic messages connected to each check node and variable node are independent, which holds valid when LDPC code block-size is very large. (3) In the procedure of the density evolution analysis and design, optimized degree profiles, $\lambda(x)$ and $\rho(x)$, are first obtained, from which irregular LDPC codes are then randomly constructed; according to the theorem of concentration around ensemble average and the theorem of convergence to cycle-free ensemble average [9], such randomly constructed LDPC codes are guaranteed to have vanishing probability

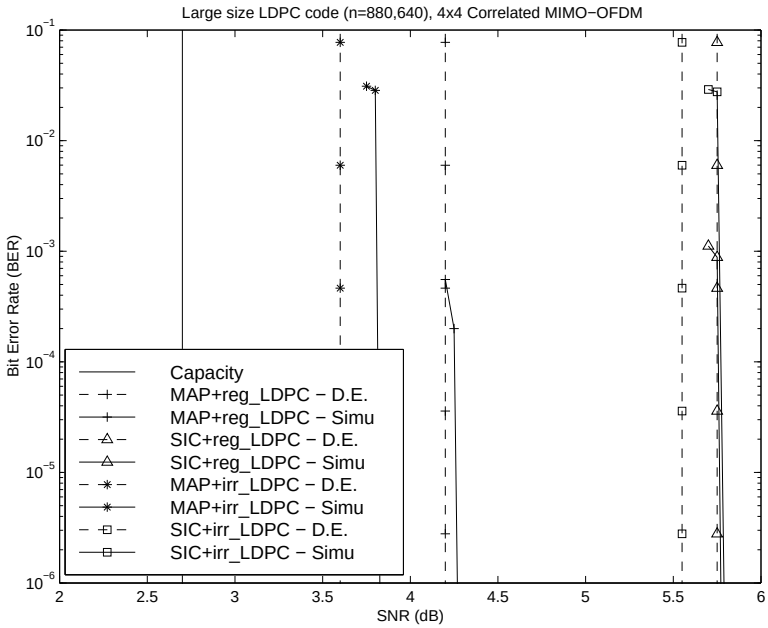

Fig. 18. Performance computed by density evolution analysis and computer simulations for ergodic 4×4 MIMO OFDM systems with spatial correlation.

of error above the $\text{SNR}_{min.op}$ threshold (correspond to the optimized $\lambda(x)$ and $\rho(x)$), when its code block-size is very large. In reality, however, the price paid for achieving the ergodic channel capacity (or error-free communications) by employing very large block-size codes is large decoding delay. Usually, if small amount of fading outage is tolerable, it is a more common practice to employ a small block-size LDPC code, which spans a small number of fading channel states. The sensible performance measure accordingly is outage capacity (see Eq.(3.4)). Unlike that for the ergodic channels, a systematic way of designing small block-size LDPC codes to achieve the outage channels is so far unknown to the best of our knowledge; instead, a heuristic design approach which claims no theoretical optimality is adopted here. The design begins with the degree profiles that have been optimized above for the ergodic channels (i.e., $\tilde{n} \to \infty$). Based on these degree profiles, a small block-size LDPC code is randomly constructed by trial-and-error; more specifically, we drop the constructed LDPC codes

with small girth in the bipartite graph, which to some extent leads to error-floor in FER performance. (It is also possible to construct small block-size LDPC codes by other methods, e.g., the method of bit-filling [45].)

The heuristically constructed small block-size LDPC codes ($n = 2048$) are simulated in outage MIMO OFDM channels ($\tilde{n} = 1$). In Figures 19-21, the performance of regular and irregular LDPC codes when employed in systems with different number of antennas and different types of demodulator is presented. Similar to the conclusions we drew above in ergodic channels, the proposed LDPC coded MIMO OFDM systems can achieve both information rate increase and performance improvement when using multiple antennas; the MAP demodulator based iterative receiver can perform within 1.5dB from the outage capacity; and the low-complexity SIC-MMSE demodulator based receiver incurs additional small performance loss ($<$ 1dB). In addition, in order to demonstrate the process of receiver convergence, we present the results in Figures 19-21 in another form in Figure 22, namely the required SNR (dB) to achieve a FER of 10^{-2} versus the number of turbo receiver iteration. In a spatially uncorrelated 4×4 MIMO OFDM system, for both the MAP and the SIC-MMSE demodulator based receivers, we see that although the performance difference between regular and irregular LDPC codes after receiver convergence (the curve "Iter #6") is negligible, the irregular LDPC codes help to speed up the receiver convergence. Around 0.5dB gain is achieved after the first receiver iteration for both the MAP and the SIC-MMSE demodulator based receiver. This observation suggests another benefit of optimizing LDPC codes, that is to help reduce the number of receiver iterations and consequently the receiver complexity in the outage MIMO OFDM channels.

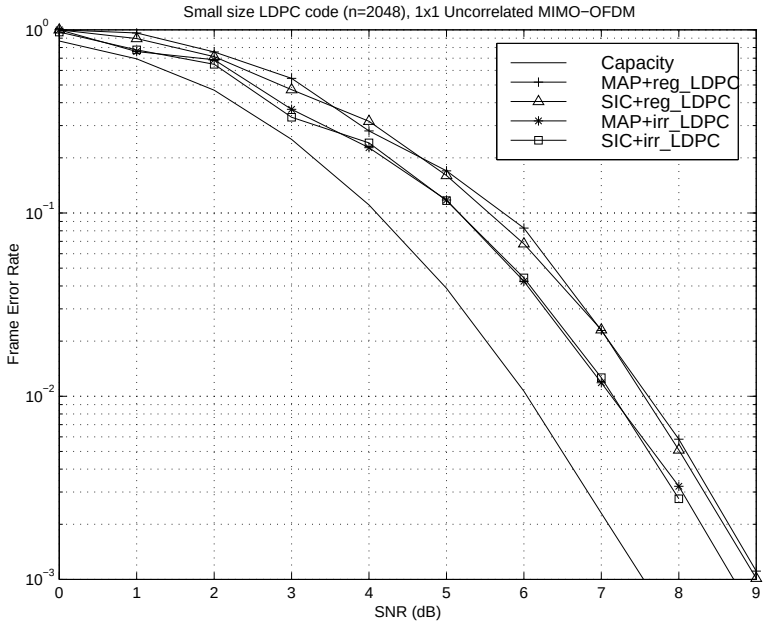

Fig. 19. Performance for outage 1×1 MIMO OFDM channels with no spatial correlation.

5. A Mismatch Study

In the above, the performance of the optimized LDPC coded MIMO OFDM is demonstrated, with LDPC codes being optimized for specific MIMO channels. As suggested by one reviewer, it is perhaps in the readers' interest to exhibit the reward of the channel-specific LDPC code design, by comparing the performance of the MIMO-channel-optimized irregular LDPC codes with that of the AWGN-channel-optimized irregular LDPC codes in MIMO OFDM channels. The results are shown in Table I. In general, the channel-specific design gain increases for systems with larger number of antennas. In addition, in outage channels, a good AWGN-optimized irregular LDPC code also exhibits the faster convergence of turbo iterative receiver than the non-optimized regular LDPC codes.

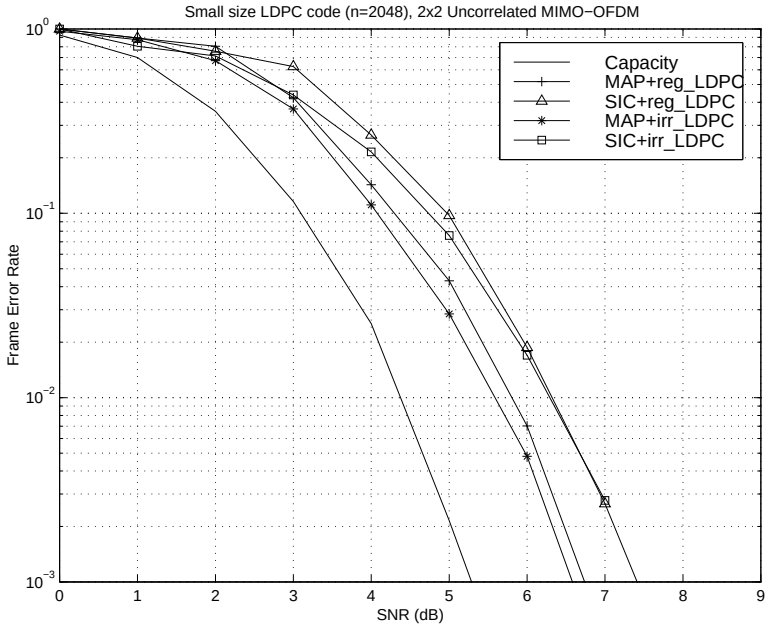

Fig. 20. Performance for outage 2×2 MIMO OFDM channels with no spatial correlation.

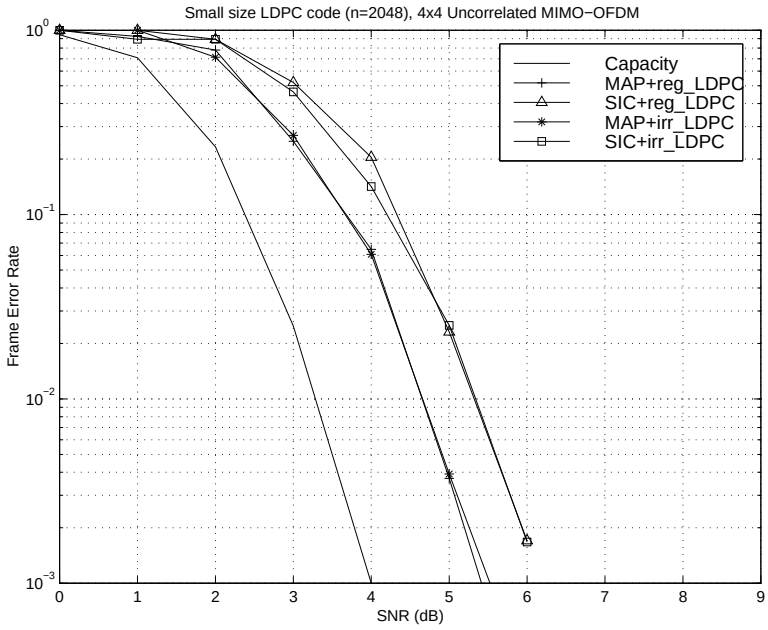

Fig. 21. Performance for outage 4×4 MIMO OFDM channels with no spatial correlation.

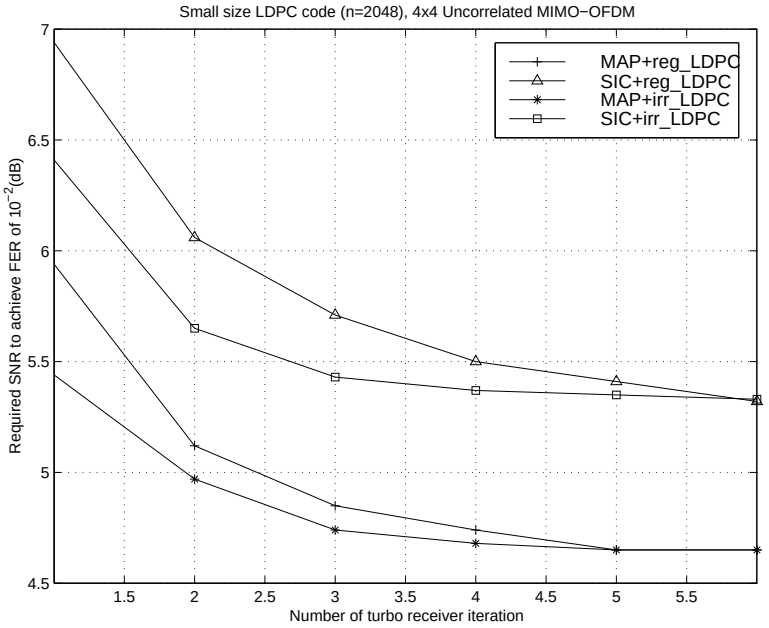

Fig. 22. For short block-size LDPC codes in 4×4 MIMO OFDM systems with no spatial correlation, the performance is plotted as the required SNR (dB) to achieve the FER of 10^{-2} versus the number of turbo receiver iteration. Note that flatter curves indicate faster receiver convergence.

E. Conclusions

In this chapter, we have considered the performance analysis and design optimization of LDPC coded MIMO OFDM systems for high data-rate wireless transmission. The tools of density evolution with mixture Gaussian approximations have been used to optimize irregular LDPC codes and to compute minimum operational signal-to-noise ratios for ergodic MIMO OFDM channels. Furthermore, based on the LDPC profiles that were already optimized for ergodic channels, we also heuristically constructed small block-size irregular LDPC codes for outage MIMO OFDM channels. Several main conclusions are as follows.

1. Based on the optimized irregular LDPC codes, a turbo iterative receiver that consists of a soft maximum *a posteriori* (MAP) demodulator and a belief-propagation LDPC decoder can perform within 1 dB above the ergodic channel capacity for various system configurations under consideration.

2. Likewise, based on the heuristically constructed small block-size irregular LDPC codes, a turbo iterative receiver based on MAP demodulator can perform within 1.5 dB above the outage channel capacity.

3. Compared to the receiver employing the MAP demodulator, the receiver employing a low-complexity linear minimum mean-square-error soft-interference-cancellation (SIC-MMSE) demodulator has limited performance loss (less than 1 dB) in spatially uncorrelated channels, but suffer extra performance loss in spatially correlated channels.

4. In ergodic MIMO OFDM channels, the optimization gain of the irregular LDPC codes over the regular LDPC codes tends to be smaller for systems with larger number of antennas. In outage MIMO OFDM channels, both the regular and

irregular LDPC codes perform close to each other after receiver converges, however the irregular LDPC codes are helpful to expedite the convergence of iterative receiver.

Table I. A mismatch study to demonstrate the reward of channel-matching irregular LDPC design. The performance is obtained through simulations in the spatial-uncorrelated MIMO OFDM channels. *LDPC.I* denotes the irregular LDPC codes optimized for the corresponding MIMO OFDM channels; *LDPC.II* denotes the irregular LDPC codes originally designed for AWGN channels. The performance (SNR) of the short block LDPC coded MIMO OFDM is measured at FER of 10^{-2}.

	Large Block Irregular LDPC			Small Block Irregular LDPC		
SNR (dB)	LDPC.I	LDPC.II	Design Gain (LDPC.II - I)	LDPC.I	LDPC.II	Design Gain (LDPC.II - I)
MAP (1×1)	2.57	2.57	0.00	7.08	7.08	0.00
MAP (2×2)	2.56	2.61	0.05	5.57	5.72	0.15
MAP (4×4)	2.46	2.65	0.19	4.48	4.81	0.33
SIC (1×1)	2.52	2.52	0.00	7.06	7.06	0.00
SIC (2×2)	2.75	2.92	0.17	6.32	6.44	0.12
SIC (4×4)	2.82	3.17	0.35	5.33	5.70	0.37

CHAPTER IV

CODING-SPREADING TRADEOFF IN LDPC-CODED CDMA WITH TURBO MULTIUSER DETECTION

A. Introduction

Based on the notion of Shannon bandwidth introduced by Massey [46], general definitions of spreading and coding are given in [47] to distinguish these operations for signaling with bandwidth redundancy. In [47], the operation of spreading is defined as any bandwidth redundancy scheme which increases the Fourier bandwidth while preserving the Shannon bandwidth, if this bandwidth redundancy mapping can be expressed as a unitary linear mapping; the coding is a signal set mapping, after which the Shannon bandwidth of the signal set remains equal to the Fourier bandwidth. These definitions are shown to lead to a separation result: every bandwidth redundancy scheme can be considered as a concatenation of coding followed by spreading [46, 48]. Coding and spreading are two aspects of signaling, and contribute differently to the performance of CDMA systems. Then it is natural to ask what portions of a given bandwidth expansion should be allocated to coding and spreading respectively in order to achieve maximum spectral efficiency. This tradeoff problem has been considered in [49] for single-user detection. An information theoretic treatment of this problem for multiuser detection is found in [50, 28]. In [28], it is shown that the MMSE receiver achieves the same optimum spectral efficiency as the single-user matched filter for low E_b/N_0. When E_b/N_0 is greater than 2.5dB, the efficiency gain for the MMSE receiver increases with E_b/N_0 over the single-user matched filter. A coding-spreading tradeoff study on linear multiuser detection in [47] gives the same conclusion in single-cell systems but finds that in the multi-cell scenario, the linear

MMSE receiver offers little advantage over the conventional matched-filter receiver in terms of capacity; and it is speculated there that by joint decoding as in [14], such a conclusion may no longer hold. In this chapter, we treat the coding-spreading tradeoff problem for CDMA systems employing joint decoding in the form of turbo multiuser detection [51, 52, 53, 14].

Unlike the turbo multiuser detectors discussed in this chapter, the front-end filters in [47] are assumed to be executed only once before sending the soft or hard outputs to the per-user channel decoders. The channel decoders are assumed to achieve the residual capacities of the resulting single-user channels. For systems employing turbo multiuser detection, such an ideal decoding assumption will not facilitate a coding-spreading analysis due to the indispensable role of soft decoding dynamics in the turbo decoding process. Here we assume that the users employ capacity-achieving LDPC codes [8, 10, 9]. By using the density evolution technique for analyzing the turbo decoding process [54], we can obtain the maximum spectral efficiency by searching the tangent point between the extrinsic information SNR evolution curves of the SISO detectors and that of the LDPC decoders when increasing the system load. Since the LDPC codes offer near-capacity performance, we expect the results based on such a system reflect that of a system employing ideal joint decoding.

The performance of CDMA systems with multiuser receivers depends on the specific choice of spreading sequences used. To reap the benefits of multiuser detection (MUD) in CDMA systems, it is important to obtain fundamental understanding of system design independent of the fine system structure. To this end, one can resort to large-system analysis, with both the number of users K and the processing gain N going to infinity while keeping their ratio $\alpha = \frac{K}{N}$ fixed. Built on some recent results on random matrix theory, large-system analysis of CDMA systems with random spreading and linear multiuser detection has recently garnered much

attention [55, 56, 57]. The large-system asymptotic performance analysis of turbo multiuser detection was considered in [58]. Another contribution of this chapter is analysis of coding-spreading tradeoff for turbo multiuser detection based on large-system analysis for both single-cell and multi-cell scenarios.

The rest of this chapter is organized as follows. In Section B, we describe the single-cell and multi-cell systems under consideration with turbo multiuser receivers. Section C presents the large-system asymptotic performance analysis for turbo multiuser detectors. Section D describes our approach to the coding-spreading tradeoff analysis using density evolution techniques. Simulation results are provided in Section E. Section F contains the conclusions.

B. System Descriptions

1. Turbo Receivers in Single-cell Systems

We consider an LDPC-coded K-user synchronous CDMA system with spreading gain N, powers $A_1^2, A_2^2 \cdots, A_K^2$, spreading sequences $\boldsymbol{s}_1$, $\boldsymbol{s}_2, \cdots, \boldsymbol{s}_K$, and signaling through their respective channels with additive white Gaussian noise. The block diagram of the transmitter-end of such a system is shown in the upper half of Fig. 1. The binary information data $\{d_k(m)\}$ for User k are LDPC encoded. The interleaved code bits of the kth user are BPSK symbol-mapped to $\{b_k(i)\}$. Shown in the lower part of Fig. 1, the overall receiver is an iterative receiver which performs turbo multiuser detection by passing extrinsic messages on the code bits between a soft-input soft-output (SISO) multiuser detector and an LDPC decoder.

The received discrete-time signal sequence is given by

$$\boldsymbol{r}(i) = \boldsymbol{S}(i)\boldsymbol{A}\boldsymbol{b}(i) + \sigma\boldsymbol{\nu}(i), \quad i = 1, \cdots, M, \tag{4.1}$$

where $\boldsymbol{S}(i) = [\boldsymbol{s}_1(i), \cdots, \boldsymbol{s}_K(i)]$ is an $N \times K$ matrix whose columns are user spreading sequences corresponding to symbol i, $\boldsymbol{A} \stackrel{\triangle}{=} \text{diag}\,(A_1, \cdots, A_K)$, $\boldsymbol{b}(i) = [b_1(i), \cdots, b_K(i)]^T$, and $\boldsymbol{\nu}(i) = [\nu_1(i), \cdots, \nu_N(i)]^T$ is a white noise vector, $\nu_l(i) \stackrel{\text{iid}}{\sim} \mathcal{N}(0,1)$, M is the total number of symbols transmitted by each user.

A sufficient statistic for demodulating the ith code bits of the K users is given by the K-vector $\boldsymbol{y}(i)$ whose kth component is the output of a filter matched to $\boldsymbol{s}_k(i)$ in the ith code bit interval, i.e., $y_k(i) \stackrel{\triangle}{=} \boldsymbol{s}_k(i)^T \boldsymbol{r}(i),\ k = 1, \cdots, K$. Denote $\boldsymbol{y}(i) = [y_1(i), \cdots, y_K(i)]^T$, then

$$\boldsymbol{y}(i) = \boldsymbol{S}(i)^T \boldsymbol{r}(i) = \boldsymbol{R}(i)\boldsymbol{A}\boldsymbol{b}(i) + \sigma \boldsymbol{n}(i), \tag{4.2}$$

where $\boldsymbol{R}(i) \stackrel{\triangle}{=} \boldsymbol{S}(i)^T \boldsymbol{S}(i)$, $\boldsymbol{n}(i) \sim \mathcal{N}\Big(\boldsymbol{0}, \boldsymbol{R}(i)\Big)$.

SIC-MMSE SISO multiuser detector: A low-complexity approximate SISO multiuser detector was developed in [14] which is based on soft interference cancellation and instantaneous linear MMSE filtering, and is summarized as follows. Denote $\boldsymbol{e}_k$ as the kth unit vector in $\mathbb{R}^K$. Denote $L^{(q-1)}_{m \leftarrow L}[b_k(i)]$ as the extrinsic log-likelihood ratio (LLR) of the kth user's ith code bit sent from the LDPC decoder to the multiuser detector, during the $(q-1)$th turbo iteration. Define

$$\tilde{b}_j(i) \stackrel{\triangle}{=} \tanh\left(\frac{1}{2} L^{q-1}_{m \leftarrow L}[b_j(i)]\right), \quad j = 1, \cdots, K, \tag{4.3}$$

$$\text{and} \quad \boldsymbol{V}_k(i) \stackrel{\triangle}{=} \sum_{j \neq k} A_j^2 [1 - \tilde{b}_j(i)^2] \boldsymbol{e}_j \boldsymbol{e}_j^T + A_k^2 \boldsymbol{e}_k \boldsymbol{e}_k^T. \tag{4.4}$$

Denote $\tilde{\boldsymbol{b}}(i) \stackrel{\triangle}{=} [\tilde{b}_1(i) \cdots \tilde{b}_K(i)]^T$ and $\tilde{\boldsymbol{b}}_k(i) \stackrel{\triangle}{=} \tilde{\boldsymbol{b}}(i) - \tilde{b}_k(i)\boldsymbol{e}_k$. Then the extrinsic LLR of $b_k(i)$ sent from the multiuser detector to the LDPC decoder during the qth turbo

iteration is given by

$$
\begin{aligned}
L^q_{m\to L}[b_k(i)] &= \frac{2z_k(i)}{1-\mu_k(i)}, && (4.5)\\
\text{with} \quad z_k(i) &= A_k \boldsymbol{e}_k^T[\boldsymbol{V}_k(i)+\sigma^2\boldsymbol{R}(i)^{-1}]^{-1}[\boldsymbol{R}(i)^{-1}\boldsymbol{y}(i)-\boldsymbol{A}\tilde{\boldsymbol{b}}_k(i)], && (4.6)\\
\mu_k(i) &= A_k^2 \boldsymbol{e}_k^T\left[\boldsymbol{V}_k(i)+\sigma^2\boldsymbol{R}(i)^{-1}\right]^{-1}\boldsymbol{e}_k. && (4.7)
\end{aligned}
$$

SIC-MF SISO multiuser detector: A further simplification on the above SIC-MMSE detector is to replace the linear MMSE filtering step after the soft interference cancellation, by a simple matched filtering step. In this case, we have

$$
\begin{aligned}
L^q_{m\to L}[b_k(i)] &= \frac{2}{\nu_k^2(i)}\left(y_k(i)-\sum_{j\neq k}A_j[\boldsymbol{R}(i)]_{k,j}\tilde{b}_j(i)\right), && (4.8)\\
\text{with} \quad \nu_k^2(i) &= \left[\boldsymbol{R}(i)\boldsymbol{V}_k(i)\boldsymbol{R}(i)+\sigma^2\boldsymbol{R}(i)\right]_{k,k}-1.
\end{aligned}
$$

Note that computationally the SIC-MF method is simpler since it avoids the matrix inversion in the SIC-MMSE method.

2. Turbo Receivers in Multi-cell Systems

Now we consider a multi-cell wireless system, in which the base station receives the sum of the in-cell signals and the interference from neighboring cells. Here we treat a typical hexagonal cell structure and consider the interference only from the first tier of the six nearest neighboring cells. We assume that all cells have the same number of users K. Let $k = 1, \cdots, K$, indicate in-cell users, and $k = K+1, \cdots, 7K$, indicate

out-cell users. With the subscript $(\cdot)_o$ denoting out-cell users, we define

$$\begin{aligned} \boldsymbol{A}_o &\triangleq \text{diag}\left\{[A_{K+1}, \cdots, A_{7K}]\right\} \ [6K \times 6K], \\ \boldsymbol{b}_o(i) &\triangleq [b_{K+1}(i), \cdots, b_{7K}(i)]^T \ [6K \times 1], \\ \boldsymbol{S}_o(i) &\triangleq [\boldsymbol{s}_{K+1}(i), \cdots, \boldsymbol{s}_{7K}(i)] \ \ [N \times 6K], \\ \text{and} \quad \boldsymbol{R}_o(i) &\triangleq \boldsymbol{S}(i)^T \boldsymbol{S}_o(i) \ \ [K \times 6K]. \end{aligned}$$

The matched-filter outputs for the in-cell users are then given by

$$\boldsymbol{y}(i) = \boldsymbol{R}(i)\boldsymbol{A}\boldsymbol{b}(i) + \boldsymbol{R}_o(i)\boldsymbol{A}_o\boldsymbol{b}_o(i) + \sigma\boldsymbol{n}(i). \tag{4.9}$$

SIC-MMSE SISO multiuser detector: Similar to the single-cell case, we form the soft estimates of all code bits of all in-cell users, $\{\tilde{b}_j(i)\}_{j=1}^K$, based on the *a priori* LLR $\left\{L_{m\leftarrow L}^{q-1}[b_j(i)]\right\}_{j=1}^K$ provided by the channel decoder from the previous stage according to (4.3). Then we perform soft cancellation only for interference from in-cell users to obtain

$$\boldsymbol{y}_k(i) \triangleq \boldsymbol{y}(i) - \boldsymbol{R}(i)\boldsymbol{A}\tilde{\boldsymbol{b}}_k(i) = \boldsymbol{R}(i)\boldsymbol{A}[\boldsymbol{b}(i) - \tilde{\boldsymbol{b}}_k(i)] + \boldsymbol{R}_o(i)\boldsymbol{A}_o\boldsymbol{b}_o(i) + \sigma\boldsymbol{n}(i), \quad k = 1, \cdots, K. \tag{4.10}$$

Then the instantaneous linear MMSE filter $\boldsymbol{w}_k(i)$ applied to $\boldsymbol{y}_k(i)$ is given by

$$\boldsymbol{w}_k(i) = \left[\boldsymbol{R}(i)\boldsymbol{V}_k(i)\boldsymbol{R}(i) + \boldsymbol{R}_o(i)\boldsymbol{A}_o\boldsymbol{A}_o\boldsymbol{R}_o(i)^T + \sigma^2\boldsymbol{R}(i)\right]^{-1}\boldsymbol{R}(i)\boldsymbol{A}\boldsymbol{e}_k; \tag{4.11}$$

and the filter output is given by

$$\begin{aligned} z_k(i) &= \boldsymbol{w}_k(i)^T\boldsymbol{y}_k(i) \\ &= A_k\boldsymbol{e}_k^T[\boldsymbol{V}_k(i) + \boldsymbol{\Sigma}(i) + \sigma^2\boldsymbol{R}(i)^{-1}]^{-1}[\boldsymbol{R}(i)^{-1}\boldsymbol{y}(i) - \boldsymbol{A}\tilde{\boldsymbol{b}}_k(i)], \\ &\quad \text{with} \quad \boldsymbol{\Sigma}(i) = \boldsymbol{R}(i)^{-1}\boldsymbol{R}_o(i)\boldsymbol{A}_o\boldsymbol{A}_o\boldsymbol{R}_o(i)^T\boldsymbol{R}(i)^{-1}. \end{aligned} \tag{4.12}$$

Following the same derivation as in [14], the extrinsic LLR from the SIC-MMSE detector to the LDPC decoder is

$$\begin{aligned} L^q_{m\to L}[b_k(i)] &= \frac{2z_k(i)}{1-\mu_k(i)}, & (4.13)\\ \text{with} \quad \mu_k(i) &= A_k^2 \boldsymbol{e}_k^T \left[\boldsymbol{V}_k(i) + \boldsymbol{\Sigma}(i) + \sigma^2 \boldsymbol{R}(i)^{-1}\right]^{-1} \boldsymbol{e}_k. & (4.14) \end{aligned}$$

SIC-MF SISO multiuser detector: In this case, after the soft cancellation of in-cell interference, match-filtering is applied to the residual signal in (4.10). We have

$$\begin{aligned} L^q_{m\to L}[b_k(i)] &= \frac{2}{\nu_k^2(i)} \left(y_k(i) - \sum_{j\neq k} A_j [\boldsymbol{R}(i)]_{k,j} \tilde{b}_j(i) \right), & (4.15)\\ \text{with} \quad \nu_k^2(i) &= \left[\boldsymbol{R}(i)\boldsymbol{V}_k(i)\boldsymbol{R}(i) + \boldsymbol{R}_o(i)\boldsymbol{A}_o^2\boldsymbol{R}_o(i)^T + \sigma^2\boldsymbol{R}(i) \right]_{kk} - 1. \end{aligned}$$

C. Large-system Asymptotic Performance Analysis

Next, we consider the asymptotic analysis where both the number of users K and the processing gain N going to infinity while keeping the ratio $\alpha = \frac{K}{N}$ fixed. A capacity analysis of large CDMA networks with linear multiuser receivers is provided in [57]. A fundamental result, the Tse-Hanly equation, is obtained, given by

$$\gamma_1 = \frac{P_1}{\sigma^2 + \alpha E_P\left[I(P, P_1, \gamma_1)\right]}, \quad \text{with} \quad I(P, P_1, \gamma_1) = \frac{PP_1}{P_1 + P\gamma_1}, \tag{4.16}$$

where P_1 and γ_1 are the power and the output SNR of the linear MMSE receiver for User 1, respectively, P denotes the power of interference from other users, and $E_P[\cdot]$ denotes the expectation with respect to the empirical distribution of the received powers of the interferers. The solution to (4.16) is the asymptotic output SNR of the linear MMSE multiuser receiver in large CDMA systems.

1. Single-cell Systems

Consider the signal after soft interference cancellation,

$$\begin{aligned} \boldsymbol{r}_k(i) &= \boldsymbol{r}(i) - \sum_{j\neq k} A_j \tilde{b}_j(i)\boldsymbol{s}_j(i) \\ &= A_k b_k(i)\boldsymbol{s}_k(i) + \sum_{j\neq k} A_j \left(b_j(i) - \tilde{b}_j(i)\right)\boldsymbol{s}_j(i) + \sigma\boldsymbol{\nu}(i). \end{aligned} \tag{4.17}$$

Note that in $\boldsymbol{r}_k(i)$, the desired user's power is A_k^2, and the jth interferer's power is $A_j^2 E\left\{\left(b_j(i) - \tilde{b}_j(i)\right)^2\right\} = A_j^2\left(1 - \tilde{b}_j(i)^2\right)$. Therefore, as far as the second-order moment is concerned, the soft-cancellation effectively adjusts the powers of the interfering signals. That is, we can equivalently write (equivalent in the second-order moment)

$$\boldsymbol{r}_k(i) = A_k b_k(i)\boldsymbol{s}_k(i) + \sum_{j\neq k}\left(A_j\sqrt{1-\tilde{b}_j(i)^2}\right) b_j(i)\boldsymbol{s}_j(i) + \sigma\boldsymbol{\nu}(i). \tag{4.18}$$

When the MMSE filter is applied to $\boldsymbol{r}_k(i)$, we can make use of the result in [57] to get the asymptotic SNR for the SIC-MMSE detector.

Assume that $A_1 = \cdots = A_K \triangleq A$. Then in (4.16) $P_1 = A^2$ and the power of the interference becomes

$$P_j = A^2\left(1 - \tilde{b}_j(i)^2\right) = A^2\left[1 - \tanh^2\left(\frac{\lambda_j}{2}\right)\right]. \tag{4.19}$$

For regular LDPC codes, the output extrinsic λ_j from LDPC decoder to the multiuser detector is approximated as symmetric Gaussian distributed, i.e., $\lambda_j \sim \mathcal{N}(m_j, 2m_j)$ [8]. The mean, m_j, can be evaluated by using the density evolution method given the pdf of the extrinsic LLR from the multiuser detector. Obviously, λ_j has same symmetric Gaussian distribution with mean m assuming equal power among all users.

The power of interference can then be written as

$$P = A^2 \left[1 - \tanh^2\left(\frac{\lambda}{2}\right)\right], \tag{4.20}$$

where $\lambda \sim \mathcal{N}(m, 2m)$. Substituting P and P_1 into (4.16), we obtain that the asymptotic SNR, γ, is the unique positive solution to the following fixed point equation

$$\gamma = \frac{1}{\dfrac{\sigma^2}{A^2} + \alpha E_\lambda \left\{ \dfrac{1 - \tanh^2(\frac{\lambda}{2})}{1 + \gamma\left[1 - \tanh^2(\frac{\lambda}{2})\right]} \right\}}. \tag{4.21}$$

Define

$$\begin{aligned} f(\gamma) &\triangleq \gamma \left(\frac{\sigma^2}{A^2} + \alpha E_\lambda \left\{ \frac{1 - \tanh^2(\frac{\lambda}{2})}{1 + \gamma\left[1 - \tanh^2(\frac{\lambda}{2})\right]} \right\} \right) - 1 \\ &= \gamma \left(\frac{\sigma^2}{A^2} + \alpha E_\lambda \left\{ \frac{1}{\cosh^2(\frac{\lambda}{2}) + \gamma} \right\} \right) - 1. \end{aligned} \tag{4.22}$$

The derivative of $f(\gamma)$ is then given by

$$f'(\gamma) = \frac{\sigma^2}{A^2} + \alpha E_\lambda \left\{ \frac{1}{\cosh^2(\frac{\lambda}{2}) + \gamma} \right\} + \alpha\gamma E_\lambda \left\{ \frac{-1}{\left(\cosh^2(\frac{\lambda}{2}) + \gamma\right)^2} \right\}. \tag{4.23}$$

Then starting from an arbitrary $\gamma^{(0)}$, γ can be solved using the following Newton iterations:

$$\gamma^{(n)} = \gamma^{(n-1)} - \mu \frac{f\left(\gamma^{(n-1)}\right)}{f'\left(\gamma^{(n-1)}\right)}, \quad n = 1, 2, \cdots. \tag{4.24}$$

On the other hand, the asymptotic output SNR of the conventional matched-filter is given by [57]

$$\gamma_1 = \frac{P_1}{\sigma^2 + \alpha E_P[P]}. \tag{4.25}$$

Using the same equivalent model (4.18) for the post soft-cancellation signals, and (4.20), we obtain the asymptotic SNR for the SIC-MF receiver described in Section B,

given by

$$\gamma = \frac{1}{\frac{\sigma^2}{A^2} + \alpha E_\lambda \left\{ 1 - \tanh^2 \left(\frac{\lambda}{2} \right) \right\}}. \tag{4.26}$$

Hence, given the mean m of the input code bit extrinsic messages $\lambda \sim \mathcal{N}(m, 2m)$, the asymptotic SNR of both the SIC-MMSE receiver and that of the SIC-MF receiver can be solved numerically based on (4.21) and (4.26), respectively.

2. Multi-cell Systems

Based on the model of the multi-cell wireless system described in Section 2, we next derive the asymptotic SNR for both the SIC-MMSE and the SIC-MF receivers in the multi-cell scenario. Again, for the post soft-cancellation signals, we consider an equivalent system which contains $7K$ users with the signal amplitudes $\left\{ \tilde{A}_k \right\}_{k=1}^{7K}$. Define $\tilde{A}_1 = A_1$, $\tilde{A}_k = A_k \sqrt{1 - \tilde{b}_k(i)^2}$, for $k = 2, \cdots, K$, and $\tilde{A}_k = A_k$, for $k = K+1, \cdots, 7K$. Assume $A_1 = \cdots = A_K \stackrel{\triangle}{=} A$, $A_{K+1} = \cdots = A_{7K} \stackrel{\triangle}{=} A/\sqrt{12}$. Our receiver performs SIC-MMSE for in-cell interference and it performs linear MMSE for out-cell interference. Therefore, there are two types of interference: the in-cell interference in the form of (4.20), and the out-cell interference with power $\frac{A^2}{12}$. Assume that all cells have the same number of users, then using (4.16), we have

$$E_P \left[I(P, P_1, \gamma) \right] = \frac{1}{7} E_\lambda \left\{ \frac{A^4 \left[1 - \tanh^2 \left(\frac{\lambda}{2} \right) \right]}{A^2 + \gamma A^2 \left[1 - \tanh^2 \left(\frac{\lambda}{2} \right) \right]} \right\} + \frac{6}{7} \frac{\frac{A^4}{12}}{A^2 + \gamma \frac{A^2}{12}}. \tag{4.27}$$

The asymptotic SNR for multi-cell system is then given by

$$\begin{aligned} \gamma &= \frac{P_1}{\sigma^2 + 7\alpha E_P \left[I\left(P, P_1, \gamma\right) \right]} \\ &= \frac{1}{\frac{\sigma^2}{A^2} + \alpha \left(E_\lambda \left\{ \frac{1 - \tanh^2(\frac{\lambda}{2})}{1 + \gamma \left[1 - \tanh^2(\frac{\lambda}{2}) \right]} \right\} + \frac{\frac{1}{2}}{1 + \frac{\gamma}{12}} \right)}. \end{aligned} \tag{4.28}$$

The unique solution γ to (4.28) can be found again using the Newton iterative method.

For the SIC-MF receiver, we have

$$E_P[P] = \frac{A^2}{7} E_\lambda \left\{ 1 - \tanh^2 \left(\frac{\lambda}{2} \right) \right\} + \frac{6}{7} \frac{A^2}{12}. \tag{4.29}$$

Substituting (4.29) to (4.25), we obtain the asymptotic SNR for the SIC-MF receiver in the multi-cell scenario, given by

$$\gamma = \frac{P_1}{\sigma^2 + 7\alpha E_P\left[P\right]} = \frac{1}{\frac{\sigma^2}{A^2} + \alpha \left(E_\lambda \left\{ 1 - \tanh^2 \left(\frac{\lambda}{2} \right) \right\} + \frac{1}{2} \right)}. \tag{4.30}$$

D. Coding-spreading Tradeoff Analysis

In [47], the theoretical analysis of coding-spreading efficiency for linear multiuser detection is based on the assumption of ideal decoding. In this chapter, since we consider the tradeoff problem for turbo multiuser detection, the ideal decoding does not facilitate the coding-spreading analysis. Thus we assume users employ LDPC codes because the LDPC code offers near-capacity performance and at the same time, admits an analytical framework on its performance analysis based on the density evolution technique.

1. Density Evolution

We first evaluate iterative turbo multiuser detection using density evolution with Gaussian approximation for the extrinsic messages. Consider a turbo receiver in Fig. 1. The receiver can be viewed as a nonlinear dynamic feedback system. The extrinsic information messages $\{\lambda_i\}$ are iteratively passed between the SISO multiuser detector and the SISO channel decoders. When the interleaver is very large and random, the extrinsic information messages are independent and identically distributed. In [8], it

is shown that the pdf of the extrinsic messages at the output of each check and bit node can be approximated as Gaussian and symmetric (i.e., the variance is twice the mean). We now demonstrate the validity of Gaussian assumption for bit node through the following example. Consider estimating the pdf for the extrinsic information at the output of the LDPC decoder for a five-user synchronous rate-$\frac{1}{2}$ (3,6) LDPC coded CDMA system with random spreading and the processing gain $N = 10$ when E_b/N_o=1.75 dB. The receiver employs the SIC-MMSE multiuser detector. Fig. 23 shows the histograms of the extrinsic information at the LDPC decoder output at different iteration stages by simulating the channel, the detector and LDPC decoder. The symmetric Gaussian pdf's with the corresponding means are also shown in the same figure. It is seen there is a little mismatch between the exact pdf and the Gaussian approximation at the first iteration. As the iteration goes on, when the probability of error becomes smaller and smaller, the match between the exact pdf and the Gaussian approximation gets quite close.

The extrinsic message of the SIC-MMSE multiuser detector is given by (4.5). As discussed in [14], the output $z_k(i)$ of the instantaneous linear MMSE filter is well approximated by a Gaussian distribution. Hence $L^q_{m\to L}[b_k(i)]$ has a Gaussian distribution with mean and variance given respectively by

$$E\{L^q_{m\to L}[b_k(i)]\} = \left(\frac{2}{1-\mu_k(i)}\right) E\{z_k(i)\} = \frac{2\mu_k(i)b_k(i)}{1-\mu_k(i)}, \tag{4.31}$$

$$\mathrm{Var}\{L^q_{m\to L}[b_k(i)]\} = \left(\frac{2}{1-\mu_k(i)}\right)^2 \mathrm{Var}\{z_k(i)\} = \frac{4\mu_k(i)}{1-\mu_k(i)}. \tag{4.32}$$

Thus the extrinsic $L^q_{m\to L}[b_k(i)]$ message has a Gaussian distribution of the form

$$L^q_{m\to L}[b_k(i)] \sim \mathcal{N}\Big(m_k(i)b_k(i), 2m_k(i)\Big), \quad \text{with} \quad m_k(i) \stackrel{\triangle}{=} \frac{2\mu_k(i)}{1-\mu_k(i)}. \tag{4.33}$$

Hence the extrinsic messages passed from the SISO multiuser detector to the LDPC

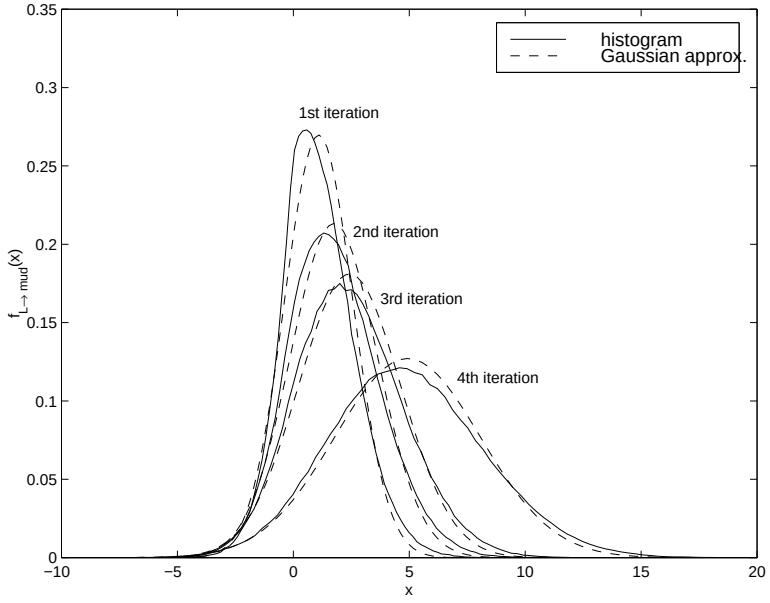

Fig. 23. The histograms for the extrinsic information of LDPC decoder in a 5-user synchronous CDMA system with the SIC-MMSE receiver, and the symmetric Gaussian approximations.

decoder are also symmetric Gaussian variable of the form $\mathcal{N}(2\text{SNR}, 4\text{SNR})$.

Consider the input and the output extrinsic messages of the multiuser detector and the channel decoder at each iteration as shown in Fig. 24, where SNR1_{in}, SNR1_{out} denote the input and the output SNRs of the multiuser detector, and SNR2_{in}, SNR2_{out} denote the input and the output SNRs of the LDPC decoder. We have the relationship $\text{SNR2}_{in} = \text{SNR1}_{out}$ and $\text{SNR1}_{in} = \text{SNR2}_{out}$. Starting with $\text{SNR1}_{in} = 0$, the multiuser detector produces a nonzero SNR2_{out} for the output extrinsic information. For a certain value of E_s/N_0, the output of the detector SNR1_{out} is the function of the input SNR1_{in} and E_s/N_0, i.e., $\text{SNR1}_{out} = \Gamma_1(\text{SNR1}_{in}, E_s/N_0)$. The output of the decoder SNR2_{out} is the function of the input SNR2_{in}, so we have $\text{SNR2}_{out} = \Gamma_2\left(\text{SNR2}_{in}\right) = \Gamma_2\left(\Gamma_1(\text{SNR1}_{in}, E_s/N_0)\right)$.

We can test the convergence by tracking the evolution of the extrinsic informa-

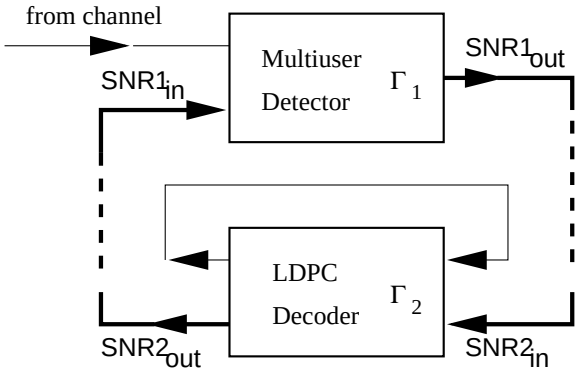

Fig. 24. Dynamic system analysis of turbo multiuser detection.

tion's SNR for both the detector and the decoder. We plot the SNR characteristic curves of output SNR of detector versus its input SNR, and the input SNR of the decoder versus its output SNR. Given the extrinsic message SNR of the LDPC decoder $\mathrm{SNR1}_{in}$, we have $\lambda \sim \mathcal{N}(2\mathrm{SNR1}_{in}, 4\mathrm{SNR1}_{in})$. The function Γ_1 can then be evaluated using Monte Carlo method for finite-size systems and using (4.16) and (4.25) for large systems. The decoder function Γ_2 is evaluated by using the density evolution method in [8], which computes the output distribution given the input distribution of the extrinsic information from the multiuser detector, i.e., $\lambda \sim \mathcal{N}(2\mathrm{SNR2}_{in}, 4\mathrm{SNR2}_{in})$. As afore mentioned, the SNRs of the input and output of Γ_1 and Γ_2 are equal to half of the mean of the extrinsic information, i.e., $\mathrm{SNR} = E\{\lambda\}/2$. An example is plotted in Fig. 25. A (3,6) regular LDPC code with $\frac{1}{2}$ code rate is used. The upper curve corresponds to the input-output function Γ_1 for the SIC-MMSE multiuser detector, and the lower curve corresponds to Γ_2^{-1} for the LDPC decoder. Fig. 25 graphically shows the progress of the turbo iterations. The improvement on the SNR of the extrinsic information follows a staircase path reflecting at right angles between the SNR characteristic curves of Γ_1 and Γ_2^{-1}. The SNR improvement steps are large when two characteristic curves are far apart, and small when they are close. There is a narrow *iterative decoding tunnel* between the curves. We can see that after five iterations,

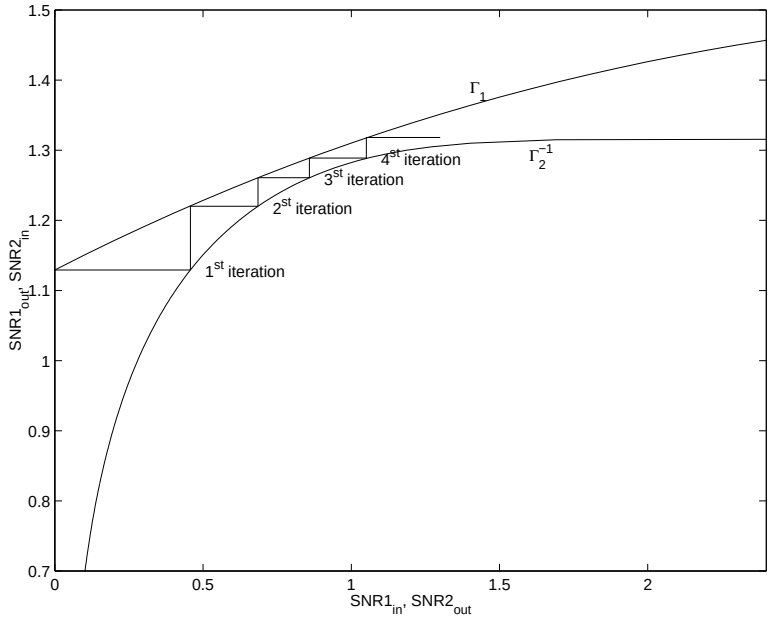

Fig. 25. SNR characteristic curves of turbo multiuser detection.

the steps pass through the tunnel successfully. This means SNR of λ goes to infinity and the bit-error-rate (BER) goes to zero.

The SNR characteristic curve of the multiuser detector, i.e., the function Γ_1, is determined by E_s/N_0. The initial displacement of the Γ_1 curve for $\text{SNR1}_{in} = 0$ depends on the value of E_s/N_0, as well as the whole SNR progress curve. Therefore, it will decide the distance between the Γ_1 and the Γ_2^{-1} curves. When E_s/N_0 increases, the Γ_1 curve moves away from the Γ_2^{-1} curve. When E_s/N_0 decreases, the Γ_1 curve moves close to the Γ_2^{-1} curve, and the tunnel becomes narrower. If at a certain value of E_s/N_0, the two curves become tangent to each other at some point, the iterative decoding tunnel is closed at the tangent point and the extrinsic SNR improvement path can not pass the point. That means the receiver can not achieve zero-error decoding. Such an E_s/N_0 value represents the threshold of the receiver.

2. Coding-spreading Tradeoff

First, we introduce the separation of coding-spreading factors. Assume each user sends information at rate of R bits/second. The transmission bandwidth available is W. The bandwidth expansion factor is then defined as

$$\Omega = \frac{2W}{R}. \tag{4.34}$$

Based on Proposition 1 in [47], we can separate the bandwidth expansion into a coding component with code rate ν bits/symbol and a spreading component with spreading factor N. We have

$$\frac{E_s}{N_0} = N\frac{E_c}{N_0}, \quad \text{and} \quad \frac{E_b}{N_0} = \Omega\frac{E_c}{N_0}, \tag{4.35}$$

where E_c is the energy per chip. Then we have

$$\Omega = \frac{N}{\nu}, \quad \text{and} \quad \frac{E_s}{N_0} = \nu\frac{E_b}{N_0}. \tag{4.36}$$

Hence Γ_1 is a function of $\nu\frac{E_b}{N_0}$ or $\frac{N}{\Omega}\frac{E_b}{N_0}$.

Now, we investigate the problem of the coding-spreading tradeoff optimization. For given values of Ω and E_b/N_0, the spreading factor N and E_s/N_0 are determined by the code rate ν. For a certain code rate ν, we use the largest number of users K_m that can transmit their bits reliably on the channel as a measurement of the system performance. Clearly K_m is a function of Ω and ν. We define the ratio of K_m and Ω as the total *spectral efficiency* of the system in bits/chip at a code rate ν, given by

$$\kappa(\Omega, \nu) = \frac{K_m(\Omega, \nu)}{\Omega}. \tag{4.37}$$

Thus, the coding-spreading tradeoff is to find the optimized code rate ν which has

the maximum spectral efficiency, i.e.,

$$\nu^* = \arg\max_{\nu} \kappa(\Omega, \nu). \tag{4.38}$$

In a practical system, K_m can be determined by fixing system performance with an information BER threshold. It is useful to draw a conclusion about the coding-spreading tradeoff based on the ideal coding. In this chapter, we pick the capacity-achieving LDPC codes to analyze the coding-spreading tradeoff.

By the analysis of the density evolution of the extrinsic information above, we can solve the tradeoff problem for turbo multiuser detection along the following line. First, fix a total bandwidth expansion Ω and E_b/N_0. For a given code rate ν, we can get the extrinsic information SNR characteristic curve for the LDPC decoder Γ_2^{-1}. E_s/N_0 is fixed as $\nu E_b/N_0$ and the spreading gain $N = \Omega\nu$. Thus, with a certain number of users K contained in the cell, we can obtain the SNR characteristic curve for the detector function Γ_1. By investigating the existence of iterative decoding tunnel, we know if the system can support this number of users. Then for each possible user number K, we can obtain the extrinsic information SNR characteristic of the multiuser detector. The largest value of K can be found by the corresponding SNR curve of Γ_1 that does not intersect with the decoder curve of function Γ_2^{-1}. An example is shown in Fig. 26. The total expansion factor is set to 64 and $E_b/N_0 = 2$dB. The function Γ_2^{-1} curve in the plot is for the rate-$\frac{1}{2}$ $(3, 6)$ regular LDPC code. Six extrinsic information SNR characteristic curves with different number of users, $K = 16, \cdots, 21$, are shown in the same plot. We find the multiuser detector SNR curve with the maximum number user without touching the decoder curve is $K = 19$. Because the number of user of K is discrete, and a real code is used, the curve corresponding to $K = 20$ is the one which just touches the curve of decoder. Hence, $K_m(64, 0.5) = 20$ for this case. Then the spectral efficiency can be computed by (4.37). We can choose different regular

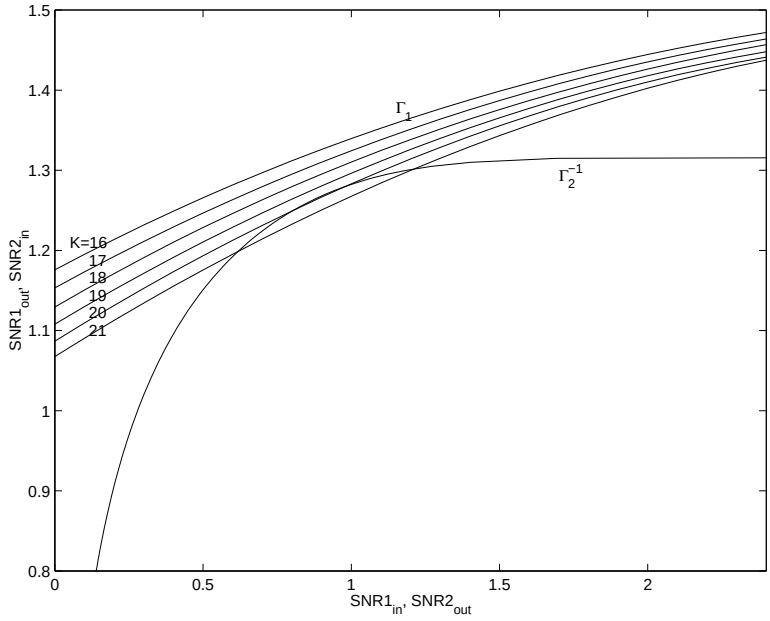

Fig. 26. Extrinsic SNR evolution curves for the SISO detector and decoder of finite-size systems.

LDPC codes to form a set of codes with different code rates. Then we can obtain the spectral efficiency for each code rate. The optimal code rate can then be obtained from (4.38).

3. Tradeoff Analysis in Large Systems

In large systems, $K, N \to \infty$. So instead of searching the largest K as in finite-size systems, we look for the largest value of $\alpha = \frac{K}{N}$ that can be supported by the system. No specific fixed bandwidth expansion Ω is required for large systems. The spectral efficiency is then defined as

$$\kappa(\nu) \stackrel{\triangle}{=} \alpha_m(\nu)\nu. \tag{4.39}$$

We can find the $\alpha_m(\nu)$ by analyzing the SNR evolution curves of the the multiuser detector and decoder. For a give code rate ν, the extrinsic information SNR evo-

lution curve of function Γ_2^{-1} is obtained in the same way as before. The curve of function Γ_1 can be obtained from the equations of the output extrinsic SNR γ derived in Section C. As afore mentioned, the extrinsic information λ is approximated as symmetric Gaussian distributed with the mean equal to twice of SNR, i.e., $\lambda \sim \mathcal{N}(2\text{SNR}, 4\text{SNR})$. Thus, the large-system output SNR of the detector SNR1_{out} is the solution of γ, the input SNR for the detector SNR1_{in} is half mean of the input λ, i.e., $\lambda \sim \mathcal{N}(2\text{SNR1}_{in}, 4\text{SNR1}_{in})$. The value of E_s/N_0 is determined by the code rate ν and E_b/N_0, which translates into A^2/σ^2 in the expressions of the asymptotic output SNR γ. We can plot the large-system multiuser detector SNR evolution curves with different values of α. By investigating the iterative detection tunnel, we can find the largest value of α which the system can support. The spectral efficiency can then be computed by (4.39).

E. Results

1. Single-cell Systems

We first present the results in the single-cell scenario. The value of the bandwidth expansion factor Ω is set to 64. For the regular LDPC code, the rate can be computed as

$$R = 1 - \frac{d_v}{d_c}, \tag{4.40}$$

where d_v and d_c are degrees of variable nodes and check nodes, respectively. The regular (d_v, d_c) LDPC codes with different code rate can be built as follows: fix $d_v = 3$, choose $d_c = 4, 5, 6, 7, \cdots$. Then we get a set of regular LDPC codes with rate equals to $0.25, 0.4, 0.5, 0.57, \cdots$. The entire code rate ν is the product of LDPC code rate and number of bits per symbol in modulation mapping. For BPSK case, $\nu = R$.

Fig. 27 shows the spectral efficiency results for finite-size systems. The curves of $\kappa(\Omega, \nu)$ over code rate ν with $E_b/N_0 = 2$dB and 3dB for both turbo receivers are plotted. In the finite system, we use aperiodic random spreading, i.e., the spreading sequence varies from symbol to symbol. We can see the SIC-MMSE receiver has high spectral efficiency at the code rate interval between $\nu = 0.4$ to 0.6, while the SIC-MF receiver favors a large range of code rate ν smaller than 0.5. For $E_b/N_0 = 3$dB, the maximum spectral efficiency (κ^*) for the SIC-MF receiver equals $22/64 \approx 0.34$ bits/chip at code rate $\nu^* = 0.4$. The maximum spectral efficiency for the SIC-MMSE receiver is $34/64 \approx 0.53$ bits/chip at code rate $\nu^* = 0.5$. For $E_b/N_0 = 2$dB, $\kappa^* = 14/64 \approx 0.22$ bits/chip at code rate $\nu^* = 0.4$ for the SIC-MF, and $\kappa^* = 22/64 \approx 0.34$ bits/chip at code rate $\nu^* = 0.4$ for the SIC-MMSE receiver. It is obvious that the maximum spectral efficiency of the SIC-MMSE receiver is much higher than that of the SIC-MF receiver, which is different from the result for the single-user LMMSE receiver in [47]. Comparing the performance at other code rates, we find that the SIC-MMSE receiver has a significant gain in spectral efficiency at the optimal code rate, while the SIC-MF receiver only sees a marginal gain in spectral efficiency at the optimal code rate.

The asymptotic spectral efficiency results in large systems are shown in Fig. 28 and Fig. 29. When $E_b/N_0 = 3$dB, the maximum spectral efficiency $\kappa^* = 0.52$ bits/chip at the code rate $\nu^* = 0.5$ for the SIC-MMSE receiver, and $\kappa^* = 0.31$ bits/chip at $\nu^* = 0.4$ for the SIC-MF receiver. When $E_b/N_0 = 2$dB, $\kappa^* = 0.32$ bits/chip at the code rate $\nu^* = 0.4$ for the SIC-MMSE receiver, and $\kappa^* = 0.19$ bits/chip at $\nu^* = 0.4$ for the SIC-MF receiver. We can see that the spectral efficiency results of large systems match very well with those of finite-size systems. Thus, we get the same conclusions of the spectral efficiency as in finite systems. The spectral efficiency results of some high E_b/N_0 values are shown in Fig. 29. The gap between the SIC-MMSE receiver

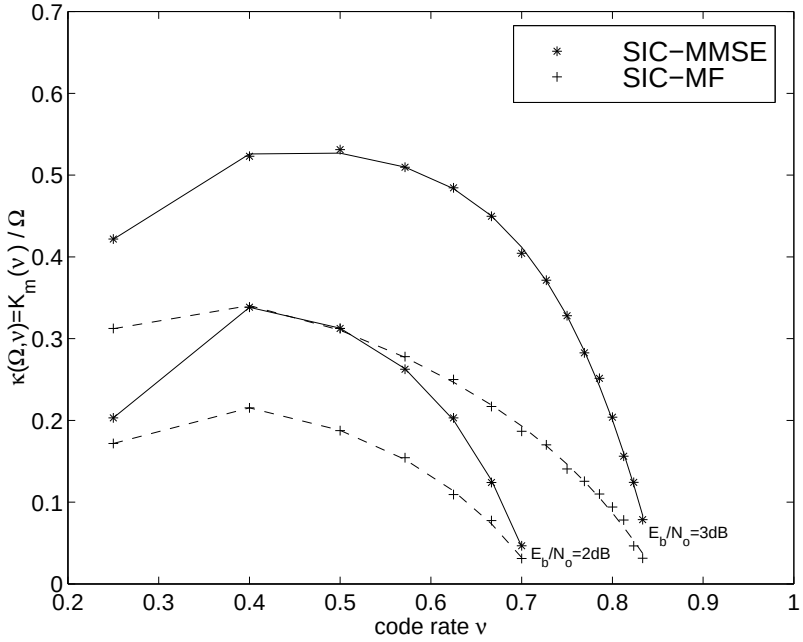

Fig. 27. Spectral efficiency of finite-size systems in the single-cell scenario; $\Omega = 64$.

and the SIC-MF receiver is enlarged. The optimal code rate for the SIC-MMSE receiver remains at the middle range of the code rate when E_b/N_0=6dB. When E_b/N_0 increases to 12dB or 18dB, the optimal code rate shifts to the range of higher code rate, i.e., (0.6, 0.85). The optimal code rate for the SIC-MF receiver exists in the range of low coding rates. This means that the SIC-MMSE receiver favors spreading while the SIC-MF receiver favors coding. The maximum spectral efficiencies for the SIC-MMSE receiver are 0.88, 1.15 and 1.23 bits/chip, for E_b/N_0 =6dB, 12dB and 18dB, respectively. And the corresponding maximum special efficiencies for the SIC-MF receiver are 0.50, 0.63 and 0.66 bits/chip. The optimum spectral efficiencies for the LMMSE receiver with single-user decoding presented in [47] are around 0.72, 1.0 and 1.1 bits/chip, respectively. Hence, the SIC-MMSE multiuser detection with joint-decoding offers better optimum spectral efficiency than the LMMSE multiuser detection with single-user decoding.

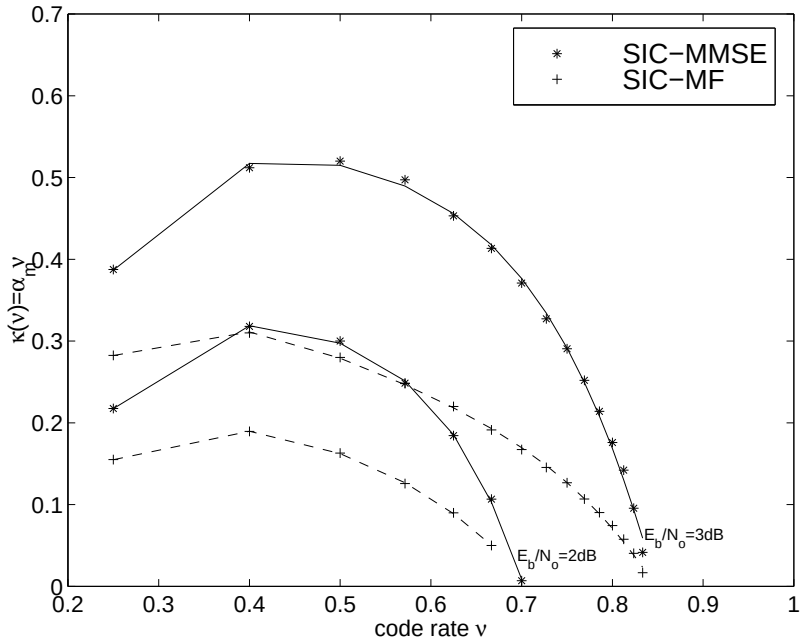

Fig. 28. Spectral efficiency of large systems in the single-cell scenario.

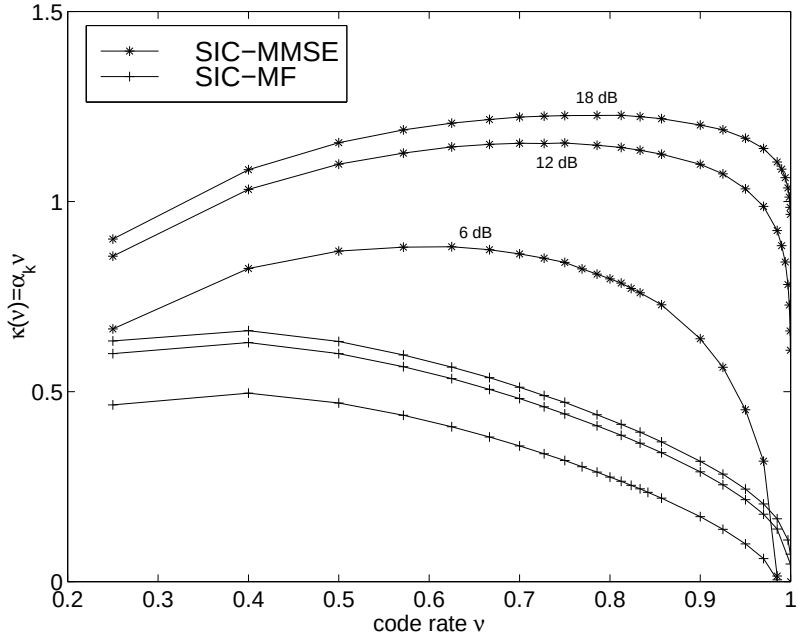

Fig. 29. Spectral efficiency of large systems in the single-cell scenario: E_b/N_0 =6dB, 12dB, 18dB.

Hence, we can see in the single-cell system, the turbo multiuser receiver with the SIC-MMSE detector has significant gain in spectral efficiency over the corresponding receiver employing the SIC-MF detector when both perform at the optimal code rate. It also offers higher optimum spectral efficiency than the linear multiuser detector.

2. Multi-cell Systems

Recall that in the multi-cell scenario, the turbo multiuser receiver only performs soft interference cancellation for the in-cell users. Fig. 30 shows the spectral efficiency curves of turbo multiuser detectors in finite-size systems. For $E_b/N_0 = 3$dB, the maximum spectral efficiency (κ^*) for the SIC-MF receiver equals to $11/64 \approx 0.17$ bits/chip at code rate $\nu^* = 0.4$. The maximum spectral efficiency for the SIC-MMSE receiver is $13/64 \approx 0.20$ bits/chip at the optimal code rate $\nu^* = 0.4$. For $E_b/N_0 =$ 2dB, $\kappa^* = 6/64 \approx 0.09$ bits/chip at the optimal code rate $\nu^* = 0.4$ for the SIC-MF receiver, and $\kappa^* = 8/64 \approx 0.125$ bits/chip at code rate $\nu^* = 0.4$ for the SIC-MMSE receiver. The SIC-MF spectral efficiency is down by a factor of 1/2 when compared with single-cell results. And the gap between the spectral efficiency curves of the SIC-MMSE and the SIC-MF receivers is reduced. The optimal code rate with the maximum spectral efficiency κ^* is located at the middle code rate range, i.e., $\nu^* = 0.4$ for both receivers. Though not as significant as in the single-cell scenario, the SIC-MMSE receiver still outperforms the SIC-MF receiver when both operate at the optimal code rate. The multi-cell asymptotic spectral efficiency results in large systems are shown in Fig. 31. The results are consistent with those for finite-size systems. The spectral efficiency results of some high E_b/N_0 values are shown in Fig. 32. The optimum spectral efficiencies of the SIC-MMSE receiver are 0.38, 0.50 and 0.53 bits/chip for E_b/N_0 =6dB, 12dB and 18dB, respectively, which are much better than the results of the SIC-MF receiver: 0.28, 0.36 and 0.36 bits/chip.

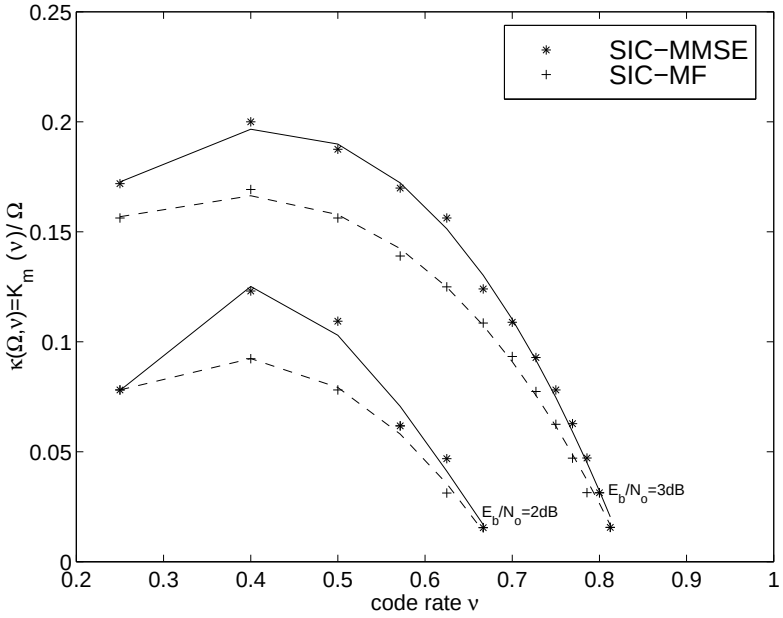

Fig. 30. Spectral efficiency of finite-size systems in the multi-cell scenario; $\Omega = 64$.

Comparing with the results of the LMMSE receiver with single-user decoding, 0.40, 0.48 and 0.50 bits/chip for E_b/N_0 =6dB, 12dB and 18dB, we find that the SIC-MMSE multiuser detector with joint-decoding has close results on optimum spectral efficiency with the LMMSE detector with single-user decoding in the multi-cell scenario.

3. Higher Order Constellations

Finally, we examine the coding-spreading tradeoff in systems with the QPSK and 8-PSK modulations. With QPSK modulation in large systems, it is shown in the Appendix A that

$$\kappa_{\mathrm{QPSK}}(\nu) = 2\kappa_{\mathrm{BPSK}}(\frac{\nu}{2}). \tag{4.41}$$

This relationship is also demonstrated by the simulation results of finite-size systems. Fig. 33 shows that the spectral efficiency results of the large systems match very well with the finite-size systems. Thus, we can use the results obtained previously for

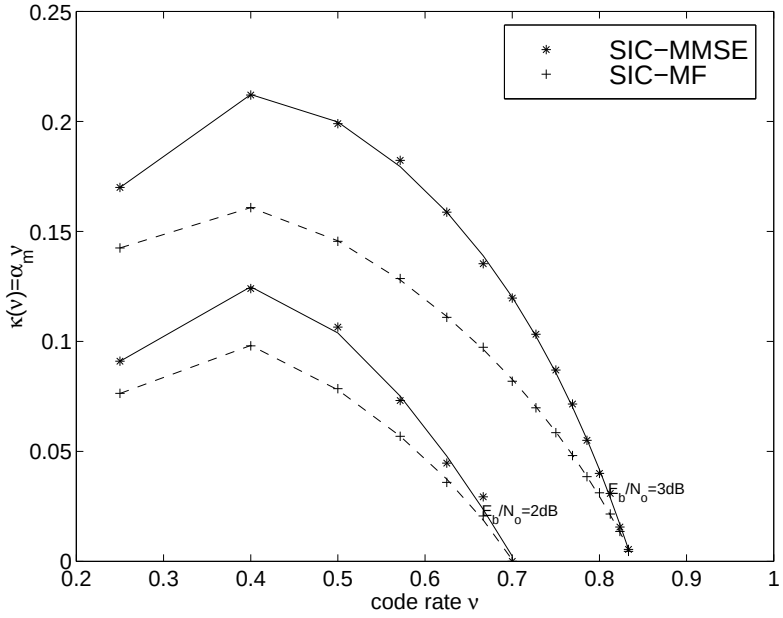

Fig. 31. Spectral efficiency of large systems in the multi-cell scenario.

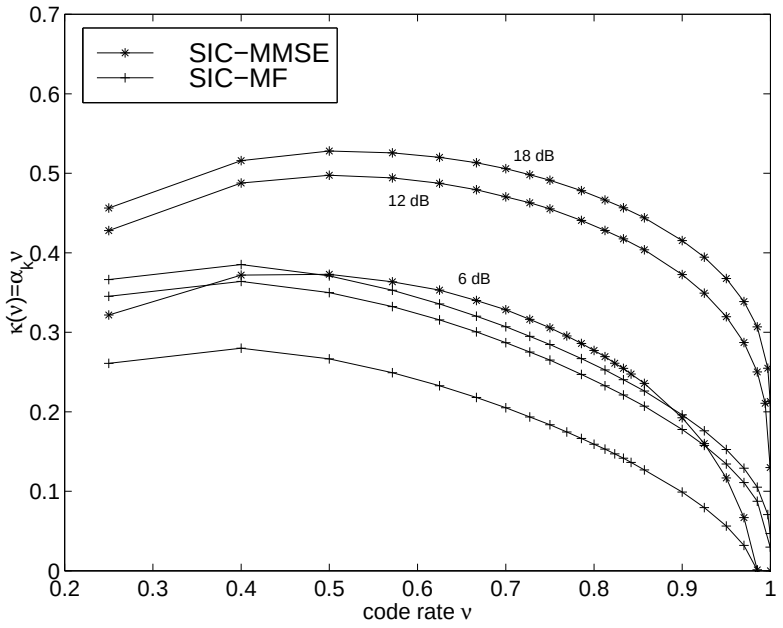

Fig. 32. Spectral efficiency of large systems in the multi-cell scenario: E_b/N_0 =6dB, 12dB, 18dB.

BPSK to present the results of QPSK, which are shown in Fig. 34 and Fig. 35. The optimal spectral efficiency of QPSK modulation is twice that of BPSK modulation in both single-cell and multi-cell scenarios.

The spectral efficiency curves of 8-PSK modulation are plotted in Fig. 36 for single-cell scenario and in Fig 37 for multi-cell scenario for large systems. Obviously, with higher order constellations the gap between the SIC-MMSE and the SIC-MF receivers is widened in both single-cell and multi-cell systems.

F. Conclusions

In this chapter, we have treated the coding-spreading tradeoff problem for turbo multiuser detection in synchronous CDMA system over AWGN channels by investigating the extrinsic SNR evolution dynamics of the SISO multiuser detectors and the LDPC channel decoders. Two types of SISO detectors, the SIC-MMSE detector and the SIC-MF detector, are considered. The spectral efficiency curves of the SIC-MMSE and the SIC-MF receiver for different code rate are obtained for both finite and large systems, in both single-cell and multi-cell scenarios. Numerical results demonstrate that in single-cell systems, the SIC-MMSE receiver offers a significant gain in spectral efficiency over the SIC-MF receiver. The results also show that the SIC-MMSE receiver outperforms the LMMSE receiver on the maximum spectral efficiency. In multi-cell systems, though the spectral efficiency gap between two receivers is reduced, the SIC-MMSE receiver still provides attendant gains over the SIC-MF receiver when both operate at the optimal code rates.

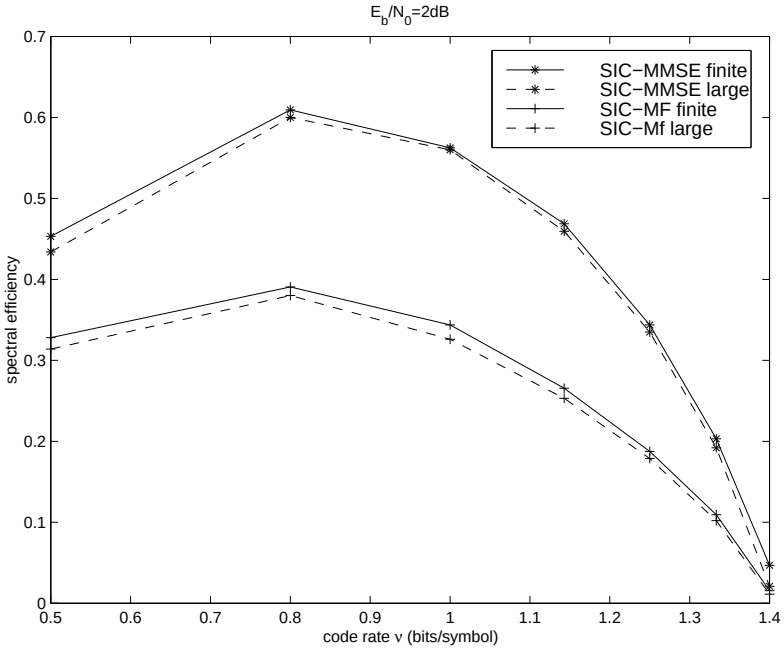

Fig. 33. Spectral efficiency of finite-size and large systems in the single-cell scenario: E_b/N_0 =2dB

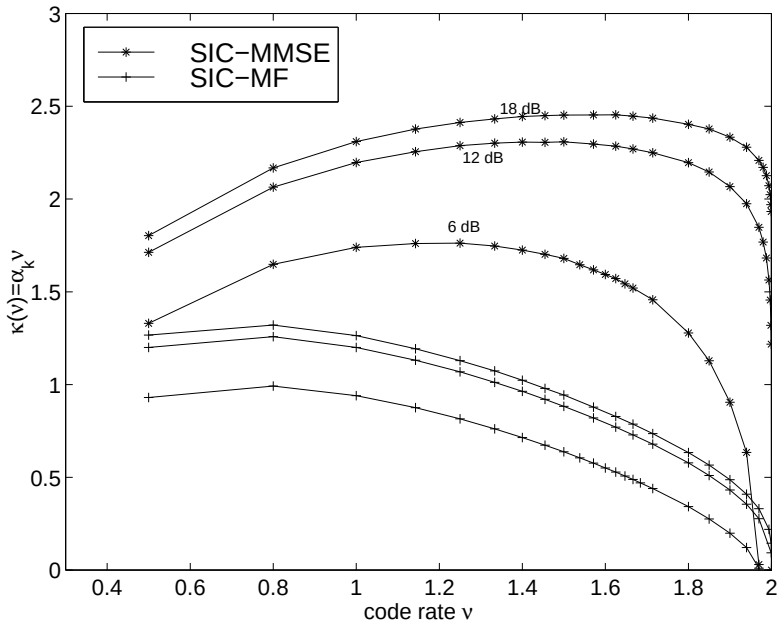

Fig. 34. Spectral efficiency of large systems in the single-cell scenario with QPSK modulation.

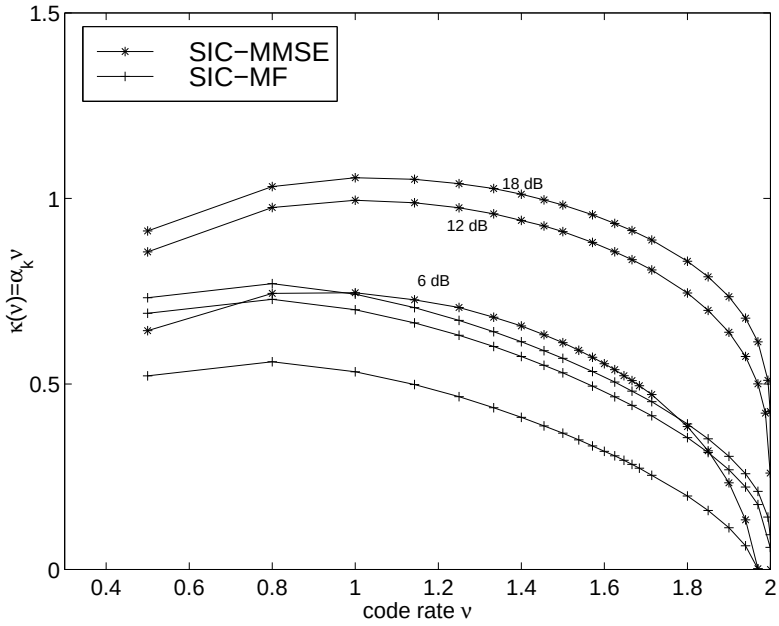

Fig. 35. Spectral efficiency of large systems in the multi-cell scenario with QPSK modulation.

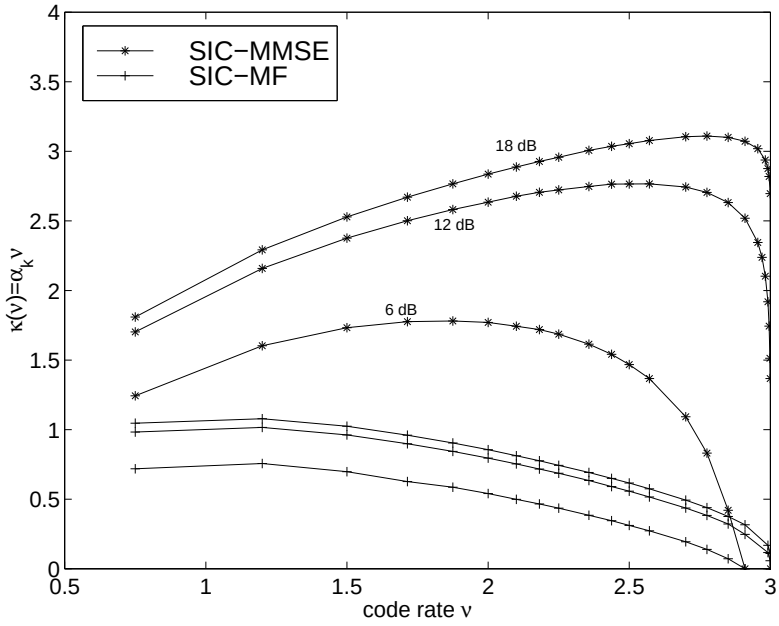

Fig. 36. Spectral efficiency of large systems in the single-cell scenario with 8-PSK modulation.

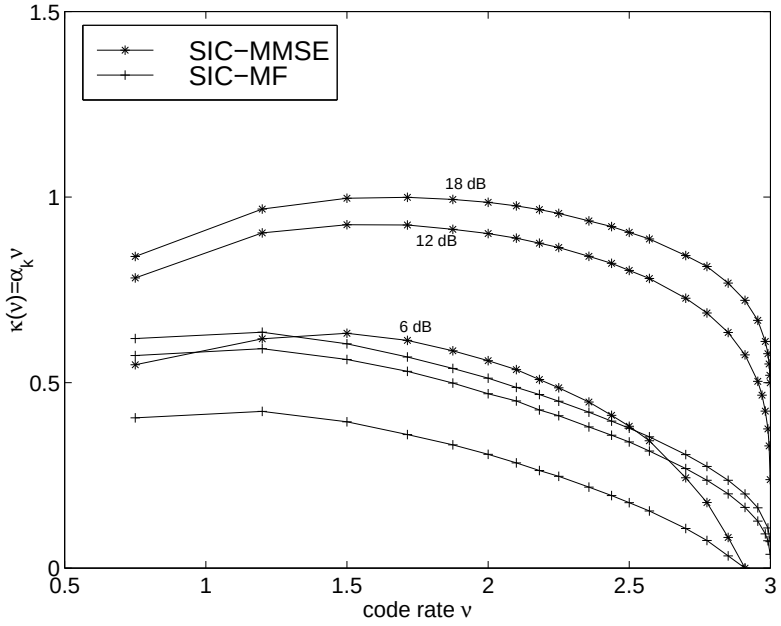

Fig. 37. Spectral efficiency of large systems in the multi-cell scenario with 8-PSK modulation.

CHAPTER V

DESIGN OF IRREGULAR REPEAT ACCUMULATE CODES FOR MIMO SYSTEMS WITH ITERATIVE RECEIVER

A. Introduction

During the past decade, random-like codes have drawn significant interest because they offer capacity-achieving performance. One of the important milestones is the re-discovery of the low-density parity-check (LDPC) codes [5], which were originally proposed by Gallager [6, 59]. The irregular LDPC codes were introduced in [7], which were shown to asymptotically achieve the capacity of the binary erasure channel (BEC) under iterative message-passing decoding. The complete design and performance analysis of irregular LDPC codes for memoryless channels based on density evolution and Gaussian approximation were treated recently in [8, 9]. It has been shown that carefully designed irregular LDPC codes can outperform parallel concatenated convolutional codes (PCCC) for long code lengths and provide performance within a fractional of a decibel from the AWGN channel capacity.

The repeat-accumulate (RA) code is another type of random-like code first proposed in [60] as turbo-like codes. It is a special case of both PCCC and serial concatenated convolutional codes (SCCC) with performance slightly inferior to the fully-fledged turbo codes [61]. The irregular repeat-accumulate (IRA) code first introduced in [62] is a systematic RA code with irregular repeat profiles. The Gaussian density evolution technique for LDPC code design is applied to the IRA code optimization in [62], and it is shown that the optimized IRA codes outperform turbo codes under different code lengths. Several design methods for IRA codes in memoryless channels are discussed and compared in [63]. The IRA codes offer performance close to that of

the irregular LDPC does. Compared with the LDPC codes, the IRA codes are more attractive from the implementation point of view, because the encoders are extremely simple and the decoding complexity is the same as that of the LDPC codes.

Communication by employing multiple transmit and receive antennas has become a promising solution for the next-generation high-speed wireless systems [31, 37, 34]. On the other hand, the turbo processing principle is a powerful paradigm for enhancing the system performance and has been successfully applied to many detection and decoding problems [12]. In this chapter, we consider the code design problem for IRA-coded MIMO systems employing iterative (turbo) receivers. Recently, the optimization of LDPC codes have been addressed in the context of turbo equalization [29] and turbo multiuser detection [43]. Here different from [29, 43] and following [64], we employ the EXIT chart technique to characterize the soft MIMO demodulator, based on which the IRA code optimization is carried out using density evolution. We also analyze the inherent relationship between the IRA code and the LDPC code ensembles based on their Tanner graph representations [65]. We show that such a relationship can be exploited to transform an optimized LDPC code into an optimized IRA code. It can also be used to design short-length IRA codes in block fading MIMO channels.

The remainder of this chapter is organized as follows. In Section B, we describe an IRA-coded MIMO system employing a turbo receiver. Two soft-input soft-output MIMO demodulation algorithms are discussed. In Section C, we discuss the density evolution analysis for IRA codes and the optimization of IRA codes for turbo MIMO systems. In Section D, we describe the mapping relationship between the IRA codes and the LDPC codes, and the transformation of an optimal LDPC code for MIMO system into the corresponding optimal IRA code. In Section E, we provide numerical results, and discuss the design of short-length IRA codes for block-fading channels.

Section F contains the conclusions.

B. System Descriptions

1. IRA Coded MIMO System

We consider an IRA coded MIMO system with n_T transmit antennas and n_R receive antennas, signaling through independent fading channels. The transmitter structure is illustrated in the upper portion of Fig. 38. A block of K information bits are encoded by a rate $R = K/N$ IRA code. The N coded bits $\{b_i\}$ are interleaved and modulated using the MPSK constellation into a block of N/M_c symbols $\{c_k\}$, where M_c is the constellation size. The MPSK symbols are demultiplexed to n_T streams and then transmitted by n_T transmit antennas simultaneously. After proper sampling, the received signal at the m-th receive antenna during the t-th time slot is given by

$$y_m(t) = \sqrt{\frac{\rho}{n_T}} \sum_{n=1}^{n_T} h_{mn}(t) c_{(t-1)n_T+n} + v_m(t), \quad m = 1, \cdots, n_R,\ t = 1, 2, \cdots, \quad (5.1)$$

where $h_{mn}(t)$ is the complex fading gain of the channel from the n-th transmit antenna to the m-th receive antenna during the t-th time slot; $v_m(t) \sim \mathcal{N}_c(0, 1)$ is the complex additive white Gaussian noise and ρ is the total received signal-to-noise ratio.

Denote $\boldsymbol{y}(t) \triangleq [y_1(t), \cdots, y_{n_R}(t)]^T$, $\boldsymbol{x}(t) \triangleq \left[c_{(t-1)n_T+1}, \cdots, c_{tn_T}\right]^T$, and $\boldsymbol{v}(t) \triangleq [v_1(t), \cdots, v_{n_R}(t)]^T$, and $\boldsymbol{H}(t)$ as an $n_R \times n_T$ matrix with $h_{mn}(t)$ being the (m, n)-th entry. Then (5.1) can be written in a vector form as

$$\boldsymbol{y}(t) = \sqrt{\frac{\rho}{n_T}} \boldsymbol{H}(t) \boldsymbol{x}(t) + \boldsymbol{v}(t). \quad (5.2)$$

With no channel state information (CSI) at the transmitter side but perfect CSI at the receiver side, assuming Gaussian signaling, the *ergodic capacity* for such MIMO

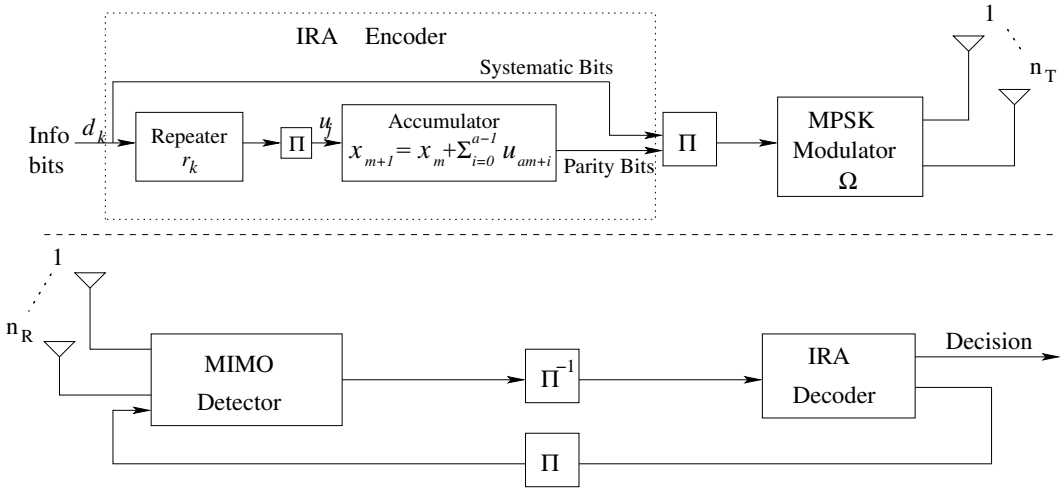

Fig. 38. An IRA-coded MIMO system with an iterative receiver.

channel is given by [34]

$$C(\rho) = \mathrm{E}\Big\{ \underbrace{\log_2 \det\left(\boldsymbol{I}_{n_R} + \frac{\rho}{n_T}\boldsymbol{H}\boldsymbol{H}^H\right)}_{\mathcal{I}(\rho,\,\boldsymbol{H})} \Big\}, \tag{5.3}$$

where $\mathcal{I}(\rho, \boldsymbol{H})$ is the instantaneous mutual information conditioned on the channel $\boldsymbol{H}$. When the transmitted symbols belong to a certain constellation, i.e., $\boldsymbol{x} \in \Omega^{n_T}$, the mutual information is computed instead as

$$\begin{aligned} \mathcal{I}(\rho, \boldsymbol{H}) \;=\; & n_T \log_2 |\Omega| \\ & - \frac{1}{|\Omega|^{n_T}} \sum_{j=0}^{|\Omega|^{n_T}-1} \mathrm{E}\Big\{ \log_2 \sum_{i=0}^{|\Omega|^{n_T}-1} \exp\Big[- \Big\| \sqrt{\frac{\rho}{n_T}}\boldsymbol{H}(\boldsymbol{x}_j - \boldsymbol{x}_i) + \boldsymbol{v} \Big\|^2 + \|\boldsymbol{v}\|^2 \Big] \Big\}, \end{aligned} \tag{5.4}$$

where the expectation is taken over the distribution of $\boldsymbol{v} \sim \mathcal{N}_c(\boldsymbol{0}, \boldsymbol{I}_{n_R})$. For MIMO systems in quasi-static block fading channels, for a given outage probability P_{out}, the

outage capacity $\overline{C}\left(\rho, P_{out}\right)$ is determined from the following equation:

$$P\left(\mathcal{I}(\rho, \boldsymbol{H}) \leq \overline{C}\right) = P_{out}. \tag{5.5}$$

2. IRA Encoding and Decoding

The schematic diagram of an IRA encoder is shown in the upper portion of Fig. 38. A block of information bits $\{d_k\}$ are encoded by an irregular repeat code with d_k repeated r_k times, where $\{r_k : 2 \leq r_k \leq D\}$ are the repetition degrees of $\{d_k\}$, D is the maximum repetition degree. The repeated bits are interleaved to obtain $\{u_j\}$, and then encoded by an accumulator, given by

$$x_{m+1} = x_m + \sum_{i=0}^{a-1} u_{am+i}, \quad m = 0, \cdots, M-1, \tag{5.6}$$

where x_m represents parity nodes with initial setting $x_0 = 0$; a is the grouping factor. The length of the parity bits is $M = n/a$, where $n = \sum_{k=1}^{K} r_k$. The final coded bits $\{b_i\}_{i=1}^{N}$ are the collection of the information bits $\{d_k\}_{k=1}^{K}$ and the parity bits $\{x_m\}_{m=1}^{N-K}$.

Similar to LDPC codes, we can represent the IRA codes by a Tanner graph [65], shown in Fig. 39. The IRA code ensemble is formed by all graphs of the form of Fig. 39. Note that $n = \sum_{k=1}^{K} r_k$ is the total number of edges connecting the information bit nodes and the check nodes. Define λ_i as the proportion of the edges connected to the information bit nodes with degree i, $i = 2, \cdots, D$, which satisfies $\sum_{i=2}^{D} \lambda_i = 1$. The rate of the codes is then given by

$$R = \frac{K}{K+M} = \frac{n \sum_i \lambda_i / i}{n \sum_i \lambda_i / i + \sum_i \lambda_i n / a} = \frac{a \sum_{i=2}^{D} \lambda_i / i}{1 + a \sum_{i=2}^{D} \lambda_i / i}. \tag{5.7}$$

We use a polynomial to represent the repetition profile of an IRA code ensemble, i.e.,

$$\lambda(x) = \sum_{i=2}^{D} \lambda_i x^{i-1}. \tag{5.8}$$

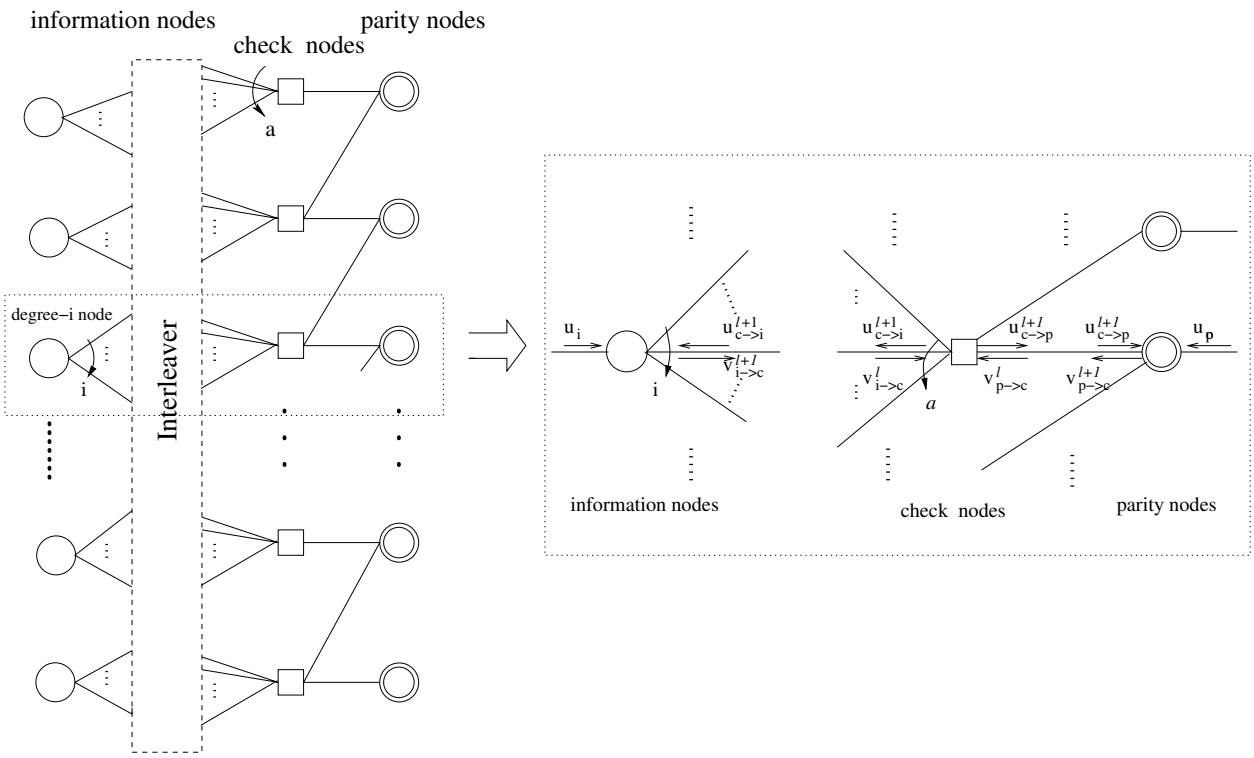

Fig. 39. Tanner graph and decoding of an IRA code.

With the Tanner graph representation, we can use the belief-propagation (BP) message-passing decoding algorithm which is similar to the LDPC decoding algorithm to decode the IRA code [66].

3. Turbo MIMO Receivers

A turbo MIMO receiver is employed for iterative joint MIMO detection and IRA decoding, as shown in the lower portion of Fig. 38. The extrinsic information of the IRA coded bits is iteratively passed between a soft MIMO detector and a soft belief-propagation IRA decoder. In each outer detection-decoding iteration, a number of inner iterations are performed within the soft IRA decoder during which the extrinsic information is passed along the edges in the Tanner graph of the IRA codes.

Two types of soft MIMO detectors are described next with the following no-

tations. All extrinsic information is in the log-likelihood-ratio (LLR) form and the variable L is used to refer to the extrinsic information. Superscript (q) is used to denote the q-th outer iteration. A subscript $M \rightarrow I$ denotes the message passed from the MIMO detector to the IRA decoder, and vice versa. For notational convenience, henceforth we drop the time index t.

MAP MIMO Detector

Assume perfect channel state information at the receiver. At the q-th turbo iteration, the soft MIMO detector computes the extrinsic information for the IRA coded bit b_i as

$$L^q_{M\rightarrow I}(b_i) = \Gamma\left(\boldsymbol{y}, \left\{L^{q-1}_{M\leftarrow I}(b_i)\right\}\right), \tag{5.9}$$

where $\boldsymbol{y}$ is the received data; $\left\{L^{q-1}_{M\leftarrow I}(b_i)\right\}$ is the extrinsic information computed by the IRA decoder in the previous stage. At the the first iteration, let $L^{q-1}_{M\leftarrow I}(b_i) = 0, \forall i$; $\Gamma(\cdot)$ denotes the MIMO detector function.

At a given time slot, n_T MPSK symbols corresponding to $M_c n_T$ IRA code bits are transmitted from the n_T transmit antennas. Denote

$$\mathcal{B}^+_k \triangleq \{(b_1, \cdots, b_{k-1}, +1, b_{k+1}, \cdots, b_{M_c n_T}) : b_j \in \{+1, -1\}, j \neq k\}. \tag{5.10}$$

Similarly define $\mathcal{B}^-_k$. With MPSK modulation, $\mathcal{B}^+_k$ is mapped to $\mathcal{C}^+_k$ and $\mathcal{B}^-_k$ to $\mathcal{C}^-_k$. Thus, the extrinsic output from the maximum *a posteriori* (MAP) MIMO detector is

given by

$$\begin{aligned} L^q_{M\to I}(b_k) &= \log\frac{P(b_k=+1|\boldsymbol{y})}{P(b_k=-1|\boldsymbol{y})} - \log\frac{P(b_k=+1)}{P(b_k=-1)} \\ &= \log\frac{\sum_{\boldsymbol{x}^+\in\mathcal{C}_k^+} P(\boldsymbol{y}|\boldsymbol{x}=\boldsymbol{x}^+)P(\boldsymbol{x}=\boldsymbol{x}^+)}{\sum_{\boldsymbol{x}^-\in\mathcal{C}_k^-} P(\boldsymbol{y}|\boldsymbol{x}=\boldsymbol{x}^-)P(\boldsymbol{x}=\boldsymbol{x}^-)} - \log\frac{P(b_k=+1)}{P(b_k=-1)} \\ &= \log\frac{\sum_{\boldsymbol{x}^+\in\mathcal{C}_k^+}\exp\Big[-\Big\|\boldsymbol{y}-\sqrt{\frac{\rho}{n_T}}\boldsymbol{H}\boldsymbol{x}^+\Big\|^2\Big]\prod_{j\neq k,b_j\in\mathcal{B}^+}P[b_j]}{\sum_{\boldsymbol{x}^-\in\mathcal{C}_k^-}\exp\Big[-\Big\|\boldsymbol{y}-\sqrt{\frac{\rho}{n_T}}\boldsymbol{H}\boldsymbol{x}^-\Big\|^2\Big]\prod_{j\neq k,b_j\in\mathcal{B}^-}P[b_j]}, \quad (5.11) \end{aligned}$$

$$\text{with}\ \ P(b_j) \triangleq P(b=b_j) = \frac{\exp\big(b_j L^{q-1}_{D\leftarrow I}(b_j)\big)}{1+\exp\big(b_j L^{q-1}_{D\leftarrow I}(b_j)\big)}. \quad (5.12)$$

SIC-MMSE MIMO Detector

We now describe a suboptimal soft MIMO detector based on soft interference cancellation and linear MMSE filtering, originally proposed for multiuser detection in [14].

Based on the *a priori* LLR of the code bits provided by the IRA decoder in the $(q-1)$-th stage, $\{L^{q-1}_{M\leftarrow I}(b_k)\}$, we first form the soft estimates of the MPSK symbol transmitted from the m-th antenna, given by

$$\tilde{x}_m = \sum_{x_q\in\Omega} x_q P(x_m=x_q) = \sum_{x_q\in\Omega} x_q \prod_{j=1}^{\log_2|\Omega|} P(\{x_q\}_j), \quad (5.13)$$

where $\{x_q\}_j$ denotes the j-th bit of the symbol x_q in constellation set Ω. Denote $\tilde{\boldsymbol{x}}_k \triangleq [\tilde{x}_1,\cdots,\tilde{x}_{k-1},0,\tilde{x}_{k+1},\cdots,\tilde{x}_{n_T}]^T$. Define

$$z_k \triangleq \sqrt{\frac{\rho}{n_T}}\boldsymbol{e}_k^T\boldsymbol{H}^H\Big(\frac{\rho}{n_T}\boldsymbol{H}\boldsymbol{V}_k\boldsymbol{H}^H+\boldsymbol{I}_{n_R}\Big)^{-1}\Big(\boldsymbol{y}-\sqrt{\frac{\rho}{n_T}}\boldsymbol{H}\tilde{\boldsymbol{x}}_k\Big), \quad (5.14)$$

$$\mu_k \triangleq \boldsymbol{e}_k^T\boldsymbol{H}^H\Big(\boldsymbol{H}\boldsymbol{V}_k\boldsymbol{H}^H+\frac{n_T}{\rho}\boldsymbol{I}_{n_R}\Big)^{-1}\boldsymbol{H}\boldsymbol{e}_k, \quad (5.15)$$

where

$$\boldsymbol{V}_k \triangleq \mathrm{diag}\left\{1-|\tilde{x}_1|^2,\cdots,1-|\tilde{x}_{k-1}|^2,1,1-|\tilde{x}_{k+1}|^2,\cdots,1-|\tilde{x}_{n_T}|^2\right\},$$

and $\boldsymbol{e}_k$ denotes an $n_R \times 1$ vector with all-zero entries, except for the k-th entry being 1. Then the extrinsic information $L^q_{D\to L}$ delivered by the SIC-MMSE MIMO detector is computed by

$$L^q_{M\to L}(b_i) = \log \frac{\sum\limits_{(x_q)_i=+1, x_q\in\Omega} \exp\Big\{-\frac{\|z_k-\mu_k x_q\|^2}{\mu_k-\mu_k^2}\Big\}\prod\limits_{j\neq i} P\Big(b=(x_q)_j\Big)}{\sum\limits_{(x_q)_i=-1, x_q\in\Omega} \exp\Big\{-\frac{\|z_k-\mu_k x_q\|^2}{\mu_k-\mu_k^2}\Big\}\prod\limits_{j\neq i} P\Big(b=(x_q)_j\Big)}, \tag{5.16}$$

where $(x_q)_i$ denote the bit in the symbol x_q corresponding to the bit b_i.

C. Optimization of IRA Codes via Density Evolution

1. Density Evolution for IRA Decoding

The details of density evolution for LDPC codes can be found in [9, 10]. In this section, following the same procedure, we formulate the density evolution for IRA decoding based on the belief-propagation decoding algorithm. Assuming the codeword length is infinite, the key of density evolution is to track the pdf of the extrinsic messages passing between the bit nodes and the check nodes in every iteration. Since there are no cycles in the Tanner graph when $N \to \infty$, the extrinsic messages can be modelled as independent random variables.

Let $u_{c\to i,j}$ denote the extrinsic message output from a check node passed along the jth edge to an information bit node and $v_{i\to c,j}$ denote the extrinsic message output from an information node passed along the jth edge to a check node. Similarly define $u_{c\to p,j}$ and $v_{p\to c,j}$. Denote u_i and u_p as the messages from the channel observation to the information node and parity node, respectively. As shown in Fig. 39, based on the sum-product algorithm [10], we can obtain the extrinsic message updated from

the ℓ-th stage to the $(\ell+1)$-th stage in the IRA decoder, given by

$$\tanh\frac{u_{c\to i,k}^{\ell+1}}{2} = \prod_{j=1,j\neq k}^{a}\tanh\frac{v_{i\to c,j}^{\ell}}{2}\prod_{j=1}^{2}\tanh\frac{v_{p\to c,j}^{\ell}}{2}, \tag{5.17}$$

$$\tanh\frac{u_{c\to p,k}^{\ell+1}}{2} = \prod_{j=1}^{a}\tanh\frac{v_{i\to c,j}^{\ell}}{2}\prod_{j=1,j\neq k}^{2}\tanh\frac{v_{p\to c,j}^{\ell}}{2}, \tag{5.18}$$

$$v_{i\to c,k}^{\ell+1} = \sum_{j=1,j\neq k} u_{p\to i,j}^{\ell+1} + u_i, \tag{5.19}$$

$$v_{p\to c,k}^{\ell+1} = \sum_{j=1,j\neq k}^{2} u_{p\to c,j}^{\ell+1} + u_p. \tag{5.20}$$

Let $f_{i\to c}^{\ell}(x)$ and $f_{p\to c}^{\ell}(x)$ denote the pdf of extrinsic messages passed from an information bit node to a check node, i.e., $v_{i\to c}^{\ell}$, and from a parity bit node to a check node, i.e., $v_{p\to c}^{\ell}$, respectively, during the ℓ-th iteration. Similarly define $f_{c\to i}^{\ell}(x)$ and $f_{c\to p}^{\ell}(x)$. From (5.19) and (5.20), we can see that the pdf of the output extrinsic message at an information or parity node is the convolution of the pdf's of the outgoing message. For (5.17) and (5.18), we can define function $\gamma(x) = \left(\mathrm{sgn}(x), \log\tanh|\frac{x}{2}|\right)$ to transform multiplication to summation. Denote $\mathcal{F}(f(x))$ as the output pdf of function $\gamma(x)$ when input $x \sim f(x)$. Similarly, $\mathcal{F}^{-1}(f(y))$ is denoted as the output pdf of function $\gamma^{-1}(y)$ when input $y \sim f(y)$. Then, the pdf's of the messages passed in the decoder at the $(\ell+1)$-th iteration can be computed by

$$f_{c\to i}^{\ell+1}(x) = \mathcal{F}^{-1}\left(\mathcal{F}\left(f_{i\to c}^{\ell}(x)\right)^{\otimes(a-1)}\otimes\mathcal{F}\left(f_{p\to c}^{\ell}(x)\right)^{\otimes 2}\right), \tag{5.21}$$

$$f_{c\to p}^{\ell+1}(x) = \mathcal{F}^{-1}\left(\mathcal{F}\left(f_{i\to c}^{\ell}(x)\right)^{\otimes a}\otimes\mathcal{F}\left(f_{p\to c}^{\ell}(x)\right)\right), \tag{5.22}$$

$$f_{i\to c}^{\ell+1}(x) = \sum_{i=2}^{D}\lambda_i f_{c\to i}^{\ell+1}(x)^{\otimes(i-1)}\otimes f_u(x), \tag{5.23}$$

$$f_{p\to c}^{\ell+1}(x) = f_{c\to p}^{\ell+1}(x)\otimes f_u(x), \tag{5.24}$$

where $\otimes$ denotes convolution, $^{\otimes i}$ denotes i-fold convolution, $f_u(x)$ is the pdf of the

channel observation messages.

We now apply the Gaussian approximation to the pdf of the extrinsic message as described in [8]. Denote m_u, $\tilde{m}_u$, m_{u_0} as the means of the extrinsic messages from the check node to the information node, from the check node to the parity node, and from the channel, respectively. Define $\phi(x) = 1 - E\left[\tanh\left(\frac{u}{2}\right)\right]$, where $u \sim \mathcal{N}(x, 2x)$, and $\phi(0) = 1$. Thus,

$$m_u^{\ell+1} = \phi^{-1}\Big(1 - \Big[1 - \sum_{i=2}^{D} \lambda_i \phi\left((i-1)m_u^{\ell} + m_{u_0}\right)\Big]^{a-1} \cdot \Big[1 - \phi\left(\tilde{m}_u^{\ell} + m_{u_0}\right)\Big]^2\Big), \tag{5.25}$$

$$\tilde{m}_u^{\ell+1} = \phi^{-1}\Big(1 - \Big[1 - \sum_{i=2}^{D} \lambda_i \phi\left((i-1)m_u^{\ell} + m_{u_0}\right)\Big]^{a} \cdot \Big[1 - \phi\left(\tilde{m}_u^{\ell} + m_{u_0}\right)\Big]\Big). \tag{5.26}$$

Next, define $r^{\ell} \triangleq \sum_{i=2}^{D} \lambda_i \phi\left((i-1)m_u^{\ell} + m_{u_0}\right)$ and $\tilde{r}^{\ell} \triangleq \phi\left(\tilde{m}_u^{\ell} + m_{u_0}\right)$. Then, substitute r and $\tilde{r}$ into (5.25) and (5.26), we obtain

$$r^{\ell+1} = \sum_{i=2}^{D} \lambda_i \phi\left(m_{u_0} + (i-1)\phi^{-1}\left(1 - (1-r^{\ell})^{a-1}(1-\tilde{r}^{\ell})^2\right)\right), \tag{5.27}$$

$$\tilde{r}^{\ell+1} = \phi\left(m_{u_0} + \phi^{-1}\left(1 - (1-r^{\ell})^{a-1}(1-\tilde{r}^{\ell})^2\right)\right). \tag{5.28}$$

For error-free decoding, m_u must grow to infinity, i.e., $m_u^{\ell+1} > m_u^{\ell}$ for any ℓ. Equivalently, we have $r^{\ell+1} < r^{\ell}$. Define

$$h(s, r, \tilde{r}) = \sum_{i=2}^{d_1} \lambda_i h_i(s, r, \tilde{r}), \tag{5.29}$$

$$\text{with} \quad h_i(s, r, \tilde{r}) \triangleq \phi\Big(s + (i-1)\phi^{-1}\left(1 - (1-r)^{a-1}\left(1-\tilde{r}\right)^2\right)\Big), \tag{5.30}$$

$$\text{and} \quad \tilde{h}(s, r, \tilde{r}) \triangleq \phi\Big(s + \phi^{-1}\left(1 - (1-r)^{a}\left(1-\tilde{r}\right)\right)\Big). \tag{5.31}$$

Therefore, we obtain the IRA code ensemble optimization method for AWGN channel

as

$$\underset{\{\lambda_i\},\, a}{\text{maximize}} \quad a\sum_{i=2}^{D}\lambda_i/i, \quad \text{s.t.} \quad r < h\left(m_{u_0}, r, \tilde{r}(r)\right) \text{ and } \sum_{i=2}^{D}\lambda_i = 1, \tag{5.32}$$

where $\tilde{r}(r)$ denotes the solution of

$$\tilde{r} = \tilde{h}\left(m_{u_0}, r, \tilde{r}\right), \tag{5.33}$$

with a given r. Note that the function $\phi(x)$ is monotonically decreasing. Then, given s, for all $r \in [0,1]$, the function $\tilde{h}\left(s, r, \tilde{r}\right)$ is monotonically increasing with $\tilde{r}$. Since $\tilde{h}(s,r,0) \geq 0$ and $\tilde{h}(s,r,1) \leq 1$, (5.33) has a unique solution in $[0,1]$.

2. IRA Code Optimization for MIMO

In this section, we present the density evolution-based IRA code optimization for MIMO systems with turbo receivers following [64]. First, let $\mathcal{G}_M(x,\rho)$ denote the EXIT transfer function of a MIMO detector and $\mathcal{G}_I(x)$ denote the EXIT transfer function of an IRA decoder. $\mathcal{G}_M(x,\rho)$ is the average mutual information between the extrinsic messages output from the MIMO detector and the IRA coded bits when the prior information input to the MIMO detector is symmetric Gaussian distributed and corresponding to an average mutual information x with a given channel SNR ρ. Similarly, $\mathcal{G}_I(x)$ is the output mutual information from the decoder when the input mutual information is x. An EXIT chart contains two curves: $\mathcal{G}_M(x,\rho)$ and $\mathcal{G}_I^{-1}(x)$. The output of the MIMO detector is the input of the IRA decoder. Hence, starting with $x = 0$, we can draw a stairway between the two curves showing the evolution of the mutual information with iterations. When $\mathcal{G}_I^{-1}(x) = 1$, it indicates error-free decoding. We have the following two properties of EXIT chart.

Convergence Property [67]: The turbo receiver evolutes to the error-free decoding state if and only if $\mathcal{G}_I^{-1}(x)$ lies below $\mathcal{G}_M(x,\rho)$ for $0 \leq x < 1$. This means no crossover

exists between the two curves and there is an iteration tunnel which ensures $\mathcal{G}_I(x)$ to approach 1.

Area Property [68]: For an erasure channel, the area $\mathcal{A}$ under the curve $\mathcal{G}_I(x)$ is equal to the rate of the outer code, i.e., $\mathcal{A} = \int_0^1 \mathcal{G}_I(x)dx = R$. This property holds only for the erasure channel. Nevertheless it is almost true in most practical situations. Or at least, it is true that the code rate is monotonically increasing with the area $\mathcal{A}$.

With these two properties, we can form the IRA code design rule for MIMO channels. Given a MIMO channel with a certain SNR and a MIMO detector, an IRA code is optimal if the EXIT transfer function of the decoder satisfies $\mathcal{G}_I^{-1}(x) = \mathcal{G}_M(x, \rho)$ with the desired code rate. Then, the optimized IRA code with the minimum SNR is our solution. Therefore, the IRA code optimization problem becomes finding the degree profile and the grouping factor of an IRA code with a target code rate such that the EXIT transfer function $\mathcal{G}_I(x)$ for the IRA decoder has the same or similar shape as that of the MIMO detector $\mathcal{G}_M(x, \rho_{\min})$. Define

$$J(x) \triangleq 1 - \int_{-\infty}^{\infty} \frac{e^{-((y-x)^2/4x)}}{2\sqrt{\pi x}} \log_2(1 + e^{-y})dy, \tag{5.34}$$

$$\gamma(\tilde{\lambda}, x, \tilde{x}) \triangleq R\sum_{i=2}^{D} \tilde{\lambda}_i J(ix) + (1 - R)J(2\tilde{x}). \tag{5.35}$$

The function $J(x)$ denotes the average mutual information between the coded bits and the extrinsic messages which are symmetric Gaussian distributed with pdf $\mathcal{N}(x, 2x)$. Therefore, $J^{-1}(x)$ denotes the mean of the extrinsic messages corresponding to an equivalent mutual information of x. The function $\gamma(\tilde{\lambda}, x, \tilde{x})$ represents the output mutual information of the IRA decoder when the extrinsic messages from the check to information bit are symmetric Gaussian distributed with mean x and variance $2x$, the check to parity bit extrinsic messages are also symmetric Gaussian with mean $\tilde{x}$ and variance $2\tilde{x}$, and $\tilde{\lambda}_i$ is the fraction of information bit nodes with degree-i in the

IRA code.

In order to design an IRA code with a desired EXIT transfer function $\mathcal{G}_I^{-1}(x) = \mathcal{G}_M(x, \rho)$, we first get G samples of the EXIT function of the MIMO detector where the input and output sequences are denoted as $\boldsymbol{u} = [u_1, \cdots, u_G]$ and $\boldsymbol{v} = [v_1, \cdots, v_G]$, respectively. That is, when the mean of input extrinsic LLRs of the IRA decoder from the channel is $J^{-1}(v_i)$, the output extrinsic information is u_i. Hence, the IRA code optimization problem for turbo MIMO channels can be summarized as follows:

$$\begin{aligned} \underset{\{\lambda_i\},\, a}{\text{maximize}} \quad & a \sum_{i=2}^{D} \lambda_i / i, \\ \text{s.t.} \quad & r > h\left(m_k, r, \tilde{r}(m_k, r)\right), \text{ with } \phi(\gamma^{-1}(\tilde{\lambda}, u_k)) < r \leq \phi(m_k),\ k = 1, 2, \cdots, G, \end{aligned} \tag{5.36}$$

where $m_k = J^{-1}(v_k)$.

The above nonlinear optimization problem can be solved by differential evolution [9]. We now simplify it to a linear optimization problem by making some approximations. The difficulty in optimizing (5.36) is that $\lambda(x)$ appears in the bound of r. To compute $\gamma^{-1}(\tilde{\lambda}, u_k)$, a pessimistic way of approximating (5.35) is to assume all information bit nodes have degree 2, i.e.,

$$\gamma(\tilde{\lambda}, x, \tilde{x}) \approx RJ(2x) + (1 - R)J(2\tilde{x}). \tag{5.37}$$

We find that this approximation is effective in obtaining good IRA codes.

The second approximation is to assume the output of the IRA decoder at the information node is a Gaussian distributed with mean $\sum_{i=2}^{D} i\tilde{\lambda}_i x$. That is,

$$\gamma(\tilde{\lambda}, x, \tilde{x}) \approx RJ\big(x \sum_{i=2}^{D} \tilde{\lambda}_i i\big) + (1 - R)J(2\tilde{x}). \tag{5.38}$$

Note that we have $\sum_{i=2}^{D} i\tilde{\lambda}_i = \frac{1-R}{R}a$. Thus,

$$\gamma(\tilde{\lambda}, x, \tilde{x}) \approx RJ\left(\frac{1-R}{R}ax\right) + (1-R)J(2\tilde{x}). \tag{5.39}$$

We further approximate $x \approx \tilde{x}$ by assuming the means of output extrinsic messages from the check nodes to the information nodes and to the parity nodes are same. Thus, given u_k, we can obtain

$$\bar{m}_k \approx \gamma^{-1}(\tilde{\lambda}, u_k), \quad \text{where} \quad u_k = \gamma(\tilde{\lambda}, \bar{m}_k) \approx RJ\left(\frac{1-R}{R}a\bar{m}_k\right) + (1-R)J(2\bar{m}_k). \tag{5.40}$$

With (5.40), the optimization problem (5.36) becomes a linear one and can be easily solved using any linear programming package. The procedure of the IRA code optimization can be summarized as follows.

Algorithm 1 [IRA code optimization for turbo MIMO]. *Given ρ, compute the output extrinsic information from the soft MIMO detector, i.e., $v_k = \mathcal{G}_M(u_k, \rho)$, $k = 1, \cdots, G$, by Monte Carlo simulation. Define $\boldsymbol{c} \stackrel{\triangle}{=} \left[\frac{1}{2}, \cdots, \frac{1}{D}\right]^T$ and $\boldsymbol{\lambda} \stackrel{\triangle}{=} [\lambda_2, \cdots, \lambda_D]$. Set $a_{\min}$ and $a_{\max}$.*

- *For $a = a_{\min}, \cdots, a_{\max}$*
  - *Draw samples r_j, $r_j \in \bigcup_k \big(\phi(\bar{m}_k), \phi(m_k)\big]$, $j = 1, 2, \cdots, Q$, where $\bar{m}_k = \gamma^{-1}(\tilde{\lambda}, u_k)$ according to (5.40), $m_k = J^{-1}(v_k)$. Compute $h_i(m_k, r_j, \tilde{r}_j)$ according to (5.30), $i = 2, \cdots, D$, where $\tilde{r}_j$ is the solution to $\tilde{r}_j = \tilde{h}(m_k, r_j, \tilde{r}_j)$ given by (5.31).*
  - *Define $\boldsymbol{b} \stackrel{\triangle}{=} [r_1, \cdots, r_Q]^T$ and form a matrix $\boldsymbol{A}$ by $[\boldsymbol{A}]_{j,i} = h_i(m_k, r_j, \tilde{r}_j)$.*
  - *Solve the following optimization problem via linear programming*

$$\max_{\boldsymbol{\lambda}} \ \boldsymbol{c}^T\boldsymbol{\lambda} \quad \text{s.t. } \boldsymbol{A}\boldsymbol{\lambda} - \boldsymbol{b} \leq \boldsymbol{0}. \tag{5.41}$$

- *Compute the IRA code rate R according to (5.7).*

- *Find the maximal code rate, R^*, and the corresponding $\{\boldsymbol{\lambda}, a\}$.*

If R^* reaches the target rate, the corresponding $\{\boldsymbol{\lambda}, a\}$ is the optimized profile for the turbo MIMO system. Otherwise, increase ρ and repeat the above procedures.

D. IRA-LDPC Mapping and Optimization

In this section, we propose another design method for IRA-coded MIMO systems. First, we discuss the relationship between the IRA and LDPC code ensembles. The optimization of the IRA code or the LDPC code is based on the density evolution which manipulates ensemble pdf of extrinsic messages passing along edges. Therefore, the design procedure is not related to the specific structure of the codes. The IRA code can be viewed as a specific class of LDPC codes. Hence, we can directly apply the LDPC design procedure to the turbo MIMO systems. The optimized IRA code profile can be obtained from the optimized LDPC code profile through IRA-LDPC mapping.

We can decode IRA using two different schemes. One is message-passing decoding algorithm which is the same as that for the LDPC codes. The other is turbo-like decoding algorithm employed with BCJR decoding for accumulator. It was shown in [69] that the message-passing decoder is identical to the BCJR algorithm for the $1/(1+D)$ inner code. Therefore, the trellis in IRA code can be simply treated as a special implementation of the mapped LDPC code. Then, the mapping between an IRA code ensemble and an LDPC code ensemble is fairly straightforward. As shown in the Tanner graph of an IRA code in Fig. 39, the check nodes are the same as the check nodes in an LDPC code with degree $a+2$. The parity nodes of an IRA code can be viewed as degree-2 variable nodes in an LDPC code. The information bit nodes of

an IRA code are also viewed as LDPC variable nodes with the same degree as they are in an IRA code. Thus, we can build a mapping relationship between the IRA code profile and the corresponding LDPC profile as follows.

Denote (λ^L, ρ^L) as the profile of the mapped LDPC code ensemble. Define d_r as the concentrated degree of the check node in an LDPC code. The edge profile of the check nodes of the mapped LDPC code is $\rho^L_{d_r} = \rho^L_{a+2} = 1$. The node profile of the IRA code is given by

$$\tilde{\lambda}_i = \frac{\lambda_i / i}{\sum_{j=2}^{D} \lambda_j / j}, \quad i = 2, \cdots, D. \tag{5.42}$$

Thus, the node profile of the mapped LDPC code is given by

$$\tilde{\lambda}^L_2 = \frac{\tilde{\lambda}_2 + 1/R - 1}{1/R} \text{ and } \tilde{\lambda}^L_i = \frac{\tilde{\lambda}_i}{1/R}, \quad i = 3, \cdots, D \tag{5.43}$$

Therefore, the profile of the corresponding LDPC code from the edge perspective is given by

$$\lambda^L_i = \frac{\tilde{\lambda}^L_i i}{\sum_{i=2}^{D} \tilde{\lambda}^L_j j}, \quad i = 2, \cdots, D. \tag{5.44}$$

The reverse mapping from the IRA code profile to the LDPC code profile is finally given by

$$a = d_r - 2, \tag{5.45}$$

$$\tilde{\lambda}_2 = \frac{\tilde{\lambda}^L_2 - (1 - R)}{R}, \quad \tilde{\lambda}_i = \frac{\tilde{\lambda}^L_i}{R}, \quad i = 3, \cdots, D, \tag{5.46}$$

$$\lambda_i = \frac{\tilde{\lambda}_i i}{\sum_{j=2}^{D} \tilde{\lambda}_j j}, \quad i = 2, \cdots, D. \tag{5.47}$$

Using above mapping, we can first apply the LDPC code design procedures developed in [29, 43] to LDPC-coded turbo MIMO systems, and then map the optimized LDPC code ensemble profile to the corresponding IRA code profile using (5.45)–

(5.47). Here another constraint should be specified when designing the corresponding LDPC code. As shown in Fig. 39, we have $M/N = 1 - R$. Thus, the portion of the degree 2 nodes in the LDPC code cannot be less than $1 - R$, otherwise we can not get an IRA code from the LDPC profile. Hence,

$$\tilde{\lambda}_2^L \geq 1 - R = \frac{1/d_r}{\sum_{j=2}^{D} \lambda_j^L / j} \implies \lambda_2^L \geq \frac{2}{d_r}. \tag{5.48}$$

Define

$$\gamma(\tilde{\lambda}^L, x) \triangleq \sum_{i=2}^{D} \tilde{\lambda}_i^L J(ix). \tag{5.49}$$

Thus, the recursion of r^ℓ for an LDPC code can be expressed as follows [8]

$$r^\ell = h(s, r^{\ell-1}) \quad \text{with} \quad h(s,r) = \sum_{i=2}^{D} \lambda_i^L h_i(s,r), \tag{5.50}$$

$$\text{where} \qquad h_i(s,r) = \phi\left(s + (i-1)\phi^{-1}(1-(1-r)^{d_r-1}\right). \tag{5.51}$$

When designing LDPC codes for AWGN channels, the optimization problem can be stated as follows: for a given $\rho(x)$ and m_{u_0},

$$\underset{\{\lambda_i\}}{\text{maximize}} \quad \sum_{i=2}^{D} \lambda_i^L / i \quad \text{s.t. } r > h(m_{u_0}, r), \quad 0 < r \leq \phi\left(m_{u_0}\right). \tag{5.52}$$

Note here $\rho(x) = x^{d_r-1} = x^{a+1}$. The constraints for the IRA-induced LDPC code optimization for MIMO system are then

$$r > h(m_k, r), \quad \phi(\gamma^{-1}(\tilde{\lambda}^L, v_k)) < r \leq \phi(J^{-1}(u_k)), k = 1, \cdots, G, \tag{5.53}$$

$$\text{and} \qquad \lambda_2^L \geq \frac{2}{d_r}. \tag{5.54}$$

Similar to (5.37), we can approximate (5.49) by $\gamma(\tilde{\lambda}^L, r) \approx J(2r)$. Then, we can solve the optimization problem using linear programming.

Now, we validate the above IRA code design method through LDPC mapping

by the following example. We consider designing an IRA code for AWGN channels. The repetition profile obtained from IRA code optimization is $\lambda(x) = 0.694938x + 0.102280x^2 + 0.001864x^3 + 0.143135x^4 + 0.056941x^5 + 0.034554x^6 + 0.007591x^7 + 0.190411x^{18} + 0.393731x^{19}$. The group factor $a = 7$ and the rate is 0.5002. We evaluate the asymptotic thresholds by simulation with information block length 10^5. The bit-error-rate (BER) is less than 10^{-5} when $E_b/N_0 \geq 0.5$dB, only 0.3dB dB from the capacity. Next we obtain the optimized IRA profiles from design LDPC profiles, given by $\lambda(x) = 0.139238x^2 + 0.141527x^3 + 0.118489x^4 + 0.133268x^5 + 0.410668x^6 + 0.340540x^7 + 0.765814x^{17} + 0.173816x^{18} + 0.273896x^{19}$, and $a = 7$. The rate of IRA code is 0.5001. The simulation results show that the BER reaches to 10^{-5} when $E_b/N_0 \geq 0.55$dB, 0.35dB away from the capacity. It is fairly good with maximum repetition degree of 20 for an IRA code.

E. Numerical Results

In this section, we present numerical results of the design and optimization of IRA codes for turbo MIMO systems. The fading matrix $\boldsymbol{H}$ varies at each time slot and changes independently from one slot to the next. The modulator uses the QPSK constellation with Gray mapping. All the IRA codes designed here have target rate of $\frac{1}{2}$.

1. EXIT Charts of MIMO Detectors

First, we illustrate the EXIT curves $\mathcal{G}(x, \rho)$ for the two soft MIMO detectors described in Section B. We consider two different MIMO configurations, namely, 2×2 and 4×4. Set $\rho = 2$dB and potential coding rate $R = 0.5$. We evenly choose some values u_i from $[0, 1)$ as the input mutual information of the MIMO detectors and obtain mean

of the extrinsic log-likelihood-ratio (LLR) by $m_i = J^{-1}(u_i)$. We then draw samples of LLRs, $x_n \sim \mathcal{N}(m_i, 2m_i)$, and calculate the output LLRs from MIMO detectors by Monte Carlo simulation. We compute the output mutual information v_i by the distribution of output LLRs from the detector.

Figure 40 shows the EXIT curves for the MAP detector and the SIC-MMSE detector. We can see that with the same antenna settings, the output extrinsic mutual information from the SIC-MMSE detector, with no *a priori* information input, is slightly smaller than that of the MAP detector. This initial offset determines the performance of the detector. The EXIT curves merge when the input $I_{in} = 1$. This is easy to understand because at $I_{in} = 1$, all the interference bits are perfectly detected, thus the SIC-MMSE detector and the MAP detector offer the same performance when the channel SNR is the same. It is also seen that the extrinsic mutual information output in the 4×4 system with the same detector is worse than that of the 2×2 case when the input EXIT values are small, i.e., $I_{in} < 0.3$. With stronger extrinsic information input, the 4×4 system provides better extrinsic output.

2. IRA Code Optimization Results

We next present the IRA code optimization results following the design procedure described in Section 2. The maximum repetition degree $D = 30$. With the approximations in (5.38) and (5.39), we use linear programming to obtain the best profiles of the IRA code ensemble. As a sample result, for the 2×2 case, with the MAP detector, we obtain $R = 0.5050$, $a = 7$, $\lambda(x) = 0.082818x^1 + 0.147731x^2 + 0.000331x^3 + 0.001790x^4 + 0.083303x^5 + 0.039609x^6 + 0.093325x^7 + 0.054323x^8 + 0.004153x^9 + 0.054851x^{26} + 0.096975x^{27} + 0.147768x^{28} + 0.192974x^{29}$; and with the SIC-MMSE detector, we obtain $R = 0.5001$, $a = 7$, $\lambda(x) = 0.091158x^1 + 0.133820x^2 + 0.086313x^5 + 0.024131x^6 + 0.096559x^7 + 0.044099x^8 + 0.000727x^9 + 0.082999x^{27} + 0.207612x^{28} + 0.232583x^{29}$.

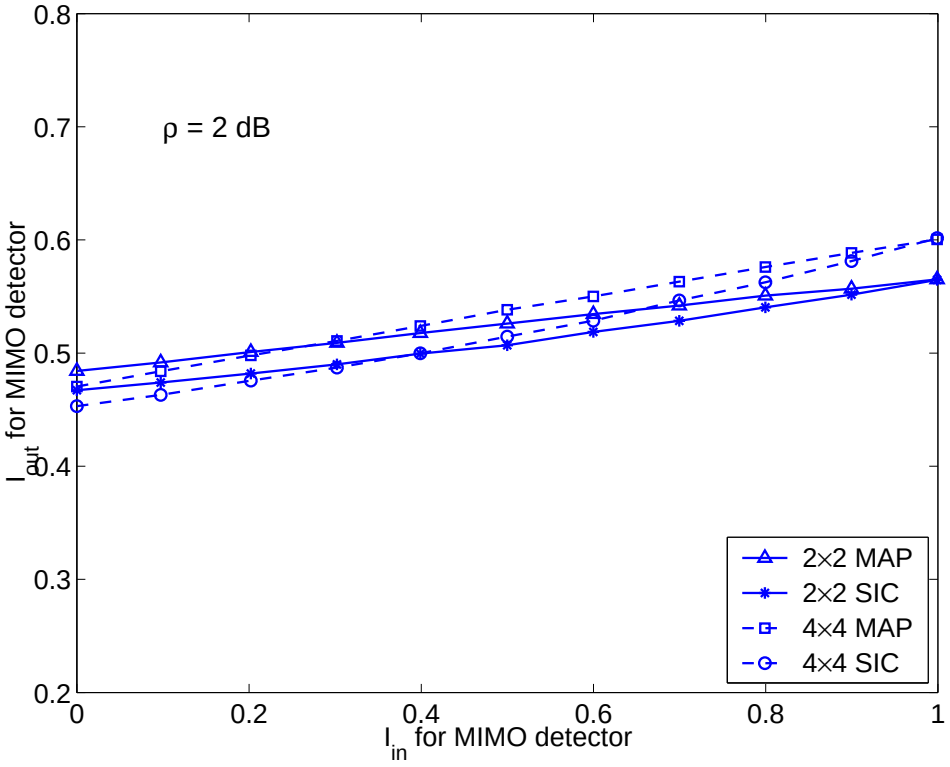

Fig. 40. EXIT curves for soft MIMO detectors.

Figure 41 shows the EXIT curves of the MAP detector of the optimized IRA code for this MIMO channel, and of the optimized IRA code for the AWGN channel. It can be seen that the EXIT curve of the designed IRA code matches very well with that of the detector, indicating the usefulness of the IRA code design techniques discussed in Section C. The EXIT chart of the optimized IRA code for AWGN channel is parallel to the horizontal axis in the transition range. The rate is 0.4771 which is lower than that of the MIMO optimized IRA code. Hence, the AWGN optimized code is not efficient for ergodic MIMO channels. And simulations indicate that if the AWGN optimized IRA code is used in the tubo MIMO system, the 4×4 MIMO system will have a worse performance than the 2×2 system because it has a smaller initial extrinsic output. An actual trajectory of the demodulation and decoding for 2×2

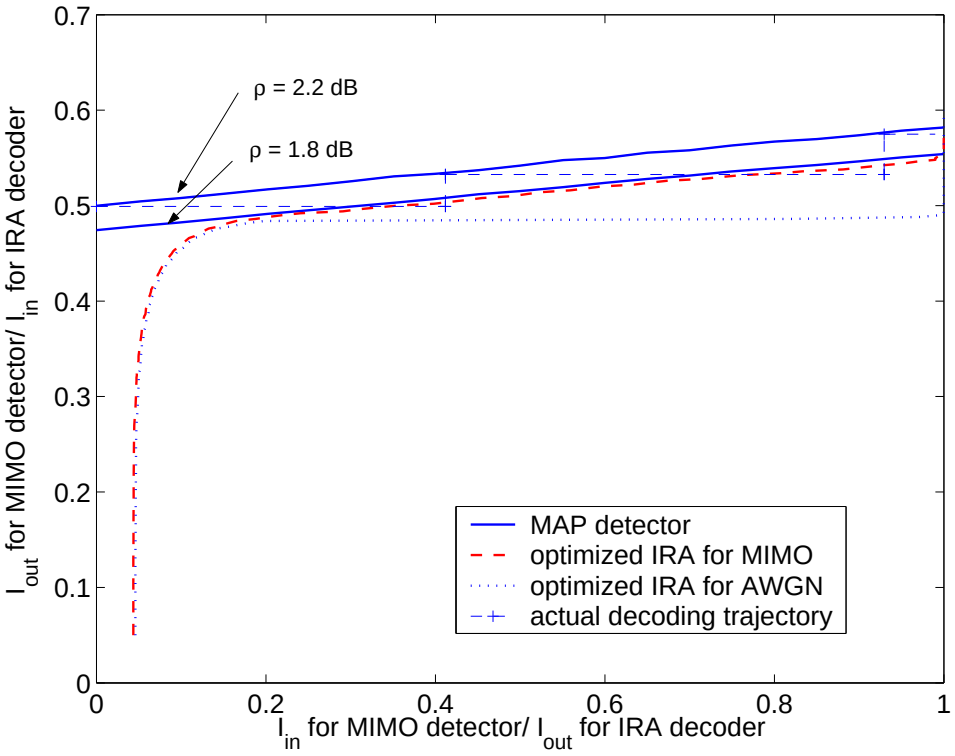

Fig. 41. EXIT charts for 2×2 MAP MIMO detector and IRA decoder.

MIMO system with MAP detector is also illustrated in Fig. 41. It is seen that an iterative tunnel exists between the EXIT curves of detector for $\rho = 2.2$dB and IRA decoding to ensure the decoding output evolve to 1. The decoder output is a little off the EXIT curve because of the approximation in the density evolution of IRA decoding.

We next evaluate the threshold for the MIMO-optimized IRA code. The information block length is 10^5. The final results are shown in Fig. 42. The required SNRs to achieve the constrained capacities [c.f. Eq. (5.4)] with QPSK constellation of the 2×2 and 4×4 ergodic MIMO channels with rate-$\frac{1}{2}$ code are 1.5dB and 1.6dB, respectively. The SNR thresholds to achieve zero-error decoding for the optimized IRA code with the MAP detector are 1.8dB for both 2×2 and 4×4 systems. The

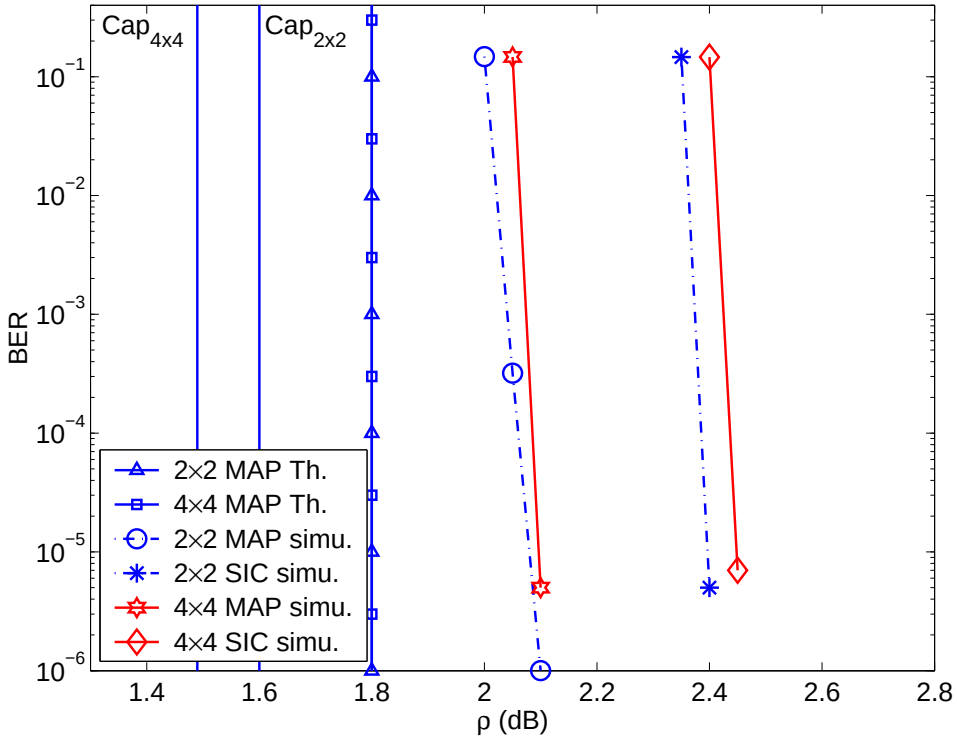

Fig. 42. BER performance of the optimized IRA codes using density evolution in ergodic MIMO channels.

simulation results show that for the 2×2 system with the MAP detector, the BER approach 10^{-5} when $\rho > 2.1$dB, only 0.5dB from the capacity. For the 4×4 system with the MAP detector, the simulated performance is 0.6dB from the capacity and 0.3dB off the designed threshold. The SIC-MMSE detector performs around 0.3dB worse than the MAP detector in each antenna setting.

3. IRA Code Optimization with LDPC Mapping

First, we design LDPC codes with additional constraint (5.48) for turbo MIMO channels. Then, we obtain the IRA code profiles from the optimized LDPC code using the mapping given by (5.45)–(5.47). The numerical results are illustrated in Fig. 43. For the 2×2 system, the optimized LDPC with the MAP detector has the threshold at

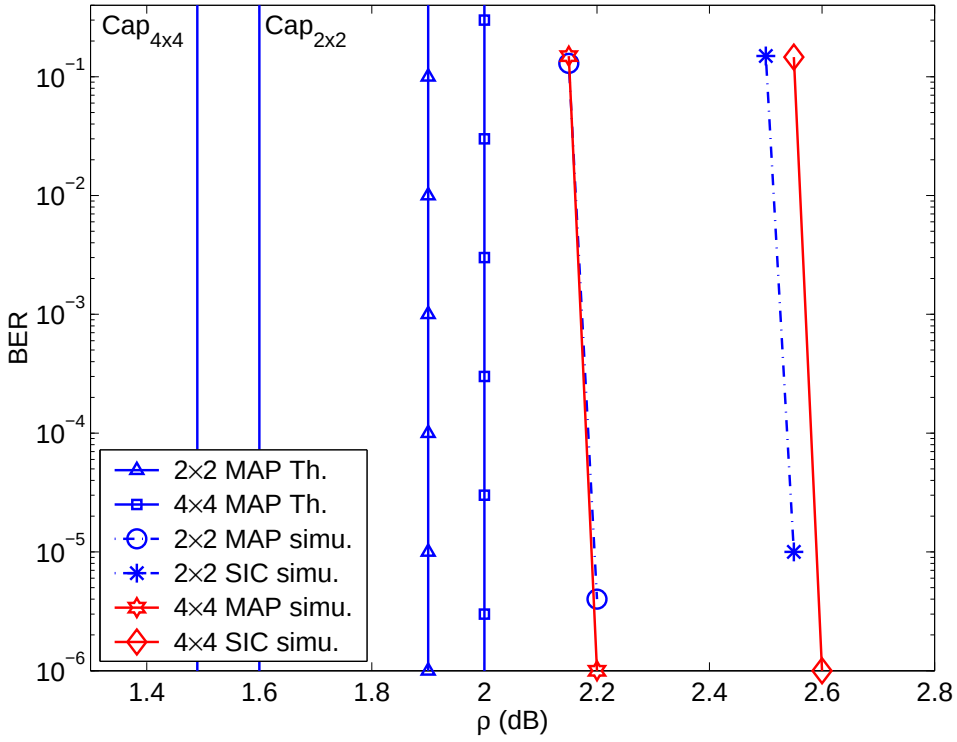

Fig. 43. BER performance of the optimized IRA codes using LDPC mapping in ergodic MIMO channels.

1.9dB, 0.3dB from the capacity; the simulated BER is below 10^{-5} when $\rho > 2.20$dB. For the 4×4 MIMO system, the threshold of the optimized LDPC with the MAP detector is 2.0dB; the simulated BER is below 10^{-5} when $\rho > 2.20$dB. Comparing with Fig. 42, the performance of optimized IRA code using the LDPC mapping is only slightly worse than that obtained by direct design.

4. IRA in Block Fading MIMO

Finally, we consider the IRA coded system in block fading MIMO channels. The channel gain matrix $\boldsymbol{H}$ remains constant in one block and changes independently from one block to the next. Still we assume the transmitter does not know the channel but the receiver has perfect knowledge of the channel. We assume each codeword fully

occupies one static fading block. Based on the optimal IRA profiles, we implement a finite-size IRA code with information block length $K \approx 1024$ for the block fading case. The S-random interleaver is adopted after the repetition in the IRA encoder. The performance is evaluated in terms of block or frame error rate (FER). Six turbo iterations are implemented in the receiver.

Figure 44 shows the FER curves for the 2×2 system at different iterations. The outage capacity curve is also plotted for comparison. It is seen that with the MAP MIMO detector, the FER performance is less than 2dB from the outage capacity curve. The SIC-MMSE detector performs 1.5dB worse than the MAP detector. We also find that the error floor occurs to the SIC-MMSE detector at 10^{-3} FER. Figure 45 shows the FER performance for the 4×4 system, as well as the outage capacity curve. The turbo receiver with the MAP detector performs only 1.5dB from the outage capacity. And with the SIC-MMSE detector, the performance is only 0.6dB worse than that of the MAP detector. The error floor occurs again to the MAP receiver at 10^{-3} FER.

Improving Short-length IRA Codes

From the above results, we find the designed IRA codes perform well even with short-length and in block fading channel. However, the error floor unpredictably occurs due to the difficulty in controlling the S-random interleaver structure. We need to lower the error floor since it degrades the performance dramatically. The mapping between the IRA code and the LDPC code opens some ways to solve the problem. As discussed in Section D , in the IRA code, the information bit nodes and the parity nodes are equivalent to the variable nodes of the LDPC code. It is known that the degree-2 nodes have very poor FER performance for short-size LDPC code though it is important for the irregular LDPC code to achieve the capacity with the infinite

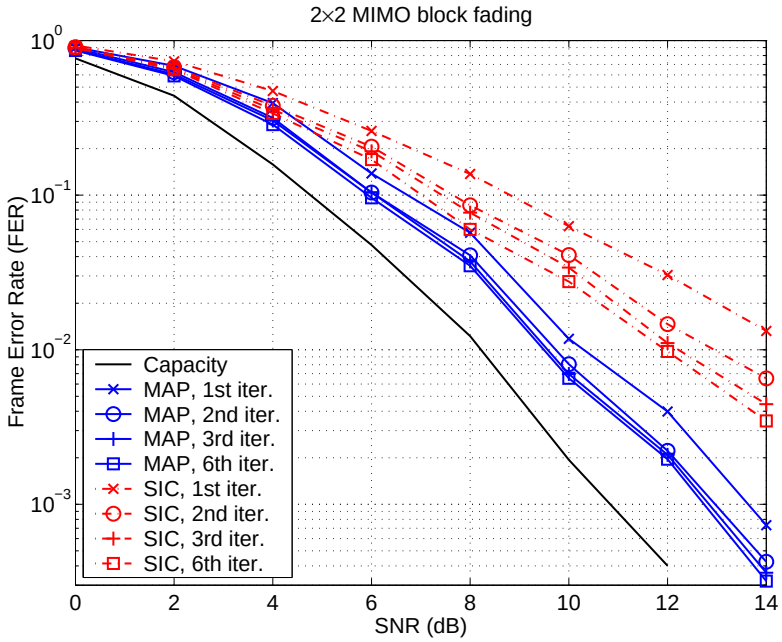

Fig. 44. FER performance of the short-length IRA codes in block fading 2×2 MIMO channels.

code length [9]. One solution is to deterministically arrange the edges of the degree-2 nodes adjacent to each other to ensure no cycles within degree-2 nodes. The parity nodes in an IRA code are viewed as degree-2 variable node in the LDPC code. From the Tanner graph in Fig. 39, we can see that the parity nodes are exactly arranged in this deterministic way. This can be another important advantage of the IRA code. However, the information nodes also contain some degree-2 nodes in the optimized profiles. Thus, in the whole code, the degree-2 nodes are not in a good design feature for short-length code. This is one reason that causes error floor. Due to the explicit encoder structure of the IRA code, we can easily find a solution by putting all the degree-2 nodes to the parity bits to give more protection on the information nodes with high degrees. This feature is hard to find in an LDPC code. Based on this, we design the IRA code for MIMO systems with additional constraint that information bit nodes contain no degree-2 node, i.e., $\lambda_2 = 0$. The resulting optimized IRA code

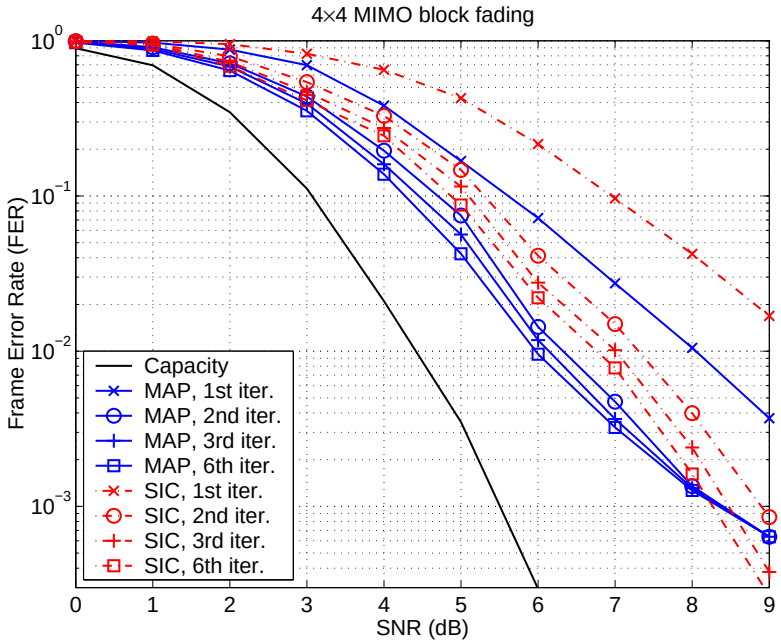

Fig. 45. FER performance of the short-length IRA codes in block fading 4×4 MIMO channels.

may not be the best IRA for long-length IRA code in the BER sense, but it offers a better FER performance for short-length code. We consider an example of the 4×4 system with the MAP detector. Figure 46 shows the FER curves of the IRA code implemented from the optimized profile without degree-2 information node, as well as the previous code without eliminating the degree-2 information nodes. We can see that the final FER curve of the new code is 0.4 dB closer to the outage capacity and has a lower error floor.

In short-length LDPC code design, eliminating cycle 4 is another important issue [70]. By eliminating the cycle 4 with all information nodes and parity nodes, we expect to have better performance and lower error floor for short-length IRA code. We consider a special IRA code with repetition profile as $\lambda_3 = 1$ and $a = 3$. Thus, it does not contain degree-2 information nodes. This special IRA code is shown to have good performance in the infinite code-length case with BER below 10^{-5} when

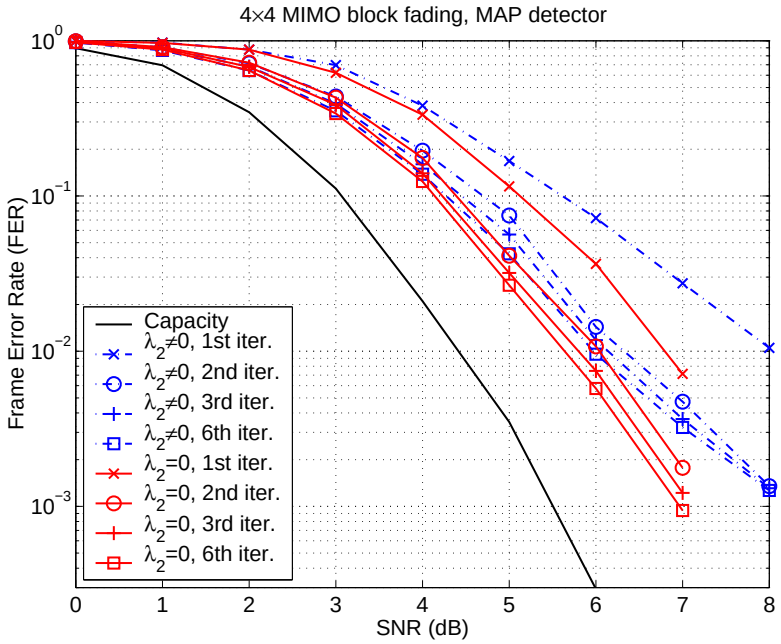

Fig. 46. FER performance of optimized no-degree-2 IRA code for block fading MIMO (4×4).

$\rho \geq 2.35$dB. We implement it with $K = 1024$ and eliminate all the cycle 4. We also eliminate small cycles (cycle 6 and up) involved with parity nodes as much as possible. The results are shown in Fig. 47. The FER performance form the final iteration is 0.6 dB better than the optimized IRA code with degree-2 information node and containing many cycle 4. It is now within 1 dB from the outage capacity.

Hence the IRA-LDPC mapping relationship not only provides an alternative way to design IRA code, but also reveals venues to build good short-length IRA codes.

F. Conclusions

In this chapter, we have considered the design of optimal IRA codes for MIMO systems employing turbo receivers. Two design approaches are discussed. One is based on the density evolution technique and the EXIT chart characteristic of the soft MIMO

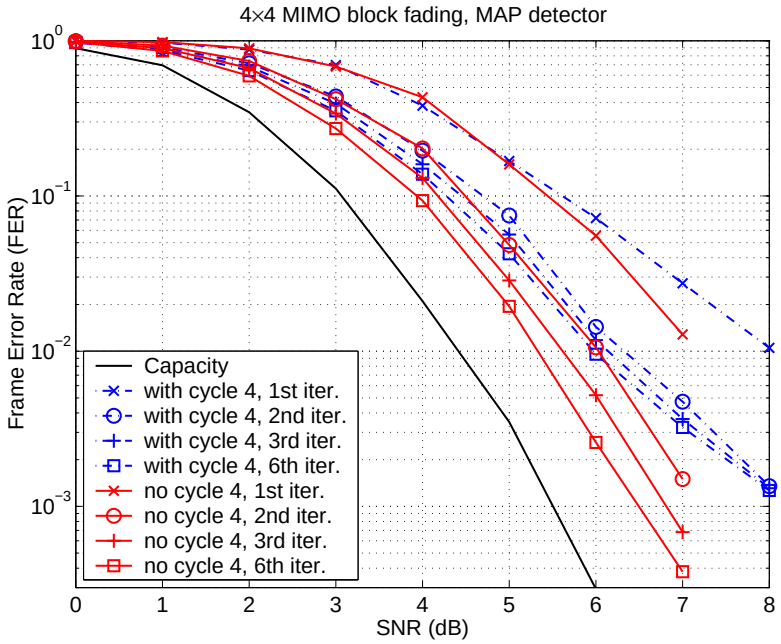

Fig. 47. FER performance of special IRA code for block fading MIMO (4×4): $\lambda_3 = 1$, no cycle 4.

detector and that of the IRA decoder. Another approach is based on mapping an optimized LDPC code for turbo MIMO systems to a corresponding IRA code under certain constraints. Two types of soft MIMO detectors are treated, namely, the MAP detector and the low-complexity SIC-MMSE detector. The resulting thresholds from simulations are within 1dB from the ergodic capacities of the MIMO systems under consideration. The design of short-length IRA codes for block fading MIMO channel is also considered which is based on the existing design methods for short-length LDPC codes. Compared with the LDPC codes, the IRA codes are extremely simple to encode and offer comparable performance. Hence, IRA code is a promising coding scheme for the next-generation wireless systems.

CHAPTER VI

CONCLUSIONS

In this dissertation, we have presented code optimization and analysis for several wireless communication systems with iterative joint decoding and demodulation, namely, LDPC code optimization for turbo CDMA systems, performance analysis and design optimization of LDPC coded MIMO-OFDM systems, coding-spreading tradeoff in LDPC coded CDMA with turbo multiuser detection, and design of irregular repeat accumulate codes for MIMO systems with iterative receiver. Provided by these code design methods, the optimized LDPC or IRA codes with large block size performs only several tenth decibel to information theoretical bound with MAP demodulators or ML detectors. Both LDPC codes and RA codes are promising coding schemes for the fourth generation (4G) wireless communication systems. Compared with the LDPC codes, IRA codes are extremely simple to encode and offer comparable performance. The frameworks of code optimization presented in this dissertation can also be applied to other wireless communication systems with iterative receivers.

REFERENCES

[1] C. Berrou, "The ten-year-old turbo codes are entering into service," *IEEE Commun. Mag.*, vol. 41, no. 8, pp. 110–116, Aug. 2003.

[2] T. Richardson and R. Urbanke, "The renaissance of Gallager's low-density parity-check codes," *IEEE Commun. Mag.*, vol. 41, no. 8, pp. 126–131, Aug. 2003.

[3] F.R. Kschischang, "Codes defined on graphs," *IEEE Commun. Mag.*, vol. 41, no. 8, pp. 118–125, Aug. 2003.

[4] C. Berrou, A. Glavieux, and P. Thitimajshima, "Near shannon limit error-correcting and decoding: Turbo codes," in *Proc. of Int. Conf. Commun. (ICC)*, Geneva, Swizerland, May 1993, pp. 1064–1070.

[5] D.J.C. MacKay and R.M. Neal, "Near shannon limit performance of low density parity check codes," *Elect. Lett.*, vol. 33, no. 6, pp. 457–458, Mar. 1997.

[6] R.G. Gallager, "Low-density parity check codes," *IRE Trans. Inform. Theory*, vol. 39, no. 1, pp. 37–45, Jan. 1962.

[7] M. Luby, M. Mitzenmacher, A. Shokrollahi, and D. Spielman, "Analysis of low-density codes and improved designs using irregular graphs," in *Proc. ACM Symp. Theory Comp.*, Dallas, Texas, 1998, pp. 249–258.

[8] S.Y. Chung, T. Richardson, and R. Urbanke, "Analysis of sum-product decoding of low-density parity check codes using a Gaussian approximation," *IEEE Trans. Inform. Theory*, vol. 47, no. 2, pp. 657–670, Feb. 2001.

[9] T. Richardson, M.A. Shokrohalli, and R. Urbanke, "Design of capacity approaching irregular low density parity check codes," *IEEE Trans. Inform. Theory*, vol. 47, no. 2, pp. 619–637, Feb. 2001.

[10] T. Richardson and R. Urbanke, "Capacity of low density parity check codes under message passing decoding," *IEEE Trans. Inform. Theory*, vol. 47, no. 2, pp. 599–618, Feb. 2001.

[11] S.Y. Chung, G.D. Forney, T.J. Richardson, and R. Urbanke, "On the design of low-density parity-check codes within 0.0045 dB of the shannon limit," *IEEE Commun. Lett.*, vol. 5, no. 2, pp. 58–60, Feb. 2001.

[12] J. Hagenauer, "The turbo principle: Tutorial introduction and state of the art," in *Proc. Int. Symp. Turbo Codes & Related Topics*, Brest, France, Sept. 1997, pp. 1–11.

[13] C. Douillard, A. Picart, P. Didier, M. Jezequel, C. Berrou, and A. Glavieux, "Iterative correction of intersymbol interference: Turbo equalization," *European Trans. on Telecommun.*, vol. 6, pp. 507–511, Sept.–Oct. 1995.

[14] X. Wang and H.V. Poor, "Iterative (turbo) soft interference cancellation and decoding for coded CDMA," *IEEE Trans. Commun.*, vol. 47, no. 7, pp. 1046–1061, July 1999.

[15] M. Sellathurai and S. Haykin, "Turbo-BLAST for wireless communications: Theory and experiments," *IEEE Trans. Sig. Proc.*, vol. 50, no. 10, pp. 2538–2546, Oct. 2002.

[16] A. Worthen and W. Stark, "Unified design of iterative receivers using factor graphs," *IEEE Trans. Inform. Theory*, vol. 47, no. 2, pp. 843–849, Feb. 2001.

[17] J. Hou, P. Siegel, and L. Milstein, "Performance analysis and code optimization of low density parity-check codes on rayleigh fading channels," in *Proc. 38th Annu. Allerton Conf. Commun., Control, & Comp.*, Monticello, IL, Nov. 2000, pp. 266–275.

[18] H.V. Poor, "Turbo multiuser detection: A primer," *J. Communications and Networks*, vol. 3, no. 3, pp. 196–201, Sept. 2001.

[19] J. Chen and M.P.C. Fossorier, "Density evolution for two improved BP-based decoding algorithms of LDPC codes," *IEEE Commun. Lett.*, vol. 6, no. 5, pp. 208–210, May 2002.

[20] J. Hagenauer, E. Offer, C. Meason, and M. Mörz, "Decoding and equalization with analog non-linear networks," *Euro. Trans. Telecom.*, vol. 10, no. 6, pp. 659–680, Nov.-Dec. 1999.

[21] S. ten Brink, "Convergence of iterative decoding," *Elec. Lett.*, vol. 35, no. 13, pp. 1117–1118, June 1999.

[22] E.L. Lehmann and G. Casella, *Theory of Point Estimation*, New York: Springer-Verlag, 1998.

[23] G.J. McLachlan and T. Krishnan, *The EM Algorithm and Extensions*, New York: Wiley, 1997.

[24] P. McKenzie and M. Alder, "Selecting the optimal number of components for a gaussian mixture mode," in *Proc. IEEE Int. Symp. Inform. Theory*, Trodheim, Norway, 1994, pp. 393–393.

[25] J. Rissanen, *Stochastic Complexity in Statistical Inquiry*, River Edge, New Jersey: World Scientific Publishing Co., 1989.

[26] K. Price and R. Storn, "Differential evolution - a simple and efficient heuristic for global optimization over continuous spaces," *Journal of Global Optimization*, vol. 11, pp. 341–359, 1997.

[27] S. Verdu, *Multiuser Detection*, p. 111, Cambridge, U.K: Cambridge Univ. Press, 1998.

[28] S. Verdu and S. Shamai, "Spectral efficiency of CDMA with random spreading," *Elec. Lett.*, vol. 45, no. 2, pp. 622–640, Mar 1999.

[29] K.R. Narayanan, X. Wang, and G. Yue, "LDPC code design for MMSE turbo equalization," in *Proc. IEEE Int. Symp. Inform. Theory (ISIT)*, Lausanne, Switzerland, June 2002, pp. 415–415.

[30] P. Bender, P. Black, M. Grob, R. Padovani, N. Sindhushyana, and S. Viterbi, "CDMA/HDR: A bandwidth efficient high speed wireless data service for nomadic users," *IEEE Commun. Magazine.*, vol. 38, no. 7, pp. 70–77, July 2000.

[31] G.J. Foschini, "Layered space-time architecture for wireless communication in a fading environment when using multi-element antennas," *Bell Labs. Tech. J.*, vol. 1, no. 2, pp. 41–59, 1996.

[32] S. M. Alamouti, "A simple transmit diversity technique for wireless communications," *IEEE J. Select. Areas Commun.*, vol. 16, no. 8, pp. 1451–1458, Oct. 1998.

[33] V. Tarokh, N. Seshadri, and A.R. Calderbank, "Space-time codes for high data rate wireless communication: Performance criterion and code construction," *IEEE Trans. Inform. Theory*, vol. 44, no. 2, pp. 744–765, Mar. 1998.

[34] I.E. Telatar, "Capacity of multi-antenna Gaussian channels," *Euro. Trans. Telecom.*, vol. 10, no. 6, pp. 585–595, Nov./Dec. 1999.

[35] B. Lu, X. Wang, and K.R. Narayanan, "LDPC-based space-time coded OFDM systems over correlated fading channels," *IEEE Trans. Commun.*, vol. 50, no. 1, pp. 74–88, Jan. 2002.

[36] S. ten Brink, G. Kramer, and A. Ashikhmin, "Design of low-density parity-check codes for modulation and detection," *IEEE Trans. Commun.*, vol. 52, no. 4, pp. 670–678, April 2004.

[37] G.J. Foschini and M.J. Gans, "On limits of wireless communications in a fading environment when using multiple antennas," *Wireless Personal Commun.*, vol. 6, pp. 311–335, Mar. 1998.

[38] D. Shiu, G.J. Foschini, M.J. Gans, and J.M. Kahn, "Fading correlation and its effect on the capacity of multi-element antenna systems," in *Universal Personal Communications, 1998. ICUPC'98*, Florence, Italy, Oct. 1998.

[39] E. Biglieri, G. Taricco, and A. Tulino, "Performance of space-time codes for a large number of antenna," *IEEE Trans. Inform. Theory*, vol. 48, no. 7, pp. 1794–1803, July 2002.

[40] B. Hassibi and B. Hochwald, "High-rate codes that are linear in space and time," *IEEE Trans. Inform. Theory*, vol. 48, no. 7, pp. 1804–1824, July 2002.

[41] H. Bölcskei, D. Gesbert, and A. J. Paulraj, "On the capacity of OFDM-based spatial multiplexing systems," *IEEE Trans. Commun.*, vol. 50, no. 2, pp. 225–234, Feb. 2002.

[42] G. Ungerboeck, "Channel coding with multilevel/phase signals," *IEEE Trans. Inform. Theory*, vol. 28, no. 1, pp. 55–67, Jan. 1982.

[43] G. Yue, X. Wang, and K.R. Narayanan, "Design of low density parity check codes for turbo multiuser detection," in *Proc. IEEE Int. Conf. Commun. (ICC)*, Anchorage, AK, May 2003, pp. 2703–2707.

[44] M. Stege, M. Bronzel, and F. Fettweis, "MIMO-cpacities for COST 259 scenarios," in *Proc. 2002 Inter. Zurich Seminar on Broadband Commun.*, ETH Zurich, Switzerland, Feb. 2002, pp. 29.1–6.

[45] J. Campello, D.S. Modha, and S. Rajagopalan, "Designing LDPC codes using bit-filling," in *Proc. IEEE Int. Conf. Commun. (ICC).*, Helsinki, Finland, June 2001, pp. 55–59.

[46] J.L. Massey, "Information theory aspects of spread-spectrum communications," in *Proc. IEEE ISSSTA'94*, Onlu, Finland, July 1994, pp. 16–20.

[47] V.V. Veeravalli and A. Mantravadi, "The coding-spreading tradeoff in CDMA systems," *IEEE J. Select. Areas Commun.*, vol. 20, no. 2, pp. 396–408, Feb. 2002.

[48] M. Rupf, F. Tarköy, and J.L. Massey, "User-separating demodulation for code-division multiple-access systems," *IEEE J. Select. Areas Commun.*, vol. 12, no. 5, pp. 786–795, June 1994.

[49] J.Y.N. Hui, "Throughput analysis for code division multiple accessing of the spread spectrum channel," *IEEE J. Select. Areas Commun.*, vol. 2, no. 4, pp. 482–486, Jan. 1984.

[50] S. Shamai and S. Verdú, "The impact of frequency-flat fading on the spectral efficiency of CDMA," *IEEE Trans. Inform. Theory*, vol. 47, no. 4, pp. 1302–1327, May 2001.

[51] H. El Gamal and E. Geraniotis, "Iterative multiuser detection for coded CDMA signals in AWGN and fading channels," *IEEE J. Select. Areas Commun.*, vol. 18, no. 1, pp. 30–41, Jan. 2000.

[52] M. Moher, "An iterative multiuser decoder for near-capacity communications," *IEEE Trans. Commun.*, vol. 46, no. 7, pp. 870–880, July 1998.

[53] M. Reed, C. Schlegel, P. Alexander, and J. Asenstorfer, "Iterative multiuser detection for CDMA with FEC: Near single-user performance," *IEEE Trans. Commun.*, vol. 46, no. 12, pp. 1693–1699, Dec. 1998.

[54] D. Divsalar, S. Dolinar, and F. Pollara, "Iterative turbo decoder analysis base on density evolution," *IEEE J. Select. Areas Commun.*, vol. 19, no. 5, pp. 891–907, May 2001.

[55] E. Biglieri, G. Caire, and G. Taricco, "CDMA system design through asymptotic analysis," *IEEE Trans. Commun.*, vol. 48, no. 11, pp. 1882–1896, Nov. 2000.

[56] J. Evans and D.N.C. Tse, "Large system performance of linear multiuser receivers for multiuser receivers in multipath fading channels," *IEEE Trans. Inform. Theory*, vol. 46, no. 6, pp. 2059–2078, Sept. 2000.

[57] D.N.C. Tse and S. Hanly, "Linear multiuser receivers: Effective interference, effective bandwidth and user capacity," *IEEE Trans. Inform. Theory*, vol. 45, no. 2, pp. 614–657, Mar. 1999.

[58] J. Boutros and G. Caire, "Iterative multiuser joint decoding: Unified framework and asymptotic analysis," *IEEE Trans. Inform. Theory*, vol. 48, no. 7, pp. 1772–1793, July 2002.

[59] R.G. Gallager, *Low-Density Parity-Check Codes*, Cambridge, MA: MIT Press, 1963.

[60] D. Divsalar, H. Jin, and R. McEliece, "Coding theorems for 'turbo-like' codes," in *Proc. Annual Allerton Conf. Commun., Control, & Comp.*, Monticello, IL, Sept. 1998.

[61] H. Jin and R.J. McEliece, "RA codes achieve AWGN channel capacity," in *Proc. Int. Symp. Applied Algebra & Error-Correcting Codes*, Honolulu, HI, Nov. 1999, pp. 14–19.

[62] H. Jin, A. Khandekar, and R.J. McEliece, "Irregular repeat-accumulate codes," in *Proc. Int. Symp. Turbo Codes & Related Topics*, Brest, France, Sept. 2000, pp. 1–8.

[63] A. Roumy, S. Guemghar, G. Caire, and S. Verdu, "Design methods for irregular repeat accumulate codes," in *Proc. IEEE Int. Symp. Inform. Theory (ISIT)*, Yokohama, Japan, June 2003, pp. 2–2.

[64] K.R. Narayanan, D.N. Doan, and R.V. Tamma, "Design and analysis of LDPC codes for turbo equalization with optimal and suboptimal soft output equalizers," in *Proc. Annual Allerton Conf. Commun., Control, & Comp.*, Monticello, IL, Oct. 2002.

[65] R.M. Tanner, "A recursive approach to low complexity codes," *IEEE Trans. Inform. Theory*, vol. 27, no. 5, pp. 533–547, Sept. 1981.

[66] F.R. Kschischang and B.J. Frey, "Iterative decoding of compound codes by probability propagation in grphical models," *IEEE J. Select. Area Commun.*, vol. 16, no. 2, pp. 219–230, Feb. 1998.

[67] S. ten Brink, "Convergence behavior of iterative decoded parallel concatenated codes," *IEEE Trans. Commun.*, vol. 49, no. 10, pp. 1727–1737, Oct. 2001.

[68] A. Ashikmin, G. Kramer, and S. ten Brink, "Extrinsic information transfer functions: A model and two properties," in *Proc. Conf. Info. Sci. Syst. (CISS)*, Princeton, NJ, Mar. 2002.

[69] J. Li, K.R. Narayanan, and C.N. Georghiades, "Product accumulate codes: A class of codes with near-capacity performance and low decoding complexity," *IEEE Trans. Inform. Theory*, vol. 50, no. 1, pp. 31–46, Jan. 2004.

[70] J. Campello and D.S. Modha, "Extended bit-filling and LDPC code design," in *Proc. IEEE Global Telecom. Conf. (Globecom)*, San Antonio, TX, Nov. 2001, pp. 985–989.

APPENDIX A

PROOF OF (4.41)

Consider QPSK modulation with Gray mapping. Each symbol $c_k \in \{c_q\}_{q=0}^{3}$ can be represented by two binary bit $[b_k^{(0)}, b_k^{(1)}]$, where $b_k^{(l)} \in \{+1, -1\}$, by following mapping rules:

$$\begin{aligned}
(1,1) &\longleftrightarrow c_0 = \frac{1+j}{\sqrt{2}}, \\
(-1,1) &\longleftrightarrow c_1 = \frac{-1+j}{\sqrt{2}}, \\
(-1,-1) &\longleftrightarrow c_3 = \frac{-1-j}{\sqrt{2}}, \\
(1,-1) &\longleftrightarrow c_2 = \frac{1-j}{\sqrt{2}}.
\end{aligned}$$

Based on the extrinsic LLRs of code bits $\lambda_k^{(l)}, l = 0, 1$, it is easy to show

$$P(b_k^{(l)} = b) = \frac{\exp(b\lambda_k^{(l)})}{1 + \exp(b\lambda_k^{(l)})},\ b \in \{+1, -1\}. \tag{A.1}$$

Then a soft estimate of c_k is given by

$$\tilde{c}_k = \sum_{q=0}^{3} c_q P(b_k^{(1)}) P(b_k^{(0)}). \tag{A.2}$$

The power from the interferers is then given by

$$P_k = A_k^2(1 - \|\tilde{c}_k\|^2) = A_k^2 \left[1 - 0.5\tanh^2\left(\frac{b_k^{(l)}\lambda_k^{(0)}}{2}\right) - 0.5\tanh^2\left(\frac{b_k^{(l)}\lambda_k^{(1)}}{2}\right)\right]. \tag{A.3}$$

Here, $b_k^{(0)}\lambda_k^{(0)}, b_k^{(1)}\lambda_k^{(1)}$ have the same distribution, $\mathcal{N}(m, 2m)$ and $m = 2\mathrm{SNR}_{in}$. Assuming equal power, we have

$$P = A^2\left[1 - \tanh^2(\frac{\lambda}{2})\right], \tag{A.4}$$

where λ is the extrinsic LLR of LDPC coded bits assuming all zero sequence transmitted. Thus, we have exactly the same asymptotic results as (4.21) for BPSK modulation. When using BPSK modulation, all the variables are real. Thus, the noise variance $\sigma^2 = \frac{N_0}{2}$. While using QPSK modulation, all the variables are complex, $\sigma^2 = N_0$. Thus, with the same E_b/N_0, we have the same σ^2. Therefore, we obtain the same results of γ as in BPSK modulated system with same E_b/N_0.

After output SNR γ is obtained, we generate complex samples $z_k = c_k + n_k$, $n_k \sim \mathcal{N}_C\left(0, \frac{1}{\gamma}\right)$, representing estimated QPSK symbols given by the soft multiuser detectors. Without loss of generality, assume all $c_k = c_0$. Then the *a posteriori* LLRs of code bits are given by

$$\lambda'^{(0)}_k = \log \frac{P(z_k|c_k = c_0) + P(z_k|c_k = c_2)}{P(z_k|c_k = c_1) + P(z_k|c_k = c_3)}; \tag{A.5}$$

$$\lambda'^{(1)}_k = \log \frac{P(z_k|c_k = c_0) + P(z_k|c_k = c_1)}{P(z_k|c_k = c_2) + P(z_k|c_k = c_3)}; \tag{A.6}$$

where $P(z_k|c_k = c_p) = \frac{1}{\pi/\gamma} e^{-\gamma \|z_k - c_p\|^2}, p = 0, 1, 2, 3$. Then we have

$$\lambda'^{(0)}_k = \log \frac{e^{\gamma(z_k c_0^* + z_k^* c_0)} + e^{\gamma(z_k c_2^* + z_k^* c_2)}}{e^{\gamma(z_k c_1^* + z_k^* c_1)} + e^{\gamma(z_k c_3^* + z_k^* c_3)}} = \log \frac{e^{\gamma\left(\frac{1}{\sqrt{2}} z_k^* + \frac{1}{\sqrt{2}} z_k\right)}}{e^{-\gamma\left(\frac{1}{\sqrt{2}} z_k^* + \frac{1}{\sqrt{2}} z_k\right)}} = \gamma \cdot \frac{4}{\sqrt{2}} \Re\{z_k\}, \tag{A.7}$$

$$\lambda'^{(1)}_k = \log \frac{e^{\gamma(z_k c_0^* + z_k^* c_0)} + e^{\gamma(z_k c_1^* + z_k^* c_1)}}{e^{\gamma(z_k c_2^* + z_k^* c_2)} + e^{\gamma(z_k c_3^* + z_k^* c_3)}} = \log \frac{e^{\gamma\left(\frac{j}{\sqrt{2}} z_k^* - \frac{j}{\sqrt{2}} z_k\right)}}{e^{-\gamma\left(\frac{j}{\sqrt{2}} z_k^* - \frac{j}{\sqrt{2}} z_k\right)}} = \gamma \cdot \frac{4}{\sqrt{2}} \Im\{z_k\}, \tag{A.8}$$

Apparently, $\lambda'^{(0)}_k, \lambda'^{(1)}_k$ have the same symmetric Gaussian pdf. Assume $\lambda'^{(0)}_k, \lambda'^{(1)}_k$ are independent. Hence, $\lambda'^{(0)}_k, \lambda'^{(1)}_k$ are i.i.d., denoted by λ'. Then the output SNR for the binary extrinsic message is

$$\mathrm{SNR}_{out} = \frac{1}{2} E\left[\lambda'\right] = \gamma. \tag{A.9}$$

Thus, we have the same output SNR for the coded bits with QPSK as that of BPSK modulation which leads same results of $\alpha_m(\nu)$. We have spectral efficiency

$$\kappa(\nu) = \alpha_m(\nu)\nu. \tag{A.10}$$

Since the code rate ν bits/symbol with QPSK modulation are twice of the one with BPSK modulation, the final result of the spectral efficiency is then doubled, i.e.,

$$\kappa_{\text{QPSK}}(\nu) = 2\kappa_{\text{BPSK}}\left(\frac{\nu}{2}\right). \tag{A.11}$$

Same results can be obtained for the SIC-MF detector.

VITA

Guosen Yue was born in Nanjing, Jiangsu, China. He received his B.S. degree in physics and M.S. degree in electrical engineering from Nanjing University, Nanjing, China in 1994 and 1997, respectively. He began his Ph.D. program in the department of Electrical Engineering at Texas A&M University in 2000 and received his Ph.D. in August 2004. He may be contacted at the following address: Department of Electrical Engineering, Texas A&M University, College Station, TX 77843.